HORIZONTAL AND VERTICAL STRUCTURE OF VELOCITY,
POTENTIAL VORTICITY AND ENERGY IN THE GULF STREAM

by
Melinda M. Hall

B.A. Duke University, Durham, North Carolina
(1979)

SUBMITTED IN PARTIAL FULFILLMENT OF THE
REQUIREMENTS FOR THE DEGREE OF
DOCTOR OF PHILOSOPHY

at the

MASSACHUSETTS INSTITUTE OF TECHNOLOGY

and the

WOODS HOLE OCEANOGRAPHIC INSTITUTION

February, 1985

Signature of Author_____
Joint Program in Oceanography, Massachusetts
Institute of Technology-Woods Hole Oceanographic
Institution

Certified by _____
Thesis Supervisor

Accepted by _____
Chairman, Joint Committee for Physical
Oceanography, Massachusetts Institute
of Technology - Woods Hole Oceanographic
Institution.

1

Horizontal and Vertical Structure of Velocity,

Potential Vorticity, and Energy in the Gulf Stream

by

Melinda M. Hall

Abstract

From October, 1982 to October, 1983 a current meter mooring reaching

from the bottom into the thermocline was deployed for the first time in

the Gulf Stream at 68°W. The temperatures, pressures, and velocities at

the uppermost instrument indicate the Gulf Stream moved back and forth

across the mooring site, so that the entire Stream was sampled in time;

hence the data may be used to examine horizontal as well as vertical

structure of the Stream. The two key points to the success of the

analysis are: 1)the well-defined relationship between temperature and

cross-stream distance in the thermocline, enabling the use of the former

as a horizontal coordinate; and 2)a daily-changing definition of Gulf

Stream flow direction based on the shear between the thermocline and

2000 m depth. Time-series of daily-rotated velocities may be used to calculate empirical orthogonal functions for the long- and cross-stream vertical structures, which are decoupled and are respectively baroclinic and barotropic. Using the inferred horizontal coordinate one can estimate mass, momentum and kinetic energy fluxes for four individual events when the entire Stream swept by the mooring. The results agree well with historical data. Bryden's (1980) method has been used to calculate vertical velocities from the temperature equation; the resulting time-series of w are visually coherent throughout the water column and their vertical amplitude structure is reminiscent of that for a two-layer system. The rms vertical velocities are large (O(.05 cm/s)), and these as well as other estimates have been used to explore the validity of the quasi-geostrophic approximation at the mooring site. The Rossby number for the thermocline flow is about 0.3, and for the deep flow is $\leq$ 0.1.

The entire data set may also be used to construct a horizontal and vertical profile of velocity in the Gulf Stream, from which a cross-section of the mean potential vorticity can be produced. The latter shares many common feature with cross-sections from past work for a nearby site, as well as analogous data from a three-layer numerical model, thus suggesting that they are robust features of Gulf Stream-like currents. These features are, in particular, a strong jump from low to high values crossing the Stream from south to north; and a change in the sign of the potential vorticity gradient on isothermal surfaces for $T > 12°C$.

To complement the analysis of the observational data, a set of diagnostic calculations has been performed on an eddy-resolving general circulation model, to provide a complete picture of the kinetic energy budgets of the free jet and its environs. It is found that the downstream convergence of kinetic energy in the decelerating jet is balanced primarily by an ageostrophic flow against the pressure gradient, which in turn implies some conversion of kinetic to available potential energy in the region. Energetic analysis of the observations as well as the numerical data suggests barotropic and baroclinic instabilities may be equally important to the kinetic energy budgets in the Stream.

Because there is but one mooring, the dynamics governing the fluctuations remain elusive. Nonetheless, a kinematic framework is proposed, which is consistent with the data and accounts for a variety of unusual features that arise in the original analysis (for example, distinct asymmetries in the four Gulf Stream crossings, and the rather large vertical velocities). It is suggested that the data we are now capable of collecting is proffering fundamentally new attributes of the Gulf Stream, which must be included and accounted for in future theoretical work.

ACKNOWLEDGMENTS

I want to thank my advisor Harry Bryden for never failing to encourage me during my years as a student, and for his guidance and many stimulating suggestions in the development of this thesis. My other committee members -- Joe Pedlosky, Mike McCartney, Nick Fofonoff and Paola Rizzoli -- provided me with insight in their respective areas of expertise. Dr. William Holland of NCAR generously provided the numerical data for the calculations of Chapter 3. I would also like to thank Bill Schmitz for a number of stimulating discussions related to the thesis.

I want to thank Audrey Williams for her help in typing the thesis (especially the equations in Chapter 3!).

Finally, I thank Larry for his continuing support as well as many scientific discussions, and for helping me to keep things in perspective throughout the trials and tribulations of being a student.

TABLE OF CONTENTS

Chapter 1. Introduction

Perhaps the most remarkable feature of the general circulation of the world oceans is the persistence of strong western boundary currents closing the subtropical gyre circulations of each ocean to the west. The Gulf Stream in the North Atlantic, the Brazil Current in the South Atlantic, the Kuroshio in the North Pacific and the Agulhas in the Indian Ocean are all narrow, energetic swiftly flowing currents carrying large mass transports. Indeed, these boundary currents are responsible for transporting interior, wind-driven equatorward flow poleward to maintain mass continuity; presumably a large fraction of the energy and vorticity input by wind must be dissipated in these currents as well. They are clearly an integral part of the general circulation, and until we fully understand what governs their behavior, we cannot claim to understand the ocean's general circulation fully.

The Gulf Stream was first described over 450 years ago (Stommel, 1950, traces the development of ideas and observations in the Stream), and since then has been observed and monitored in a number of ways. While it is probably the most heavily documented feature in the deep North Atlantic, it is also terribly complicated, and continues to defy complete understanding. Part of the problem lies in the type of observations that have been feasible in the Gulf Stream. The earliest data came from ship drift measurements, which served to outline the general currents associated with the surface flow along the coast and eastward into the North Atlantic. Once it was recognized that a temperature front was a feature of the Stream, temperature measurements

were used to define the surface path of the current. Early versions of floats and drifters were employed as well. Around 1900 the geostrophic relationship was employed to determine oceanic currents (Stommel, 1950). In more recent years the surface thermal front has been monitored by satellite, which has the advantage of producing continuous long time-series of front position, but which has the disadvantage that clouds often obscure the front, severely reducing the amount of data collected, particularly in winter.

To understand the dynamics of this energetic current, however, one must know something of the three-dimensional structure of its velocity field, and how it varies with time. Hydrographic surveys such as Gulf Stream '60 (Fuglister, 1963) have served to define the baroclinic structure rather well, but since that study had but a few float trajectories to aid in choice of a reference level for geostrophic velocities, the barotropic aspects of the flow remained largely unknown. Moreover, a hydrographic survey is at best a snapshot of the flow in time. The deployment of large numbers of floats over the past twenty years has helped in describing gross features of the Gulf Stream's time variability, -- e.g., how meanders and eddies affect the eddy kinetic energy patterns in the North Atlantic (Richardson, 1983) -- but because there is little control over the floats after deployment, it has been virtually impossible to learn how the baroclinic structure itself varies with time. Clearly, this aspect must be monitored by long-term fixed arrays with instruments throughout the water column, but until recently, mooring technology was incapable of successfully deploying such moorings

in a current as strong as the Gulf Stream. Now that the technology is available, we need to proceed carefully in interpreting the data obtained from such moorings, particularly when there is data from but a single mooring, as is the case here.

Development of theoretical Gulf Stream investigations began with explanations of a steady structure, primarily determined by either friction (Stommel, 1948; Munk, 1950) or inertial effects (Fofonoff, 1954). Attempts to predict the time-varying path of the free eastward Gulf Stream from upstream inlet conditions began with Warren (1963), and later continued with a model by Robinson and Niiler (1967). Various types of instability models have been used to explain the time-variability of the Stream. Orlanski (1969) used a two-layer linear model with different bottom topographies to predict time and space scales for instablilities of the Stream on the continental shelf and in deeper water over the continental rise. Luyten and Robinson (1974) and Robinson, Luyten, and Flierl (1975) have discussed the long-wavelength instabilities of a thin, quasi-geostrophic meandering jet (assumed to move coherently from top to bottom). Talley (1982) has used a horizontally unbounded, two-layer, linear model to examine the radiation of energy by instabilities away from various jet configurations meant to approximate the Gulf Stream. In the past decade, great progress has been made numerically, as well. Holland and Lin (1975) were the first to run a numerical model of a baroclinic ocean in which the horizontal resolution was small enough (on the order of the deformation radius), and the viscosity was low enough, to demonstrate that mesoscale eddies are

generated spontaneously in a steadily-forced model. The numerical simplification involved in introducing quasi-geostrophic eddy-resolving general circulation models (Holland, 1978) led to extensive parameter studies of the models (Holland and Haidvogel, 1980) as well as investigations of the stability properties of the model jets (Haidvogel and Holland, 1978).

The interpretaion that will unfold in succeeding chapters is seated in the body of knowledge accumulated from these theories and observations. Two approaches may be adopted for interpreting the data: in the first, the mean flow at the mooring site is assumed to "define" the Gulf Stream there. In the second, the well documented baroclinic structure of the Stream is used to infer a daily-changing "Streamwise direction of flow." That is, the Stream is recognized as a permanent front that may change its orientation, with quasi-permanent attributes such as strong vertical shear of the flow velocity. Recent work by Johns (1985) demonstrates that the primary mode of displacement for the Gulf Stream thermocline is the simple translation of a coherent feature; this result is crucial in determining some horizontal structure from a single mooring. The basic tenet of this thesis is that such a well-defined feature exists and that its description, in a time-averaged sense, differs from the mean measured flow at the mooring site. In particular, the analysis concentrates on developing a description of this feature and enumerating the distinctions between the two possible interpretations of the Gulf Stream.

Chapter 2 first presents the vertical structure of the flow at the mooring site and places it in the context of past work. Next the

machinery is developed to extract horizontal information from the data set, allowing: 1) estimates of mass, momentum, and kinetic energy transports; 2) calculation of vertical velocities from the temperature equation; and 3) an assessment of the quasi-geostrophic approximation at the mooring site.

Little has been said thus far of the downstream changes in the Gulf Stream, but that is an area in which little progress has been made. The average downstream changes in potential vorticity structure of the Stream, for example, are so gradual that they are swamped by local variability. Fofonoff and Hall (1983) documented downstream changes in Gulf Stream transports of mass, momentum and kinetic energy , but had difficulty in accounting for the changes. Long time-series at several downstream positions are necessary to assess energetic balances in the vicinity of the Stream, and at this point such data are available only from numerical simulations of oceanic circulation. In Chapter 3 the energety budgets are discussed for the numerical Gulf Stream analog and its environs in a Holland (1978) model, assessing the relative importance of various mechanisms in accelerating and decelerating the jet, as well as their roles in the inertial recirculations and the primarily wind-driven portions of the domain. It should be pointed out that this analysis resorts to the first rather than second Gulf Stream flow definition described above: that is, the time-averaged Eulerian flow in the jet region is assumed to be the time-averaged jet.

Chapter 4 is an extension of the classical development of the data, as a cross-section of potential vorticity in the Stream is constructed

and described. As previously mentioned, the structure is far from
simple. However, comparisons with other data and with numerical model
data point up the salient features in cross-sections of potential
vorticity in the observed Gulf Stream and its analog in the numerical
model. These are evidently robust features, which have immediate
implications for the dynamics of the flow.

In Chapter 5, an effort is made to analyze the energetic budgets at
the mooring site for comparison with past work and with the numerical
analysis of Chapter 3. Then a kinematic interpretation of the flow
regime is explored, which is consistent with the data and accounts for
some of the more unusual results described in Chapter 2. Finally, some
suggestions are made for the future directions Gulf Stream observational
work might profitably take.

Chapter 2. Profiling the Gulf Stream with a current meter mooring

2.1 Introduction

The GUSTO mooring, deployed for one year at 37°37' N, 68°00' W, the mean position of the Stream at that longitude (Halliwell and Mooers, 1983), represents the first opportunity to examine long time series of current measurements throughout the water column in the Gulf Stream. Currents, temperature, and pressure were recorded at the nominal deployment depths of 400, 700, and 1000m, while current and temperature only were measured at 2000 and 4000 m. The only missing data is at the middle instrument (1000 m), where the VACM stopped working after 64 days, but resumed after 56 more days. Although only one mooring was deployed, yielding only vertical resolution of the flow, a remarkable amount of horizontal structure can be inferred: as the Stream meanders back and forth across the mooring, the temperature and pressure measurements at the uppermost instruments can be used, in conjunction with historical data, to determine how far north or south of the current axis the mooring is. Thus, the data profiles the horizontal structure of the Stream in time. Inspection of the National Weather Service analyses of satellite data, indicating the approximate surface expression of the Gulf Stream, shows that the mooring was in the Stream 58 percent of the time, in the Slope Water to the north 12 percent of the time, and Sargasso water to the south 30 percent of the time.

Because the strong currents tilted the mooring -- average pressure at the top instrument was 498 dbar, with a minimum of 433 dbar and a

maximum of 680 dbar -- temperatures and velocities were interpolated or extrapolated to intermediate standard pressures of 575 dbar, 875 dbar, and 1175 dbar to create time series that could be used in a consistent manner (Raymer, Spencer, and Bryden, 1984). Even a cursory inspection of the records reveals that while the mean velocity vector at 575 dbar was directed nearly due east, instantaneously the flow was usually north or south of east. It has been pointed out that there are at least two ways to discuss a "mean" Gulf Stream, either as the Eulerian average flow in a particular region or as a discrete feature that may change its position or orientation while retaining certain fundamental characteristics. The former is a more traditional approach and is discussed first, for comparison with past work. The second approach is more fruitful for describing a meandering, frontal jet like the Gulf Stream.

2.2 Mean statistics of the flow

All the data from the mooring was low-pass filtered with a 24-hour Gaussian filter, then subsampled daily, to provide time series of 360 daily values. Table 2-1 shows the record-length mean east and north velocities and temperatures at the five standard depths. Also shown are the variances of these quantities. In spite of the often large deviation from East of the current direction at 575 dbar, the mean velocity there is directed essentially due East. It is, however, much smaller than the maximum speeds recorded there, which are well over 100 cm/s. Mean northward velocities throughout the water column are extremely small and are nearly barotropic, though on a daily basis there may be considerable

Depth (db)	Days of data	$\bar{u}$ (cm/s)	$\bar{v}$ (cm/s)	$\bar{T}$ (°C)	$\overline{u'^2}$ (cm^2/s^2)	$\overline{v'^2}$ (cm^2/s^2)	$\overline{T'^2}$ (°C^2)
575	360	38.402	-0.952	12.598	1487.63	601.95	16.936
875	360	17.320	-1.042	7.635	448.33	192.03	5.840
1175	240	6.906	-0.809	4.880	126.87	89.65	0.572
2000	360	4.816	-0.944	3.711	68.65	67.18	0.028
4000	360	-1.038	-0.599	2.311	54.16	61.79	0.001

Table 2-1. Record-length statistics for east and north velocity and temperature corrected time series at the "standard" depths (see text).

shear in that direction (Figure 2.1a). Since v is barotropic while u is baroclinic, the mean velocity vectors turn cyclonically with increasing depth, implying a mean downward vertical velocity (Bryden, 1980). The mean velocity at 4000 m is directed nearly along-isobath, which is about 70° true (bottom depth is 4688 m), and the average zonal velocity there is westward rather than eastward. This deep flow is reminiscent of what Luyten (1977) found in his "upper rise" regime at 70°W, with along-isobath flow directed mostly westward. The mean temperature at 575 dbar is very close to that associated with the Gulf Stream axis, as discussed in Section 2.3, suggesting that this was indeed the average location of the Stream for the year.

The eddy kinetic energy is surface intensified, as Richardson (1983) found in constructing a vertical section of EKE (eddy kinetic energy) along 55°W from drifter, float, and current meter data. In that section, however, the values at 575 db in the Gulf Stream region are roughly 500 $cm^2 s^{-2}$, only about half that of around 1050 $cm^2 s^{-2}$ from Table 2-1. The surface intensification appearing in both velocity components indicates that baroclinicity associated with the Gulf Stream appears in north as well as east velocities. Below 1000 m or so, the EKE values decay very little with depth and are very nearly equipartitioned between the two velocity components. Richardson's 55 W values do not decay as rapidly with depth: at 2000 m he displays a value of 136 $cm^2 s^{-2}$, compared to 108 $cm^2 s^{-2}$ from Table 2-1, but his values below 1500 m or so under the Stream axis remain fairly constant at around 130-140 $cm^2 s^{-2}$. Schmitz (1984) found similar results for abyssal eddy

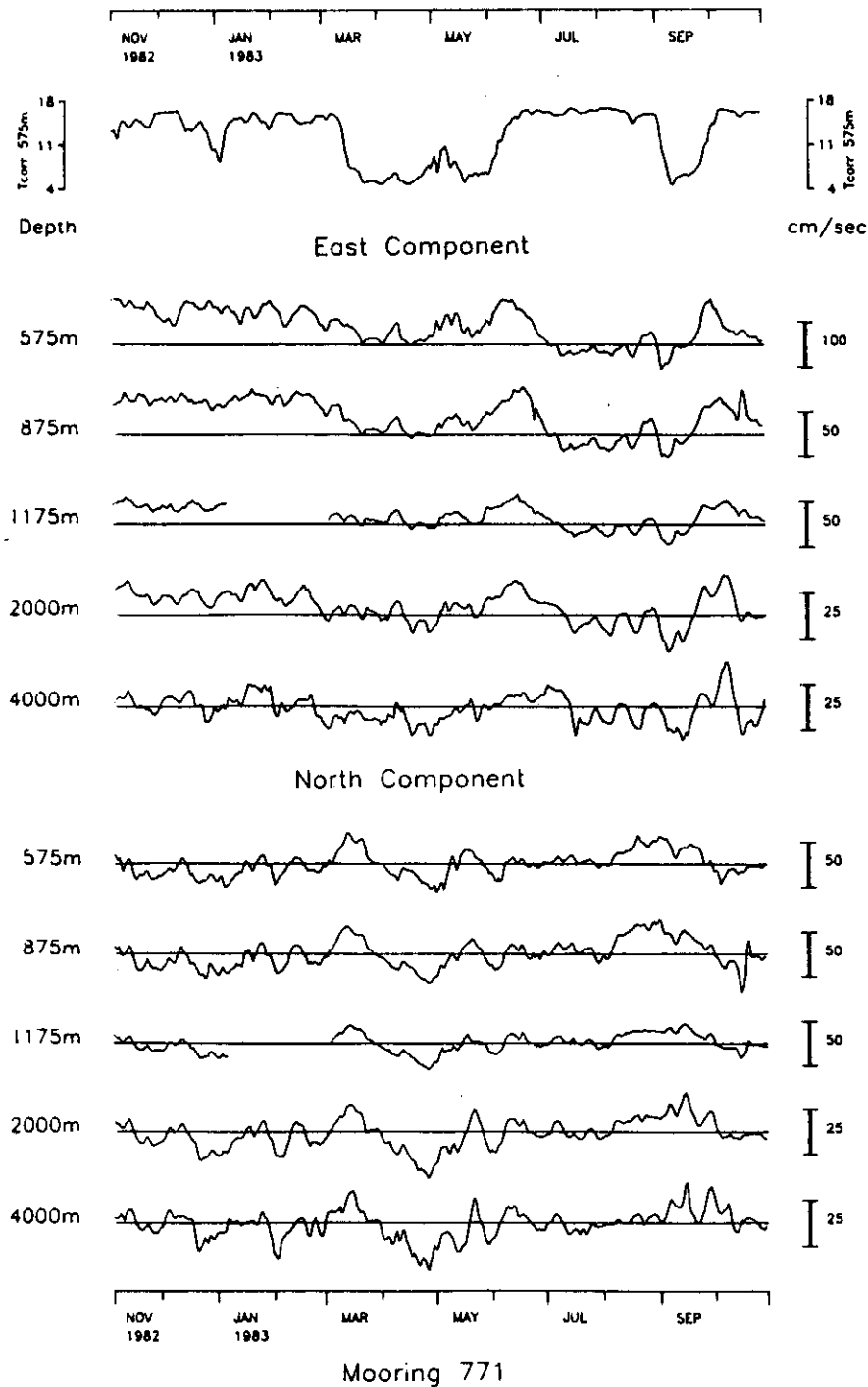Figure 2.1. a) Time series of east (top) and north (bottom) velocities at five standard depths; b) Flow direction, defined as direction of shear between 400 and 2000 m instruments; c) Time series of along- and cross-stream velocities (see text) at five standard depths. At top is time-series of T_{575}, temperature corrected to 575 dbar (see text).
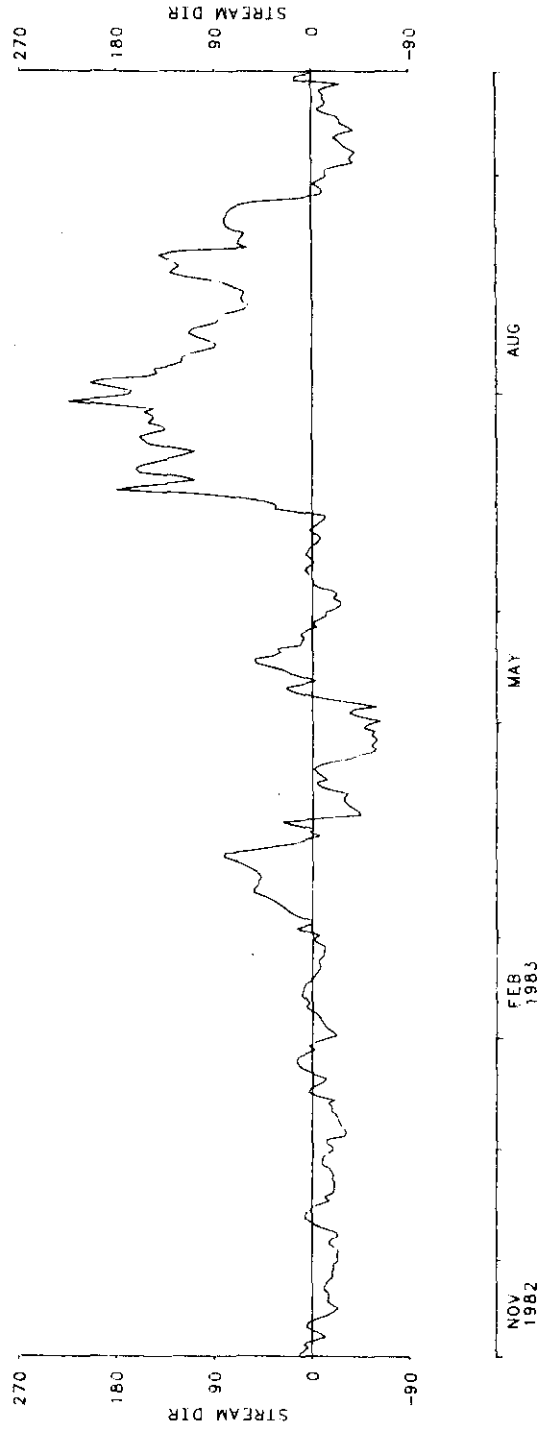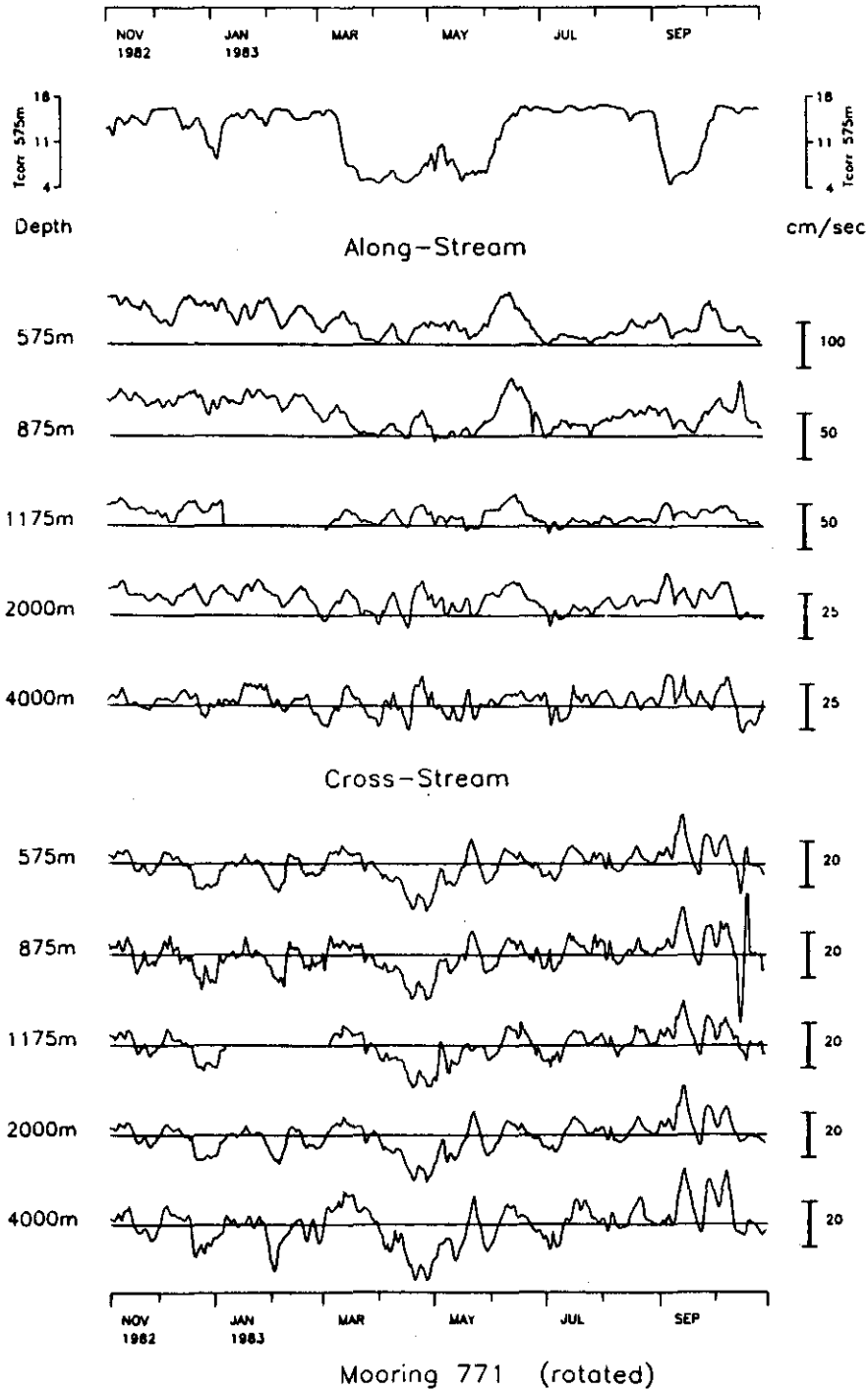
Figure 2.1b

Figure 2.1c

Mooring 771 (rotated)

kinetic energy in particular, that its variation with depth is much less in deep water than shallow; and that abyssal (4000 m) EKE displays similar scales of variation in the zonal and meridional directions. He found actual values near the Gulf Stream at $70°W$ of 104 cm^2s^{-2} at 4000 m, about twice the value of 58 cm^2s^{-2} form Table 2-1, but less than Richardson's value of 138 cm^2s^{-2}. Schmitz also points out that there is a gap in data coverage between 55 W and 70 W, but that a maximum in eddy kinetic energies might be expected there. In summary, the values in Table 2-1 seem to fit in well with other documented values in this region, both qualitatively and quantitatively.

2.3 Vertical structure of the "average Gulf Stream"

In order to obtain a description of the Gulf Stream as a discrete feature from the flow at the current meter site, it is necessary to define what is meant in referring to the Stream. As the Gulf Stream meanders and changes direction, a significant part of the "along-stream" flow may be contained in the northward component of velocity; hence a definition of what direction the Stream is flowing at any given time is required, to determine how large the along-stream flow is. The direction of the shear between the measured current at the uppermost (400 m) instrument and that at the 2000 m instrument has been chosen as the definition of the along-stream flow direction for several reasons. While the velocity vector may rotate with depth in the current records, that can be due to a small barotropic flow superimposed on the primarily baroclinic jet: strong vertical shear has long been recognized as a

signature of Gulf Stream flow. The time series of east and north
currents at the five instruments demonstrate that when the Gulf Stream is
present (as evidenced by the current speeds and the temperature at 575
dbar), it appears to penetrate all the way to the bottom instrument
(Figure 2.1a); at other times, for example the beginning of April, there
is a bottom-intensified westward flow in the deep water. To avoid any
problems with such reversals at 4000 m, the direction of shear between
that and the 400 m instrument was not chosen. Furthermore, the choice of
2000 m is a classical reference level of no motion used in the North
Atlantic. With such a definition, the along-stream direction changes day
by day as shown in Figure 2.1b.

The time series of along- and cross-stream velocities are shown in
Figure 2.1c, along with T_{575} (temperature corrected to 575 db). A
monotonic increase or decrease in T_{575} signals the passage of the Gulf
Stream across the mooring site: four clear examples occur in March,
June, late August/early September, and later September. The Gulf Stream
also occupied the mooring site for long periods when it did not sweep
completely across, such as from November, 1982 to March, 1983.
Comparison of Figures 2.1a and c shows that the third event is an
excellent argument for defining a daily along-stream direction: the flow
then was to the northwest (Figure 2.1b), yet according to T_{575} and
corroborating evidence from the NOAA satellite pictures, this flow was
indeed the Gulf Stream. In fact, the top-to-bottom coherence of Gulf
Stream flow is more apparent in Figure 2.1c than 2.1a. The baroclinicity
of the along-stream flow is obscured due to the changing velocity scales

with depth, which were chosen so that the 4000 m velocities, e.g., would in fact be discernible. However, note that all the scales on the cross-stream velocities are the same, displaying the remarkably barotropic character of the cross-stream velocities: this feature would never have been isolated in strictly east/north coordinates.

To quantify the baroclinic and barotropic structures of the along- and cross-stream velocities, empirical orthogonal functions (EOF's) for their vertical structures were computed. Time series from the standard depths were used, and EOF's were computed using data from the four complete (360-day) records. EOF's may be computed for the separate velocity components as well as for the vector velocity as a function of depth. If there is a strong coupling between the two components, the structure of the latter may be considerably different thatn the structure obtained by adding the EOF structures for the individual components. EOF's were computed both ways and compared, but no such differences were found, indicating that there is little coupling between along- and cross-stream velocity components. The correlation coefficient for the two amplitude time series attains a maximum value of $C = 0.1$, when the cross-stream series is not lagged at all. For an estimated 30 degrees of freedom, C must be ≥ 0.3 for a significant correlation at the 95 percent confidence level. Only calculations for the separate components are described here. Note that when data is available at N points in the vertical, N EOF's will be computed.

When data from the 575, 875, 2000, and 4000 dbar records are used, 92.4 percent of the variance in cross-stream velocity is accounted for by

the first mode, with the vertical structure shown in Figure 2.2a. Notice
how nearly barotropic the mode is. The second, third, and fourth modes
contain, respectively, 5.9, 1.7, and 0.03 percent of the variance and are
thus of little importance in comparison to the first mode. In the
along-stream direction, the first calculated EOF accounts for 89.8
percent of the variance, and has the strongly baroclinic vertical
structure shown in Figure 2.2b. There is no reversal of the amplitude at
4000 m, indicating that the deep flow in these coordinates is
statistically in the same direction as the thermocline flow. The second,
third, and fourth modes contain 6.2, 3.7, and 0.3 percent of the energy,
respectively.

Using hat notation to denote rotated velocities, the along- and
cross-stream velocities may be expressed in terms of east and north
velocities, and the direction α of the flow (see Figure 2.6 for
schematic):

$$\hat{u} = u\cos\alpha + v\sin\alpha \qquad\qquad u = \hat{u}\cos\alpha - \hat{v}\sin\alpha$$

$$\hat{v} = v\cos\alpha - u\sin\alpha \qquad\qquad v = \hat{v}\cos\alpha + \hat{u}\sin\alpha \qquad (2\text{-}1).$$

Since the time mean (denoted by $\overline{(\ )}$) is first removed when calculating
EOF's, the first EOF actually yields time series for

$$\begin{Bmatrix} u_1'(t) \\ u_2'(t) \\ u_3'(t) \\ u_4'(t) \end{Bmatrix} = a(t) \begin{Bmatrix} m_1 \\ m_2 \\ m_3 \\ m_4 \end{Bmatrix} \qquad \begin{Bmatrix} v_1'(t) \\ v_2'(t) \\ v_3'(t) \\ v_4'(t) \end{Bmatrix} = b(t) \begin{Bmatrix} n_1 \\ n_2 \\ n_3 \\ n_4 \end{Bmatrix} \qquad (2\text{-}2)$$

where $m_1^2 + m_2^2 + m_3^2 + m_4^2 = 1$, $n_1^2 + n_2^2 + n_3^2 + n_4^2 = 1$, and $\int a^2(t)\,dt = \lambda_1$,

$\int b^2(t)\,dt = \mu_1$, the first eigenvalues. Thus, in terms of east and

Figure 2.2. a)Vertical structure of the first EOF calculated for cross-stream velocity (see text for definition), using complete (360-day) records at 4 depths; b)same, but for long-stream velocity.
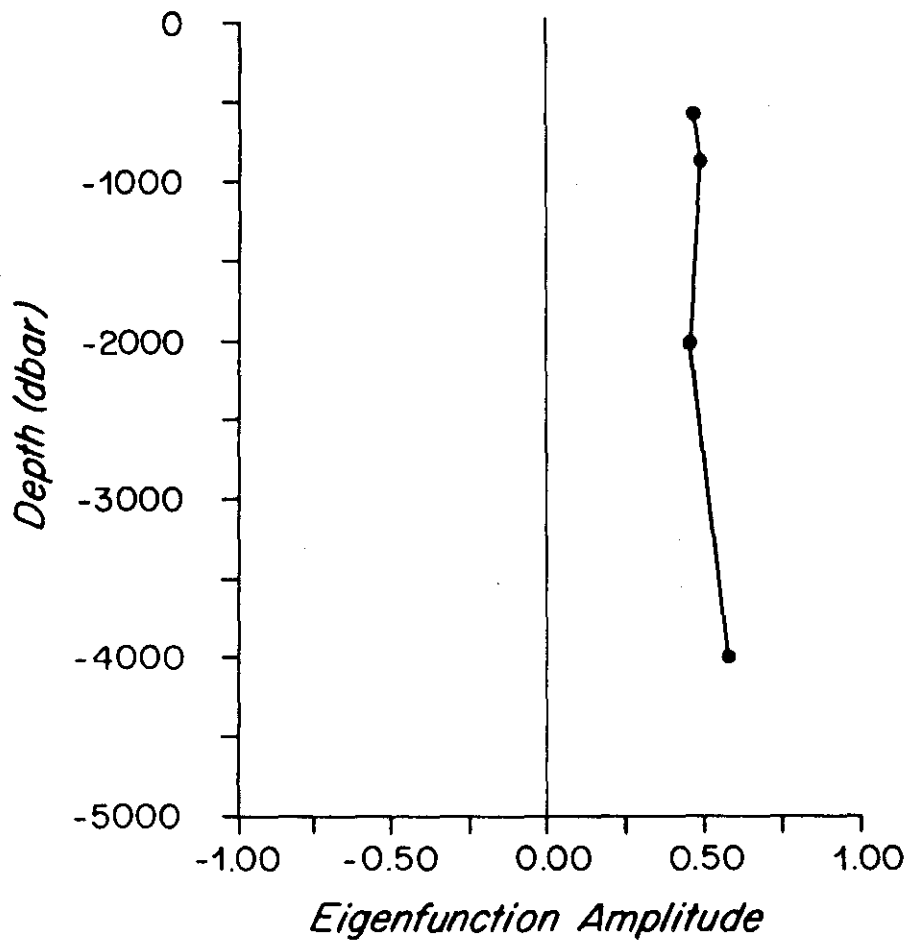
Figure 2.2b
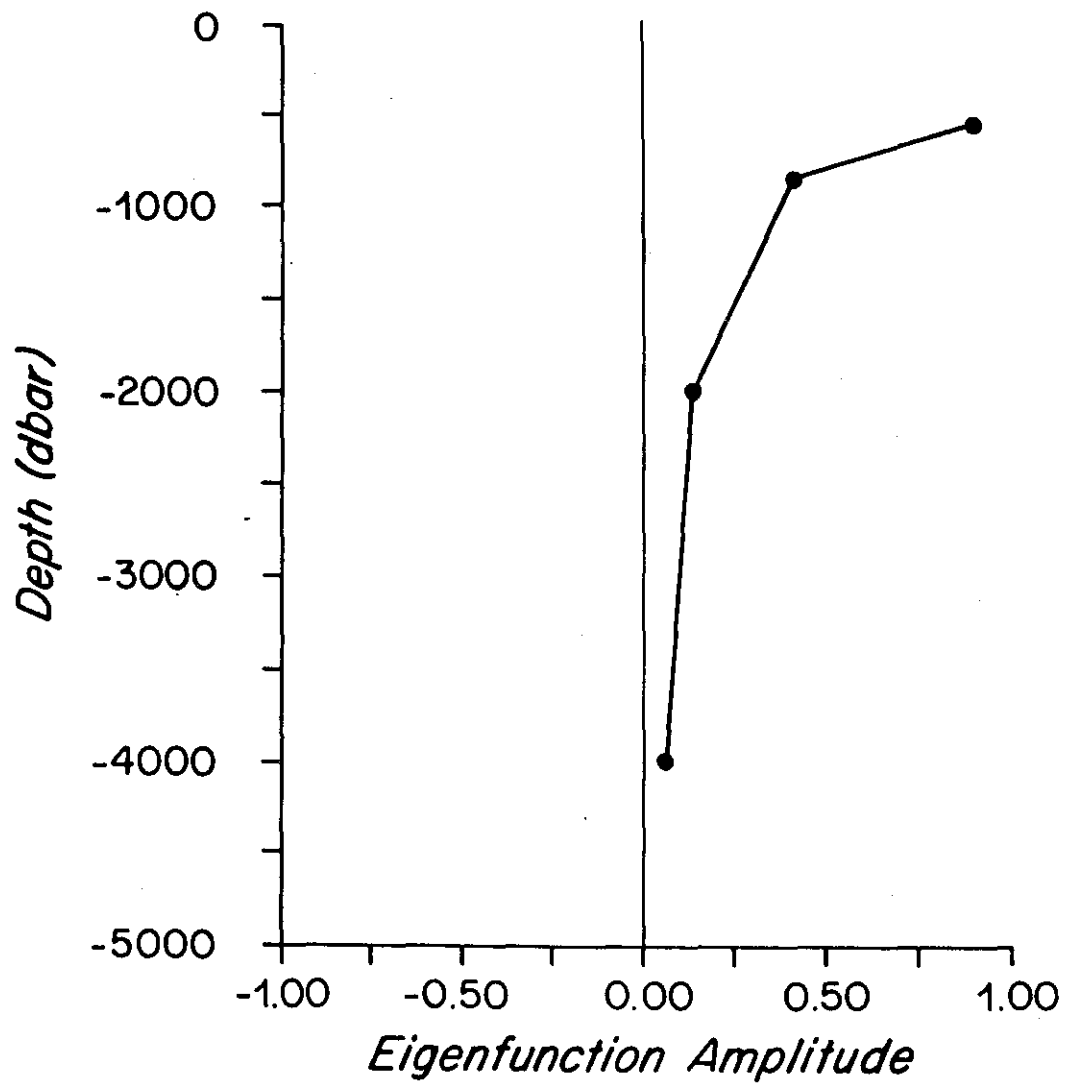
north velocities, what the EOF's actually yield is the following

description:

$$
\begin{Bmatrix} u_{575} \\ u_{875} \\ u_{2000} \\ u_{4000} \end{Bmatrix} \sim \left[\begin{Bmatrix} \bar{u}_{575} \\ \bar{u}_{875} \\ \bar{u}_{2000} \\ \bar{u}_{4000} \end{Bmatrix} + a(t) \begin{Bmatrix} m_1 \\ m_2 \\ m_3 \\ m_4 \end{Bmatrix} \right] \cos\alpha \quad -
$$

$$
\left[\begin{Bmatrix} \bar{v}_{575} \\ \bar{v}_{875} \\ \bar{v}_{2000} \\ \bar{v}_{4000} \end{Bmatrix} + b(t) \begin{Bmatrix} n_1 \\ n_2 \\ n_3 \\ n_4 \end{Bmatrix} \right] \sin\alpha \qquad (2\text{-}3a)
$$

$$
\begin{Bmatrix} v_{575} \\ v_{875} \\ v_{2000} \\ v_{4000} \end{Bmatrix} \sim \left[\begin{Bmatrix} \bar{v}_{575} \\ \bar{v}_{875} \\ \bar{v}_{2000} \\ \bar{v}_{4000} \end{Bmatrix} + b(t) \begin{Bmatrix} n_1 \\ n_2 \\ n_3 \\ n_4 \end{Bmatrix} \right] \cos\alpha \quad +
$$

$$
\left[\begin{Bmatrix} \bar{u}_{575} \\ \bar{u}_{875} \\ \bar{u}_{2000} \\ \bar{u}_{4000} \end{Bmatrix} + a(t) \begin{Bmatrix} m_1 \\ m_2 \\ m_3 \\ m_4 \end{Bmatrix} \right] \sin\alpha \qquad (2\text{-}3b).
$$

The two decoupled modes of the rotated frame combine to yield the more

complicated description of the data in terms of east and north

components. The actual time series of (u,v) and the derived series from

(2-3a,b) compare extremely well.

Depth (db)	$\bar{\tilde{u}}$(cm/s)	$\bar{\tilde{v}}$(cm/s)	$\overline{\tilde{u}'^2}(\frac{cm^2}{s^2})$	$\overline{\tilde{v}'^2}(\frac{cm^2}{s^2})$
575	51.003	-.600	918.60	45.01
875	25.020	-.448	248.67	56.55
1175	11.942	-.027	77.17	45.09
2000	8.852	-.638	36.48	44.67
4000	2.118	-.147	37.72	75.15

Table 2-2. Record-length statistics for velocities in rotated co-ordinate system at standard depths.

Table 2-2 shows the mean statistics for the velocities in the rotated coordinate system. The mean along-stream velocities are stronger than the mean east velocities throughout the water column, and are in the same direction top to bottom. The cross-stream velocity variance is very barotropic, and the total EKE throughout the water column is less for these coordinates, indicating that much of the energy calculated in Table 2-1 is associated with the meandering of the Gulf Stream rather than changes in its inherent structure.

In summary, the successful definition of an along-stream flow direction leads to a clean description of the flow's vertical structure at the mooring site. In the rotated coordinates, the fluctuations, as well as the mean, break down neatly into a baroclinic along-stream mode and a barotropic cross-stream mode, which are decoupled, and each of which contains about 90 percent of the variance. Furthermore, the structure of both the mean and fluctuating along-stream mode show no flow reversals at depth, indicating that the Gulf Stream as defined here does indeed penetrate to the bottom.

2.4 Horizontal structure of the Gulf Stream

The meandering of the Gulf Stream back and forth past the mooring site suggests that a horizontal description of the Stream might be deduced from the mooring data, to complement the vertical description. A scatter plot of along-stream velocity versus temperature at 575 dbar (Fig. 2.4) shows that the former is a strong function of the latter. If the cross-stream temperature structure at

575 dbar remains fairly constant in time (though it may meander about), then at any given time the corrected temperature at 575 dbar ought to indicate how far in the cross-stream direction the mooring is located relative to the axis of the long-stream flow. Johns (1985) has recently shown that the primary mode of displacement of the thermocline in the Gulf Stream is a strict translation of the isotherms, rather than either a tilting or squeezing, for example. Thus, this assumption of fixed cross-stream structure is justified. The much longer scales of variation in the downstream direction prevent a similar approach for a description of long-stream flow structure, which will henceforth rarely be discussed. The question is now this: how can this notion of temperature and cross-stream distance being functions of one another be quantified?

Consider Figure 2.3, which shows a scatter plot of $\partial T/\partial \hat{y}$ as a function of T at 575 db, where the $^\wedge$ notation refers to rotated coordinates. With thermal wind ($\rho_0 f \partial \hat{u}/\partial z = g \partial \rho/\partial \hat{y}$) and the assumption that salinity is a function of temperature alone such that $d\rho = -\alpha_0 dT$ where $-\alpha_0 = \partial\rho/\partial T + (\partial\rho/\partial S)(dS/dT)$, the cross-stream temperature gradient at 575 dbar may be obtined from the measured velocities and pressures at the 400 and 700 m instruments. Since rotated velocities were used, technically ($f + \partial\alpha/\partial t$) ought to be used in place of f in the geostrophic relation; however α_t is generally several orders of magnitude less than f, and so it can be ignored. The points were divided into two categories, those for which $T_{575} >$ 13°C or $T_{575} < 13°C$, and least squares linear fits were obtained

Figure 2.3. Scatter plot of ∂T/∂y vs. T at 575 db, along with linear least squares fit.
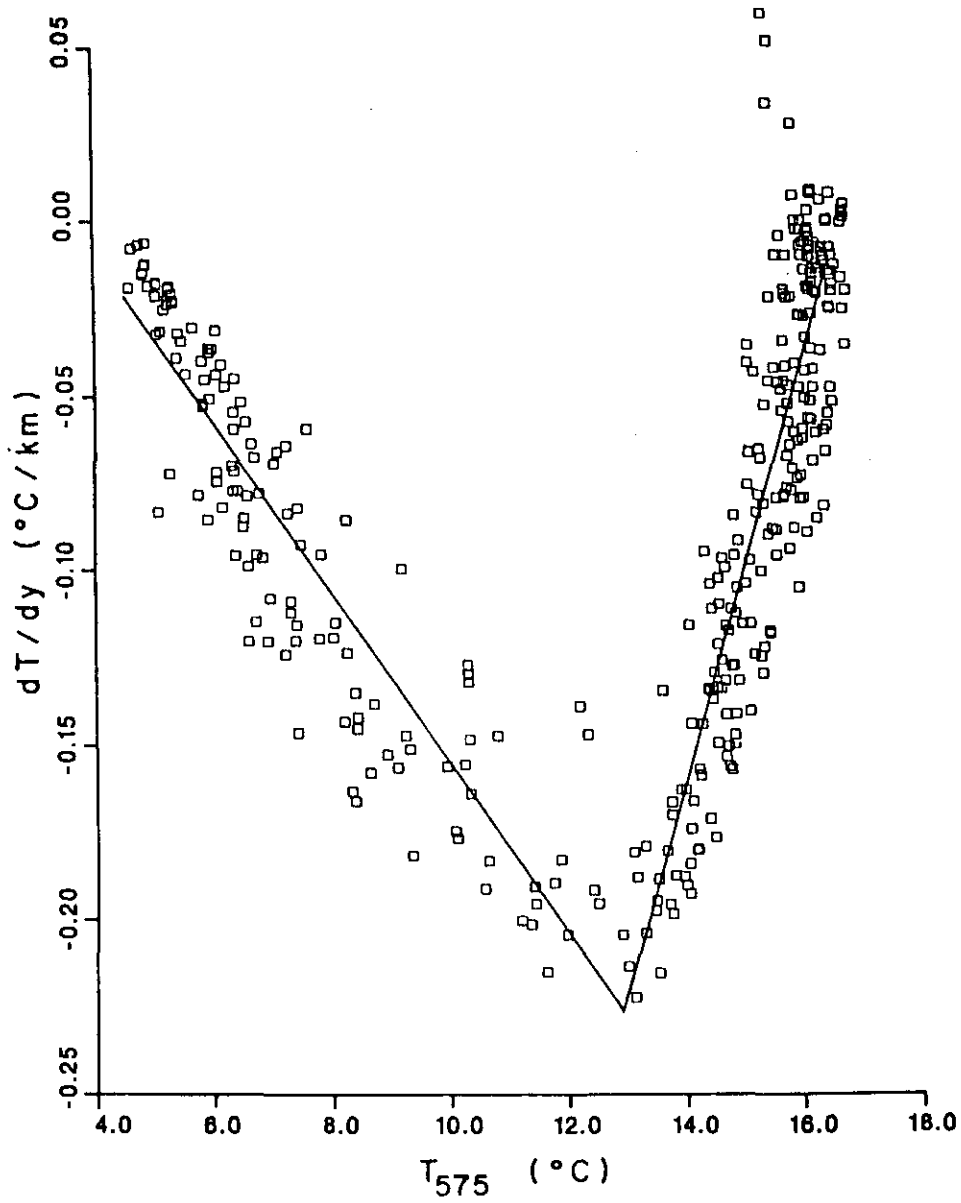
Figure 2.4. Scatter plot of û <u>vs.</u> T at 575 db, along with linear least squares fit.
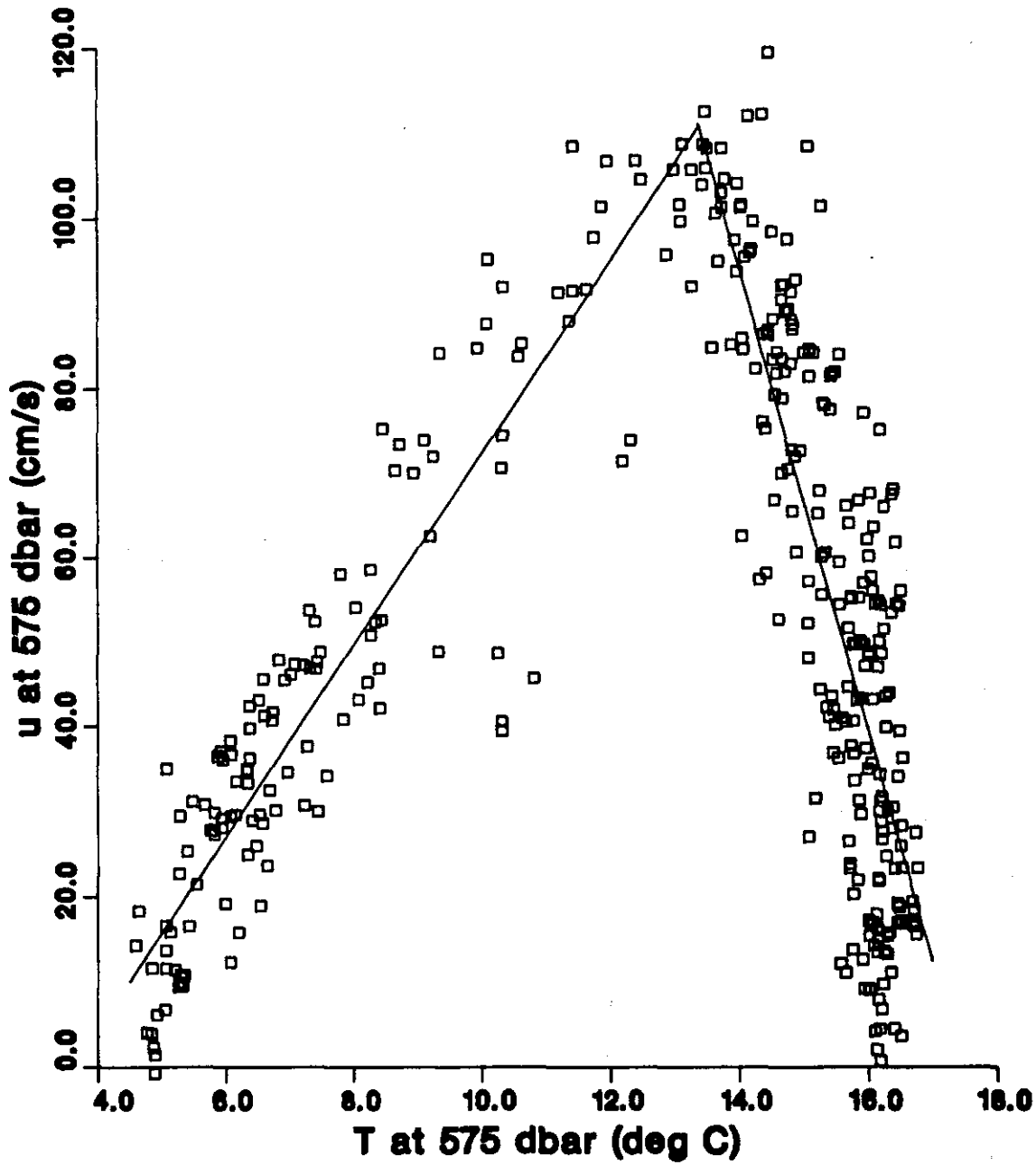
for $T_{\hat{y}}$, which are also shown. The exact forms for the two lines are

$$T < 13°C.: \quad \frac{\partial T}{\partial \hat{y}} = 0.08849\frac{°C.}{km} - 0.02438 \text{ km}^{-1}\text{x T} \quad (2\text{-}4a);$$

$$T > 13°C.: \quad \frac{\partial T}{\partial \hat{y}} = -1.0043\frac{°C.}{km} + 0.06025 \text{ km}^{-1}\text{x T} \quad (2\text{-}4b).$$

If $\hat{y} = 0$ for $T = 13°C$, (2-4 a,b) may be integrated in either direction
to obtain $T = T(\hat{y})$, and inverted to obtain $\hat{y} = \hat{y}(T_{575})$. The results
are:

$$T < 13°C.: \quad T = 3.6296°C. + 9.3704°C. \; e^{-.02438\hat{y}/km} \quad (2\text{-}5a)$$

$$\hat{y} = \frac{-km}{.02438} \ln\frac{.08849°C./km - .02438km^{-1}T}{-0.22845 \; °C/km} \quad (2\text{-}6a)$$

$$T > 13°C.: \quad T = 16.670°C. - 3.6695°C. \; e^{.06025\hat{y}/km} \quad (2\text{-}5b)$$

$$\hat{y} = \frac{km}{.06025} \ln(4.5427 - .27252(°C.)^{-1}T) \quad (2\text{-}6b)$$

It should be noted that at depths greater that 575 dbar, there is not
such a strong and clear dependence of the shear (and hence $T_{\hat{y}}$) on
temperature, making any other level less suitable for this procedure
than is the 575 dbar level.

The scatter plot of $\hat{u}_{575}$ (along-stream velocity at 575 dbar)
vs. T_{575} (Figure 2.4) again suggests that a linear least squares fit
is a reasonable description of the data-- note particularly the break
in functional form at $T \simeq 13°C$. The results of the linear fit are:

$T < 13°C.:$

$$\hat{u}_{575} = -40.951 \text{cm/s} + 11.332 \text{cm/s/°C.} \text{ x T} \quad (2\text{-}7a)$$

$T > 13°C.:$

$$\hat{u}_{575} = 479.35 \text{ cm/s} - 27.463 \text{cm/s/°C.} \text{ x T} \quad (2\text{-}7b).$$

Combining equations (2-5) with (2-7) gives $\hat{u} = \hat{u}(\hat{y})$:

$T_{575} < 13°C$:

$$\hat{u}(\hat{y}) = \hat{u}(\hat{y} = 0) - 106.19 \frac{cm}{s} (e^{-.02438 \, \hat{y}/km} - 1) \qquad (2\text{-}8a)$$

$$\frac{\partial \hat{u}}{\partial \hat{y}} = -.2589 \times 10^{-4} s^{-1} e^{-.02438 \, \hat{y}/km} \qquad (2\text{-}9a)$$

$T_{575} > 13°C$:

$$\hat{u}(\hat{y}) = \hat{u}(\hat{y} = 0) + 100.78 \frac{cm}{s} e^{.06025 \, \hat{y}/km} \qquad (2\text{-}8b)$$

$$\frac{\partial \hat{u}}{\partial \hat{y}} = .6071 \times 10^{-4} s^{-1} e^{.06025 \, \hat{y}/km} \qquad (2\text{-}9b)$$

Unfortunately, these descriptions yield discontinuities in both $\hat{u}$ and
$\partial\hat{u}/\partial\hat{y}$; however, they are used primarily for qualitative reasons and the
two regimes are often considered separately. An immediate observation
from these results is that the warm, anticyclonic side of the Stream is
actually sharper than the cold, cyclonic side in the sense

that $\left|\frac{\partial\hat{u}}{\partial\hat{y}}\right|_{T_{575}>13\ °C} > \left|\frac{\partial\hat{u}}{\partial\hat{y}}\right|_{T_{575}<13\ °C}$, in fact nearly three times as

sharp. This result contradicts the notion presented in Fofonoff and Hall
(1983) that the northern edge of the Stream, in analogy with the
two-layer inertial jet model, should exhibit a much more sudden jump in
velocity than the warm side. It may be that the structure proposed by
Fofonoff and Hall is found higher up in the water column. The North Wall
of the Gulf Stream, defined as the place where the 15°C isotherm is at
200 m depth (Fuglister, 1963) has long been used as an indicator of Gulf
Stream position, but clearly that is well above the depth range
detectable by the mooring. Analysis of the Pegasus sections at 73° W by

Halkin and Rossby (1985) shows that instantaneously as well as on average the horizontal velocity shear is much stronger on the cold than on the warm side in the upper few hundred meters; even at 600 m depth, though less pronounced, the same trend is definitely there. The velocity section constructed by Warren and Volkmann (1969), on the other hand, gives a general impression that $\partial\hat{u}/\partial\hat{y}$ is stronger on the cold side, but at 600 m depth the shear appears to be nearly symmetric about the maximum along-stream velocity at that depth. Thus, more information in the upper 500 m of the water column, taken concurrently with deeper information, will be required to resolve this question.

2.4.1 Horizontally integrated fluxes

In Hall and Bryden (1985), an average velocity profile of the Gulf Stream at the mooring site has been constructed, based on the assumption that the cross-stream temperature structure is constant (Figure 2.5). From the profile, an average transport value of 103 Sv can be calculated. However, it is also instructive to examine individually and compare the four events when the Gulf Stream swept by the mooring, for the differences in the events are illuminating.

Time may be used parametrically, with $\hat{u} = \hat{u}(t)$ and $\hat{y} = \hat{y}(T(t))$, to integrate streamwise fluxes horizontally as well as vertically. The primary difficulty in calculating integrated transports is defining the "edges" of the Stream. This has long been a troublesome problem. One example of the type of problem that can arise was discussed in Fofonoff and Hall's (1983) treatment of the Gulf Stream '60 data (Fuglister, 1963). The geostrophically calculated velocities at Section I exhibit
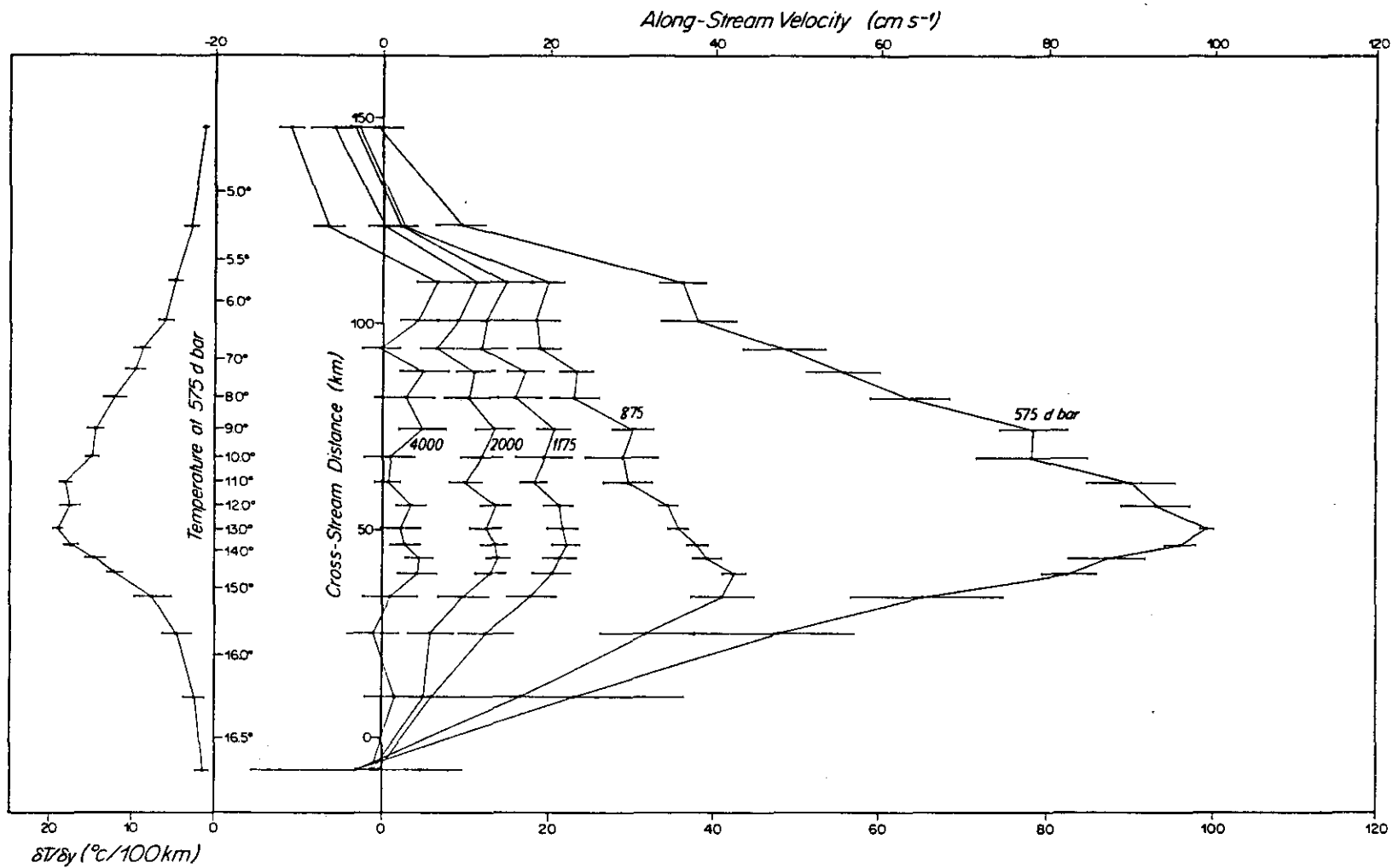
Figure 2.5. Average horizontal and vertical profile of velocity in Gulf
Stream, from year-long time series at 68°W. Details of how
profile was obtained in Hall and Bryden (1985).

closed circulations north and south of the main front: should the

contributions from these circulations be included in the transport One

way of delineating the edges is to look for the point at which either the

transport per unit width, or the velocity anywhere in the water column,

goes to zero. While that approach may be successful for the north edge,

velocities at the southern edge tend to decay very slowly. Moreover,

Schmitz(1980) has identified what is apparently a weakly depth-dependent

recirculation regime about 200-300 km south of the Gulf Stream axis at

55°W, and has suggested that it might be a recirculation increasing the

total Gulf Stream transport. In this analysis, the problem manifests

itself in that while the relationship between $\partial T/\partial \hat{y}$ and T is less tight

for temperatures far from the axis of the flow, so that a small change in

T_{575} leads to a large change in $\hat{y}$, velocities there may be too strong

to be excluded from the integration. It is best to approach each event

individually, with the restriction that only data in the temperature

range $5°C \leq T_{575} \leq 16.5°C$. are to be considered. Since none of the

passages spans this full range, temperature and/or velocity extrema are

used to define the integration limits for each event.

Since the data only extended upward as far as 575 dbar, and since

much of the transport is known to occur above that depth, some

extrapolation scheme was required to extend velocities to the surface.

Different schemes were tested on hydrographic data from Gulf Stream '60

at 68.5°W to determine which one best reproduced the actual shear in the

upper water column. If (u_4, P_4) are the measured along-stream

velocities and pressures at the 400 and 700 m instruments respectively, a

value of $u_1 = u_4 + 1/2 (u_4 - u_7)$ was assigned to the level $P_1 = 2P_4 -$

Dates of Event	Range of T_{575} (°C)	Width (km)	Axis Velocity (cm/s)	Mass Transport (10^6 m³/s)	Momentum Flux (10^9 N)	Kinetic Energy Flux (10^9 J/s)
Mar. 6, 1983– Mar. 25, 1983	16.017– 5.068	105.5	74.6	83.9	44.6	16.9
May 26, 1983– June 21, 1983	6.000– 16.442	102.6	119.5	115.5	75.7	35.3
Aug. 29, 1983– Sept. 8, 1983	15.892– 5.673	88.2	71.5	96.6	41.9	13.1
Sept. 11, 1983– Oct. 5, 1983	5.395– 16.386	109.7	99.5	111.0	62.3	27.3
Gulf Stream 60 Sect. 1	5.70– ?	111.1		98.2	89.4	60.7

Table 2-3. Summary of main features of four Gulf Stream passages across GUSTO mooring site, with values from Section 1 of the Gulf Stream 60 survey included for comparison. Axis velocity is the maximum velocity attained during an event. Other features are described in the text.

P_7 (linear extrapolation), and this value was considered to be constant to the surface. At the bottom, the velocity was assumed to decrease linearly from its value at 4000 m to zero at the bottom depth of 4688 m. The actual measured velocities and pressures were used since these are depth-integrations, not requiring standard levels.

Table 2-3 gives the pertinent information for the four events, which divide themselves more or less into two categories. In March and early September, T_{575} was decreasing, indicating that the translational cross-stream velocity of the flow was negative (southward-like); yet the average measured cross-stream velocities for those two events were positive (see Fig. 2.1c, bottom). In June and late September, translational velocities were positive, and so were the average measured cross-stream velocities. The maximum velocities at 575 db for the former two events are considerably lower than for the latter two (about 20-30 cm/s), yet mass transport is correspondingly lower only for the March event, if the narrower width of the early September passage is taken into account. A glance at Figure 2.1c shows that strong along-stream velocities at 4000 m in early September are responsible for the difference. The values in Table 2-3 are similar to other estimates near this same longitude. Fuglister (1963) used hydrographic data and an assumption of zero bottom velocity to calculate a Gulf Stream transport at 68.5°W of 136 x 10^6 m^3/s. Using velocity measurements from floats along with hydrographic data at 38°N, 69°W, Warren and Volkmann (1968) estimated a Gulf Stream transport there of 101 x 10^6 m^3/s, with an average bottom velocity of 1.5 cm/s in the same direction as the surface flow.

Integrated momentum and kinetic energy fluxes have also been calculated and are listed in Table 2-3. For comparison, values from Section I of Gulf Stream '60 (Fofonoff and Hall, 1983) are also presented. The June event most resembles the flow that was surveyed in Gulf Stream 60, in terms of total fluxes. The extrapolation scheme to the surface for the GUSTO data may be somewhat conservative, yet it is in the upper water that the greatest contributions to momentum and kinetic energy fluxes arise. That may explain why the mass transport is estimated reasonably well, while the momentum and kinetic energy transports seem to be underestimated. In conclusion, the transport values obtained here are reasonable for data from a single mooring, but it would have been helpful to have more information in the upper part of the water column.

2.4.2 Potential vorticity at 575 dbar

Ertel's theorem (see Pedlosky, 1979, for a good discussion) shows that water parcels conserve their potential vorticity in the absence of forcing, dissipation, and mixing, where potential vorticity q is defined as

$$q = \frac{(2\Omega + \omega_r) \cdot \nabla \lambda}{\rho} \tag{2-10}.$$

Here 2Ω is planetary vorticity; $\omega_r = \nabla \times u$ is relative vorticity; ρ is density; and λ is any conservative scalar property of the fluid. Taking λ to be potential temperature and ρ approximately constant yields:

$$q = (f + v_x - u_y)\theta_z + (h + u_z - w_x)T_y + (w_y - v_z)T_x$$

where $(f,h) = $ (vertical, horizontal) components of planetary vorticity.

Since terms are implicitly considered in the rotated frame, in the Gulf Stream, the following inequalities may be applied:

$$\hat{v}_{\hat{x}} \ll \hat{u}_{\hat{y}}; \quad T_{\hat{x}} \ll T_{\hat{y}}; \quad h \ll \hat{u}_z;$$
$$\hat{v}_z \ll \hat{u}_z; \quad w_{\hat{x}} \ll \hat{u}_z; \quad w_{\hat{y}} \ll \hat{v}_z$$

to get a good approximation of q as

$$q \simeq (f - \hat{u}_{\hat{y}})\theta_z + \hat{u}_z T_{\hat{y}} \simeq (f - \hat{u}_{\hat{y}})\theta_z - \frac{g\alpha_0}{\rho_0 f} T_{\hat{y}}^2$$

using thermal wind to evaluate $T_{\hat{y}}$. The analytic forms for all terms at 575 dbar as functions of $\hat{y}$ or T_{575} may be used to obtain a qualitative picture of the cross-stream potential vorticity structure at 575 dbar across the Gulf Stream. Notice that in quasi-geostrophic theory the term $-\hat{u}_{\hat{y}}T_z$ would be order Rossby number smaller than $f \times \theta_z$, while $\hat{u}_z T_{\hat{y}}$ would be order Rossby number squared smaller than $f\theta_z$. The latter would certainly be ignored in an estimate of q, and in areas of large scale flow, so is the former. Table 2-4 gives values of the various components across the Stream, estimated from the analytic forms for $\hat{u}_{\hat{y}}$, θ_z, and $T_{\hat{y}}$ at 575 dbar. Although $f\theta_z$ clearly dominates the q values, the remaining terms make important contributions near the Stream axis, where horizontal and vertical gradients are strongest. Other investigators (McDowell, Keffer and Rhines, 1982; McCartney, 1982) have pointed out that the relative vorticity contribution ought to be included in an evaluation of potential vorticity in the vicinity of strong boundary currents like the Gulf Stream. The results in Table 2-4 suggest that $\hat{u}_{\hat{y}}T_z$ and $\hat{u}_z T_{\hat{y}}$ ought to be retained when constructing a section of potential vorticity in the Gulf Stream (Chapter 4).

T_{575} (°C)	y (km)	$f_o T_z$ (10^{-6} °C/m/s)	$-u_y T_z$ (10^{-6} °C/m/s)	$u_z T_y$ (10^{-6} °C/m/s)	r_1	r_2
8.0	31.3	1.25	.17	-.12	.14	.10
10.0	15.8	1.65	.32	-.26	.19	.16
11.0	9.9	1.84	.42	-.35	.23	.19
12.0	4.6	2.03	.53	-.46	.26	.22
12.5	2.3	2.13	.59	-.51	.28	.24
12.9	0.4	2.20	.64	-.56	.29	.25
13.1	-0.5	2.07	-1.37	-.51	.66	.24
13.5	-2.4	1.95	-1.14	-.39	.58	.20
14.0	-5.3	1.82	-.90	-.28	.49	.15
14.5	-9.7	1.68	-.67	-.18	.40	.11

Table 2-4. Comparison of terms in total potential vorticity,

$$q = (f - \hat{u}_{\hat{y}})T_z + \hat{u}_z T_{\hat{y}} = (f - \hat{u}_{\hat{y}})T_z - \frac{g\alpha_o}{\rho_o f} T^2_{\hat{y}},$$ where terms have been evaluated from analytic

forms described in text; r_1 and r_2 are ratios of columns 4 to 3 and 5 to 3 respectively.

2.5 Governing equations in rotated coordinate system

Up to now, the notion of rotated velocities has been used only
mechanistically. The momentum equations for the rotated system are
actually quite complicated for this rotating system, even with the
assumption that the origins $(x,y) = (0,0)$ and $(\hat{x},\hat{y}) = (0,0)$ remain always
at the mooring site, which in turn implies that as the Stream rotates, it
always does so about an axis fixed at the site (Fig. 2.6). The change in
the Stream orientation from day to day is generally small, but away from
the origin the rotation leads to centrifugal terms which make this system
a questionable one for investigating dynamics away from the mooring site
(difficult with just one mooring in any case!). However, the rotation
has been used primarily to construct a picture of the Gulf Stream from a
number of snapshots taken at different angles. The momentum equations at
$x = y = \hat{x} = \hat{y} = 0$ are presented nonetheless. The transformations involve
terms like $\hat{u} = \hat{u}(\hat{x}(x,y,t),\hat{y}(x,y,t),t)$ whence:

$$\frac{\partial \hat{u}}{\partial t} = \frac{\partial}{\partial t}(u\cos\alpha + v\sin\alpha) + \frac{\partial}{\partial \hat{x}}(u\cos\alpha + v\sin\alpha)\frac{\partial \hat{x}}{\partial t} +$$

$$\frac{\partial}{\partial \hat{y}}(u\cos\alpha + v\sin\alpha)\frac{\partial \hat{y}}{\partial t} \qquad (2\text{-}11).$$

But $\partial\hat{x}/\partial t = (-x\sin\alpha + y\cos\alpha)\alpha_t = 0$ at $x = y = 0$, so that these terms do
not enter into the momentum equations at the site. The resulting
momentum equations (valid only at the site) are:

$$\hat{u}_t + \hat{u}\hat{u}_{\hat{x}} + \hat{v}\hat{u}_{\hat{y}} + w\hat{u}_z - (f + \alpha_t)\hat{v} = -P_{\hat{x}} \qquad (2\text{-}12a)$$

$$\hat{v}_t + \hat{u}\hat{v}_{\hat{x}} + \hat{v}\hat{v}_{\hat{y}} + w\hat{v}_z + (f + \alpha_t)\hat{u} = -P_{\hat{y}} \qquad (2\text{-}12b).$$

Thus, thinking in terms of rotated coordinates at the site adds only one

Figure 2.6. Schematic showing coordinate rotation and transformation definitions.

$$\hat{u} = u\cos\alpha + v\sin\alpha$$
$$\hat{v} = v\cos\alpha - u\sin\alpha$$
$$\hat{x} = x\cos\alpha + y\sin\alpha$$
$$\hat{y} = y\cos\alpha - x\sin\alpha$$
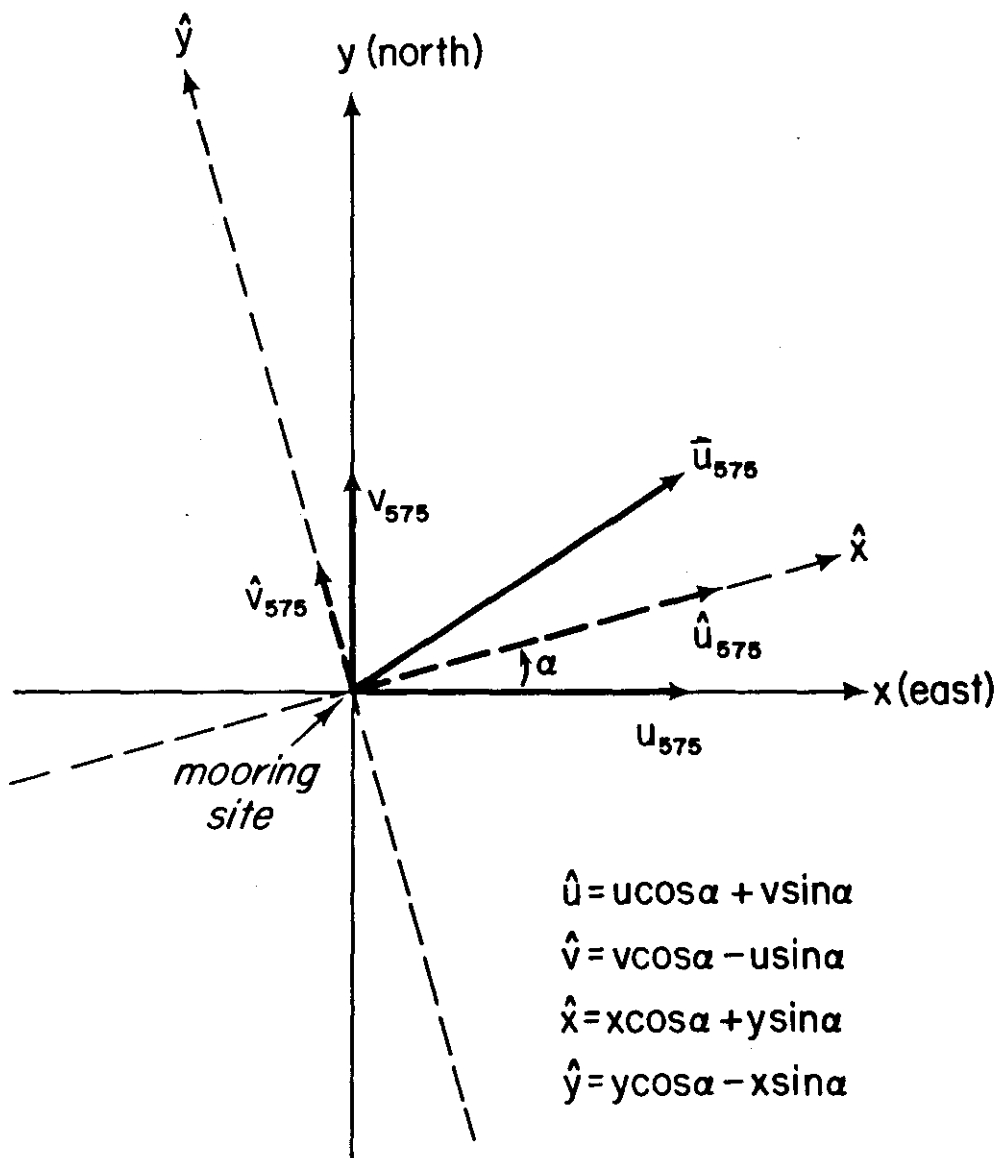
term to each equation, and $(\alpha_t/f) \leq 0.08$ during the whole time series. Notice also that possible curvature of the Stream path has been excluded essentially by taking $\alpha \neq \alpha(x,y)$.

The vorticity equation at the origin may be derived as follows: at the current meter site, the total derivative following a fluid parcel retains its form, i.e.,

$$\frac{\partial}{\partial t} + u \frac{\partial}{\partial x} + v \frac{\partial}{\partial y} = \frac{\partial}{\partial t} + \hat{u} \frac{\partial}{\partial \hat{x}} + \hat{v} \frac{\partial}{\partial \hat{y}} \qquad (2\text{-}13).$$

It is also true that $\zeta = v_x - u_y = \hat{v}_{\hat{x}} - \hat{u}_{\hat{y}}$. Thus, the vorticity equation

$$\left(\frac{\partial}{\partial t} + u \frac{\partial}{\partial x} + v \frac{\partial}{\partial y}\right)\left(\frac{\partial v}{\partial x} - \frac{\partial u}{\partial y}\right) + \beta v = f \frac{\partial w}{\partial z} \qquad (2\text{-}14a)$$

becomes

$$\left(\frac{\partial}{\partial t} + \hat{u} \frac{\partial}{\partial \hat{x}} + \hat{v} \frac{\partial}{\partial \hat{y}}\right)\left(\frac{\partial \hat{v}}{\partial \hat{x}} - \frac{\partial \hat{u}}{\partial \hat{y}}\right) + \beta v = f \frac{\partial w}{\partial z} \qquad (2\text{-}14b).$$

at the mooring site. In equation (2-14b) ζ can be approximated by $-\hat{u}_{\hat{y}}$, as noted before.

Finally, the equation for heat conservation, using standard notation, is:

$$\frac{\partial T}{\partial t} + u \frac{\partial T}{\partial x} + v \frac{\partial T}{\partial y} + w \frac{\partial \theta}{\partial z} = \text{RHS} \qquad (2\text{-}15)$$

where the RHS may include source and sink terms which will be assumed negligible. This equation assumes the same form in rotated coordinates, i.e., $T_t + \hat{u}T_{\hat{x}} + \hat{v}T_{\hat{y}} + w\theta_z = 0$.

With data from just one mooring, it is difficult to evaluate most of the terms in these equations, in order to determine what balances obtain. Certain attributes of the flow may be tested, however. It is a

straightforward matter to compare the local time derivatives with the Coriolis terms in the momentum equations to obtain some idea of the strength of geostrophic balance at the mooring site. That has been done for both the east/north and along/cross-stream velocities, by comparing the rms values of the local accelerations with those of the associated Coriolis accelerations, and assuming that the advective terms are of comparable magnitude to (or smaller than) the local accelerations. Table 2-5 shows the results for 575 and 875 dbar. There is little question that in either the north or cross-stream direction, geostrophic balance is quite strong. When data from the whole time series are used, the ratio r of the terms at 575 (875) dbar is .115 (.058) for the along-stream direction and .032 (.032) for the east momentum equation. When data from a single strong Gulf Stream event are used (the June event), r increases to .186 (.090) for along-stream and .057 (.058) for east; thus, using the geostrophic approximation to evaluate temperature gradients from velocity shear should introduce errors no larger than 20 percent.

2.5.1 Vertical velocities at the mooring site

Now consider the balance of terms in the heat conservation equation. Given that the geostrophic approximation is valid to within 20 percent at the mooring site, thermal wind yields:

$$\rho_0 f \frac{\partial \hat{u}}{\partial z} = g \frac{\partial \rho}{\partial \hat{y}} = -g \alpha_0 \frac{\partial T}{\partial \hat{y}} ; \qquad \rho_0 f \frac{\partial \hat{v}}{\partial z} = -g \frac{\partial \rho}{\partial \hat{x}} = g \alpha_0 \frac{\partial T}{\partial \hat{x}} \qquad (2\text{-}16).$$

The quantity α_0, defined before, can be evaluated from historical data and is approximately 10^{-4} gm/cm^3/°C, with variations of about 25

Depth	Direction	$(u_t)_{rms}$ (cm/s^2)	$(fv)_{rms}$	Ratio
575	East	6.98×10^{-5}	2.19×10^{-3}	.032
575	L-Stream	6.88×10^{-5}	5.99×10^{-4}	.115
875	East	3.90×10^{-5}	1.24×10^{-3}	.032
875	L-Stream	3.90×10^{-5}	6.70×10^{-4}	.058

Depth	Direction	$(v_t)_{rms}$ (cm/s^2)	$(fu)_{rms}$	Ratio
575	North	6.45×10^{-5}	4.84×10^{-3}	.013
575	X-Stream	2.15×10^{-5}	5.28×10^{-3}	.004
875	North	4.62×10^{-5}	2.42×10^{-3}	.019
875	X-Stream	3.67×10^{-5}	2.63×10^{-3}	.014

Table 2-5. Comparison of rms local and Coriolis accelerations for momentum equations in east/north and long/cross-stream coordinates, at 575 and 875 dbar, for year-long time series.

percent through the water column. Furthermore, if the velocities are expressed as $u = R \cos\phi$, $v = R \sin\phi$. where R is the speed and $\phi = \tan^{-1}(v/u)$ is the angle the velocity vector makes with east, the temperature equation (2-15) may be rewritten:

$$\frac{\partial T}{\partial t} + \frac{\rho_0 f}{g\alpha_0} R^2 \frac{\partial \phi}{\partial z} + w \frac{\partial \theta}{\partial z} = RHS.$$

Under an assumption of negligible mixing (i.e., RHS is small), vertical velocities may be calculated from

$$w = -(\frac{\partial T}{\partial t} + \frac{\rho_0 f}{g\alpha_0} R^2 \frac{\partial \phi}{\partial z})/(\frac{\partial \theta}{\partial z}) \qquad (2-17)$$

as originally pointed out by Bryden (1976). Equivalently,

$$w = -(T_t + \hat{u}T_{\hat{x}} + \hat{v}T_{\hat{y}})/\theta_z \quad (2-18).$$

If a balance between local time changes and horizontal advection is not achieved at the mooring site, then vertical velocities must exist. That is in fact the case for all depths on the mooring. At 575 dbar, $\hat{u}T_{\hat{x}}$ has generally small amplitude and is very noisy; also, T_t and $\hat{v}T_{\hat{y}}$ do not show any significant negative correlation, which would be the case if $T_t \sim -\hat{v}T_{\hat{y}}$. Although conventional scaling arguments (e.g., Pedlosky, 1979) suggest that $\hat{u}T_{\hat{x}} \sim \hat{v}T_{\hat{y}}$, the rms value of the latter at 575 dbar is about three times as great as that of the former, and the rms value of $\partial T/\partial t$ is about 2 1/2 times that of $\hat{u}T_{\hat{x}}$. These results suggested calculating w at 575 dbar from $w = -(T_t + \hat{v}T_{\hat{y}})/\theta_z$ while at 875, 1175, and 2000 dbar (2-17) was used.

To avoid introducing yet more noise by calculating θ_z from the recorded data, the analytic fits used in the temperature correction

schemes at 575, 875, and 1175 dbar were used. At 2000 dbar, a constant value of .0971 $^\circ$C./100m (determined from historical data) was used. At 575 dbar, $\partial T/\partial t$ was calculated from the corrected temperature time series at that level, $\hat{v}$ was also the corrected value, and $\partial\hat{u}/\partial z$ (used to obtain $T_{\hat{y}}$) was determined from the recorded velocity and pressure time series at 400 and 700 m. Similar schemes were used at the other depths:

$$875 \text{ dbar: } w = -\left(\frac{\partial T}{\partial t}\Big|_{875} + \frac{\rho_0 f}{g\alpha_0} R_{875}^2 \frac{\partial \phi}{\partial z} \right) / \theta_z$$

$$\frac{\partial \phi}{\partial z} = \frac{\phi_{700} - \phi_{1000}}{z_{700} - z_{1000}} \qquad \text{or} \qquad \frac{\partial \phi}{\partial z} = 2.4556 \frac{\phi_{700} - \phi_{2000}}{z_{700} - z_{2000}} ;$$

$$1175 \text{ dbar: } w = -\left(\frac{\partial T}{\partial t}\Big|_{1175} + \frac{\rho_0 f}{g\alpha_0} R_{1175}^2 \frac{\phi_{700} - \phi_{1000}}{z_{700} - z_{1000}} \right) / \theta_z ;$$

$$2000 \text{ dbar: } w = -\left(\frac{\partial T}{\partial t}\Big|_{2000} + \frac{\rho_0 f}{g\alpha_0} R_{2000}^2 \frac{\partial \phi}{\partial z} \right) / \theta_z$$

$$\frac{\partial \phi}{\partial z} = \frac{\phi_{1000} - \phi_{3000}}{z_{1000} - z_{3000}} \qquad \text{or} \qquad \frac{\partial \phi}{\partial z} = 1.0787 \frac{\phi_{700} - \phi_{3000}}{z_{700} - z_{3000}} .$$

The latter forms of ϕ_z are used when data from the 1000 m instrument is lacking, and they are based on a comparison of the time series of ϕ_z calculated in the two different ways. In the calculations for 2000 m, ϕ_{3000} is the direction of the velocity linearly interpolated between 2000 and 4000 m. At 4000 m, there is a lack of vertical information to compute w using the temperature equation; however, since this current meter was only 688 m off the bottom, a fair idea of the deep vertical velocities may be obtained by calculating $w_{4000} = \vec{u} \cdot \nabla h$, where ∇h is the slope of the bottom topography. At the time of mooring recovery, a

Depth (db)	$\bar{w}$ (10^{-3} cm/s)	w_{rms} (10^{-3} cm/s)
575	-4.38	54.66
875	3.50	83.86
1175	3.45	56.15
2000	-6.73	44.24
4000	-.90	29.32

$\overline{w'_i w'_j}$ 10^{-} cm^2/s $c\, w_i\, w_j$	w_{575}	w_{875}	w_{1175}	w_{2000}	w_{4000}
		3347.3	2193.2	1926.1	1107.2
w_{575}		.730	.735	.797	.691
			2940.6	2514.3	1273.4
w_{875}			.624	.678	.518
				1589.2	1156.3
w_{1175}				.640	.702
					1012.6
w_{2000}					.781

Table 2-6, Top: Record-length mean and rms velocities for vertical velocities calculated as described in text. Value at 1175 db is based on 240 days of data, the rest on 360 days. Bottom: Cross-products of different vertical velocity pairs, and their correlation co-efficients,

$$C_{w_i w_j} = \frac{\overline{w'_i w'_j}}{\sqrt{(w'^2_i \, w'^2_j)}} \, .$$

bathymetric survey was conducted about the mooring site; the survey indicated a slope of about 4 x 10^{-3}, with alongslope directed along 70°. true. It should be emphasized that the calculation of deep vertical velocity is absolutely independent of all those calculations made higher in the water column.

The resulting time-series of w at the five depths are displayed in Fig. 2.7, after being smoothed with a five-day running mean (except at 4000 m, where the time-series was already fairly smooth). The vertical velocities exhibit good visual coherence throughout the water column, and calculating correlation coefficients for pairs of series bears out what is evident from the plots, that vertical velocities are indeed well correlated throughout the water column. Table 2-6 lists the correlation coefficients, all of which are significant at the 95 percent confidence level for an estimated 30 degrees of freedom. Table 2-6 also shows the mean and rms values of w at the five levels. The mean values of the vertical velocities are very small, an order of magnitude smaller than the rms values, and probably not significantly different from zero. The maximum rms amplitude is attained mid-depth, at 875 db; a close look at the time series reveal that instantaneously w_{max} occurs at thermocline levels, which vary from 875 dbar on the warm side of the Stream to 575 dbar on the cold side. The monotonic decay above and below the thermocline maximum appears in the first EOF for the vertical structure of vertical velocity, which contains 81.9 percent of the variance and looks like the vertical velocity structure associated with the first baroclinic mode (Fig. 2.8). This result, taken with the neat decoupling

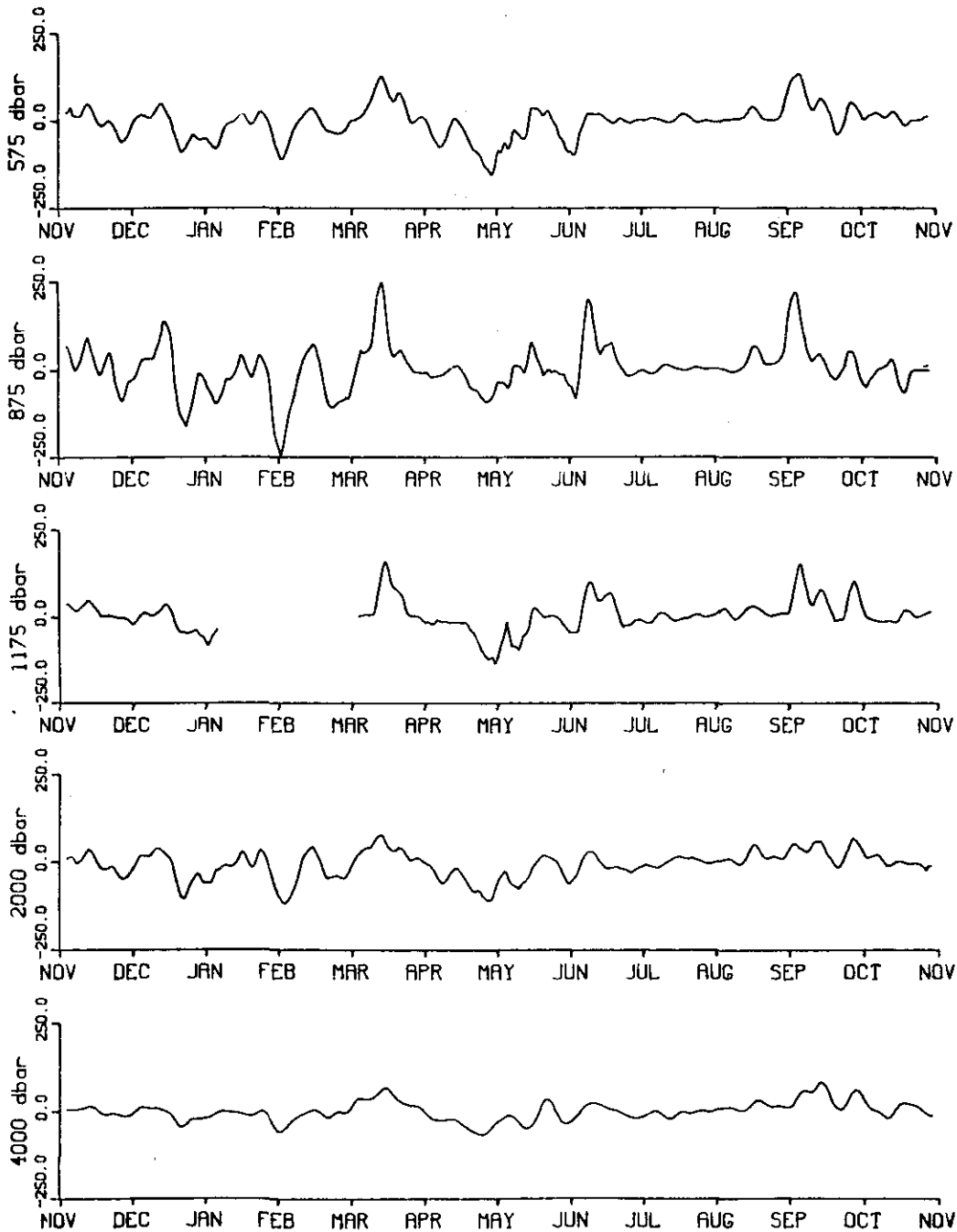Figure 2.7. Vertical velocities at designated levels, calculated as described in text. From top to bottom are vertical velocities at 575, 875, 1175, 2000, and 4000 dbar. Units are 10^{-3} cm/s.

Figure 2.8. Vertical structure of the first EOF calculated for vertical

velocity from complete (360-day) records at 4 depths. The

dashed line goes to w = 0 at the surface, which is the boundary

condition there.
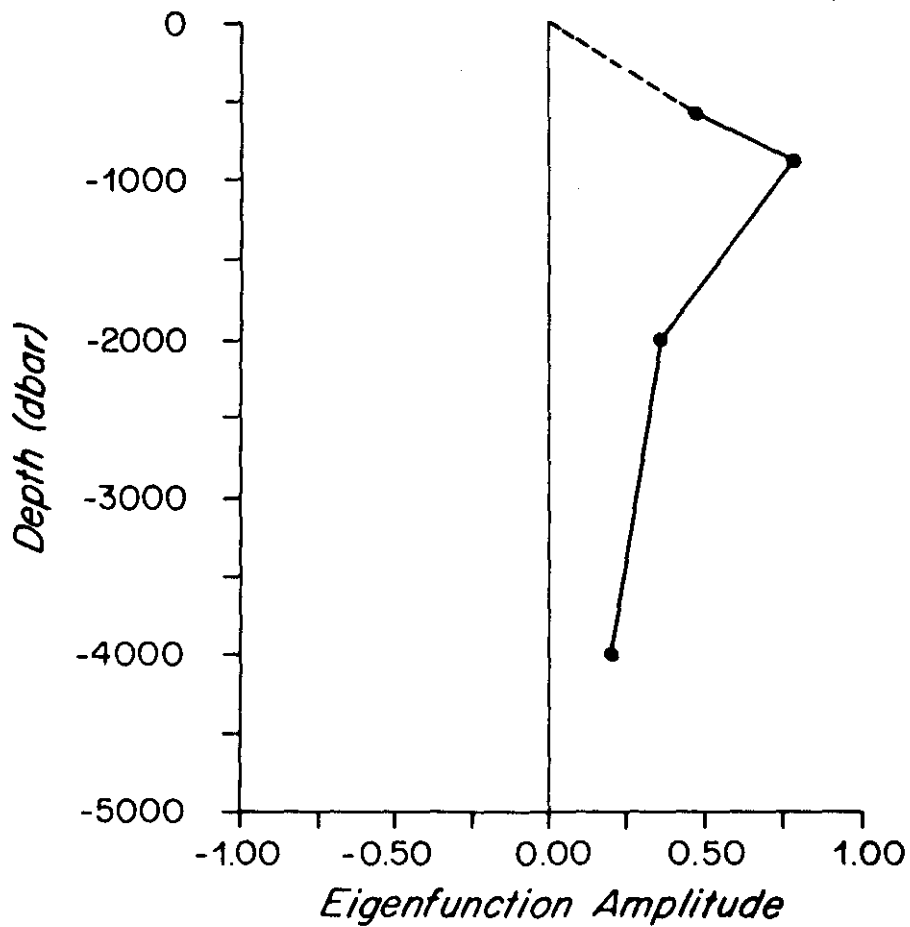
of horizontal velocities into just two modes, suggests that a two-layer
model (which reproduces a barotropic and baroclinic mode) can adequately
describe the data.

2.5.2 Vorticity balances at the mooring site

A discussion of the vorticity equation is limited by the lack of
horizontal resolution afforded by a single current meter, due to the
multiple derivatives involved, for example, in the advective terms.
However, some general features should be recognized before trying to
determine the primary balances: 1) the bottom slope, with a value of
about 4×10^{-3}, produces a β-effect of $f_0 |\nabla h|/H = (0.89 \times 10^{-4} \text{ s}^{-1})$
$\times (4 \times 10^{-3})/4000 \text{ m} = 9 \times 10^{-11} \text{m}^{-1}\text{s}^{-1})$, 4 to 5 times the planetary
β-effect; 2) on the anticyclonic side of the Stream, the analytic form
for $\hat{u}$ gives a maximum velocity curvature at 575 db of $(\hat{u}_{\hat{y}\hat{y}})_{max} =$
$3.60 \times 10^{-9} \text{ m}^{-1}\text{s}^{-1}$, two orders of magnitude greater than β, and $\beta - \hat{u}_{\hat{y}\hat{y}} < 0$
from the axis to some 87 km south of the axis; and 3) calculating fw_z
from the time series of w at various depths turns out to be fairly noisy;
but rough estimates show that it is generally an order of magnitude
larger than βv. Suppose, for example, there is a change in w of 50 $\times$
10^{-3} cm/s from 875 dbar to 4000 dbar. The v required to balance fw_z
is then

$$v = \frac{f \, \partial w/\partial z}{\beta} \simeq \frac{(0.8892 \times 10^{-4})(50 \times 10^{-3})}{3125 \times 1.9 \times 10^{-11}} \text{ cm/s} = 75 \text{ cm/s},$$

which is greater than the maximum value of v in that part of the water
column by a factor of about three. Moreover, the above is a conservative
estimate of $f \, w_z$.

Although these two terms, the only two in (2-14b) that are straightforward to evaluate, are consistently of different magnitude, they are nevertheless correlated strongly enough to suggest that there is an important dynamical connection between them. There is even a stronger correlation between v and w at any particular depth than between v and w_z, a result that may be interpreted in two ways. If the system is indeed behaving as the first baroclinic mode suggested by Figure 2.8, then w and w_z should display the same behavior in time, but w_z is in general a much noisier term-- hence the higher correlation between v and w. The second interpretation depends on water parcels conserving their temperature: to the extent that

$$w \sim \frac{-vT_y}{T_z} \quad \text{and} \quad \frac{T_y}{T_z} \sim \text{constant},$$

w and v ought to be correlated. This notion is elaborated on in Chapter 5.

The analytic values for terms like $\hat{u}_{\hat{y}\hat{y}}$ have been used to make daily estimates of $\hat{u}_{\hat{y}t}$ and $\hat{v}\hat{u}_{\hat{y}\hat{y}}$; however, the results are very noisy, and no systematic balances emerge from these calculations. It may be fairly concluded that data from the mooring alone is inadequate to make a complete dynamical investigation. The curvature of the Stream may be important to the vorticity balance, as suggested by the satellite composites for the year.

2.6 Discussion of quasi-geostrophic approximation

In quasi-geostrophic theory, the Rossby number ε is defined as U/fL (where U is a velocity scale and L a horizontal length scale), a measure

of the strength of advection relative to the Coriolis terms in the
momentum equations, or of relative to planetary vorticity. For a
strongly non-isotropic flow like the Gulf Stream, there will be a
different estimate for each momentum equation: for the long-stream
direction $\varepsilon_x \sim U/fL_y$ and for the cross-stream $\varepsilon_y \sim V/fL_x$. If $U \gg V$ and
$L_x \gg L_y$, clearly $\varepsilon_x \gg \varepsilon_y$. As long as $\varepsilon_x \ll 1$, however,
quasi-geostrophic theory still applies, and variables can be expanded in
a power series of ε_x. In what follows, all estimates are implicitly of
ε_x, since what is important is the upper bound on the Rossby number.
The subscript x is dropped for convenience. The Rossby number crops up
repeatedly as a limit on the relative size of other flow attributes, such
as vertical velocities or isotherm slopes. From the data and analytic
fits, it is possible to estimate the Rossby number from these other
quantities as well as from the original definition. When the mooring is
in the Gulf Stream, velocities range well over 100 cm/s at 575 dbar (see
Fig. 2.1c); the scale of cross-stream variation is about 50 km, from the
fits (2-7a,b). Thus, the definition $\varepsilon = U/fL_y$ gives

$$\varepsilon \sim \frac{100 \text{ cm/s}}{.89 \times 10^{-4} \text{s}^{-1} \times 50 \text{ km}} = .22.$$

It was pointed out in Section 2.4.2 that:

$$\frac{-\hat{u}_y \theta_z}{f\theta_z} = O(\varepsilon); \qquad \frac{\hat{u}_z T_{\hat{y}}}{f\theta_z} = O(\varepsilon^2).$$

Using the analytic forms only, it was found that (Table 2-4)

$$\left.\frac{-\hat{u}_{\hat{y}}}{f}\right|_{max} \sim -.60; \qquad \left.\frac{\hat{u}_z T_{\hat{y}}}{f\theta_z}\right|_{max} \sim -.25$$

where the values of ϵ fall off rapidly away from the Stream axis. These estimates are probably unrealistically large. One e-folding distance south of the maximum in $-\hat{u}_y$, (2-9c) gives $\hat{u}_y/f \sim .24$, more in line with the above estimate. The average velocity section constructed from the data may be used to estimate a maximum ratio for $-\hat{u}_y/f$ of 0.31.

When the vertical velocity calculations were presented, no mention was made of their absolute magnitude; but anyone familiar with estimates of w for other flow regimes might be uncomfortable with rms magnitudes of 0.05 cm/s (although Johns and Watts (1985) recently estimated similar values of vertical velocity in the Gulf Stream 100-200 km northeast of Cape Hatteras). Consider a scale analysis of the continuity equation. With (U,L_x), (V,L_y) denoting long- and cross-stream (velocity, length) scales, and (W,H) the corresponding vertical scales, then according to quasigeostrophic theory,

$$\frac{U}{L_x} \sim \frac{V}{L_y}, \quad \frac{W}{H} \sim \epsilon \left(\frac{U}{L_x}, \frac{V}{L_y} \right) \tag{2-19}.$$

so that the horizontal velocity can remain nondivergent to lowest order in ϵ. For the Gulf Stream, typical scales are U = 100 cm/s, V = 5 cm/s, L_x = 1000 km, L_y = 50 km, H = 1 km, and w = 5×10^{-2} cm/s. Then $\epsilon \sim$ $WL_x/UH \sim WL_y/VH = (0.05 \text{ cm/s})(100 \text{ km})/(10 \text{cm/s})(1 \text{ km}) = 0.5$. This estimate is essentially an indication of the strong isotherm slopes in the Gulf Stream. Quasi-geostrophic scaling of the temperature equation, assuming local time derivatives do not dominate, gives:

$$\left. \frac{\partial z}{\partial y} \right|_T \sim \frac{\partial T/\partial \hat{y}}{\partial \theta/\partial z} \sim \frac{w}{\hat{v}} \sim \frac{\epsilon VH/L_y}{V} = \frac{\epsilon H}{L_y}. \quad \text{In these relations, H is}$$

meant to be the vertical scale of variation, e.g., for the horizontal velocities. Quasi-geostrophy requires that an isotherm not vary its depth an O(1) amount within the length scales under consideration. However, an inspection of historical hydrographic sections shows that

$$\frac{\partial z}{\partial y}\bigg|_T \sim 10^{-2},$$

while with $H = 1$ km, and $L_y = 50$ km, $\epsilon \sim 0.5$, just the same estimate as that associated with vertical velocities.

Most of the above Rossby number estimates apply only to the flow at 575 dbar, that is, the thermocline Gulf Stream, and exclusive of the estimates depending on the strong isotherm slopes, they do not exceed values of .3. Deeper in the water column, similar estimates yield substantially lower Rossby numbers -- all, that is, except for those derived from the vertical velocities, which are substantial throughout the water column (see Table 2-6). Below the 575 dbar level, thermal wind balance holds to within 10 percent in both the along- and cross-stream directions. At 575 dbar, using the geostrophic approximation probably introduces errors of about 20-30 percent, and certainly the errors would increase at still shallower levels. Moreover, a Rossby number of 0.3 suggests that a quasi-geostrophic dynamical model may be inadequate for explaining the time-evolution of the Gulf Stream.

Chapter 3. A diagnostic investigation of energy budgets in a numerical model

3.1 Introduction

An obvious feature of the Gulf Stream as it flows eastward into the North Atlantic is its eventual weakening: mass transport decreases, and mean and eddy energies fall off from their strong maxima farther to the west. The mechanisms behind this weakening are not thoroughly understood, but radiating instabilities, topographic features, and conversions of mean kinetic to potential energy are all likely candidates. Fofonoff and Hall (1983) have documented downstream changes in mass, momentum, and kinetic energy fluxes as evaluated from hydrographic data spanning sixteen degrees of longitude, or roughly 1500 km. While mass transport decreases to the east only mildly over the survey, kinetic energy flux falls from its maximum at the westernmost section to ten percent of that value at the easternmost. Dewar and Bane (1984) have estimated a corresponding acceleration of the Stream in the South Atlantic Bight. Such dramatic change in the overall structure of this strong current has implications for the energetics throughout the subtropical gyre.

Different approaches have been taken in examining this problem. Talley (1982) discussed the possible radiation of energy by barotropic, baroclinic and mixed instabilities for a number of configurations (meant to approximate a Gulf Stream-like current) in a linear, two layer, unbounded model. A number of observational studies (Hansen, 1970; Halliwell and Mooers, 1983; Watts and Johns, 1983) have sought to document the predominant time and space scales of fluctuations in various parts of the Gulf Stream, but such studies do not establish the dynamic reason for the

existence of the fluctuations. Bryden (1979) and Wright (1981) have addressed analogous questions in the Antarctic Circumpolar Current by modelling the flow as strictly zonal and confined to a zonal channel, then investigating the normal mode linear instabilities that can arise. Haidvogel and Holland (1978) have used a similar model on both instantaneous and mean profiles of the jet from a two-layer quasi-geostrophic numerical model, and related the results to observed scales of variability in the model. Johns (1985) recently used a linear baroclinic instability model successfully to predict time and space scales of fluctuations 100-200 km northeast of Cape Hatteras, where linear theory might still be expected to apply. Pedlosky (1970, 1982) has investigated the effects of allowing the instabilities to attain finite (but still small) amplitude.

There are philosophical as well as technical problems in extending such investigations to the Gulf Stream where it becomes a free eastward-flowing current. Observations have long suggested that the Gulf Stream is strongly non-linear, so that Pedlosky's weakly nonlinear theory has dubious application. Furthermore, while channel models may be geometrically realistic for the Antarctic Circumpolar Current, the Gulf Stream is certainly not confined to a channel but is free to meander north and south. While observations serve to describe the fluctuations, they can do little to explain them: because a wave radiates energy primarily through correlations of velocity and pressure, one would like to measure these properties to evaluate the radiation. However, for the energy budget of an enclosed area, it is the divergence of the horizontal pressure work

that contributes, and in a prominently geostrophic regime, this quantity is degenerate at lowest order. Measurement techniques are not yet refined enough to give reliable estimates of correlations between pressure and small, ageostrophic velocities.

On the other hand, numerical eddy-resolving general circulation models (EGCM's) can provide not only the degree of non-linearity actually observed in the ocean, but also time-series of "data" as extensive and detailed in space and time as desired. W. R. Holland of NCAR has created several "generations" of quasi-geostrophic EGCM's, and has recently reviewed (Holland, 1984) the successes and compromises involved in comparing such models to the real ocean. In all the models, there is a strong western boundary current that turns eastward at some latitude to become either a northern boundary current (in some single-gyre models) or a free jet flowing into the interior of the basin. In a number of early models, the free jet did not penetrate realistically far into the model basin before dying out completely. Holland and Schmitz (1984) discuss the factors controlling the penetration scale, based on a study of many two-, three-, and eight-layer models. They find that the strength of friction and topography, as well as the vertical resolution of the model, affect the penetration scale.

The model chosen for analysis here was recommended by Holland (personal communication) as being the most realistic model for such an investigation, and is referred to by Holland as 3L-4; its features are summarized in Table 3-1. Figure 3.1 shows the time-mean streamfunction in each layer. The free jet penetrates about halfway across the 4000 km

Layer depths: H_1 = 300 m

H_2 = 700 m

H_3 = 4000 m

Interfaces: $g'_{3/2}$ = .0357 m s^{-2}

$g'_{5/2}$ = .0162 m s^{-2}

Rotation: f = 9.3 x 10^{-5} s^{-1}

β = 2 x 10^{-11} m^{-1}s^{-1}

Wind stress: τ_0 = 0.1 N/m^2

$\tau = -\tau_0 \cos\left(\frac{2\pi y}{4000 \text{ km}}\right)$,   0 $\leq$ y $\leq$ 4000 km

Friction: lateral: biharmonic, A = 8 x 10^9 m^{-4}s^{-2}

bottom: linear, γ = 1 x 10^{-7} s^{-1}

Horizontal dimensions: 4000 km x 4000 km

Table 3-1. Summary of features of Holland numerical model 3L-4.

Figure 3.1. Mean streamfunction for Holland numerical model 3L-4:
a)layer 1; contour from -1.5×10^5 to 1.5×10^5 m^2/s; CI $= 10^4$ m^2/s; b)layer
2: contour from -5.4×10^4 to 5.4×10^4 m^2/s; CI $= 6 \times 10^3$ m^2/s; c)layer 3:
contour from -1.8×10^4 to 1.8×10^4 m^2/s; CI $= 2 \times 10^3$ m^2/s.
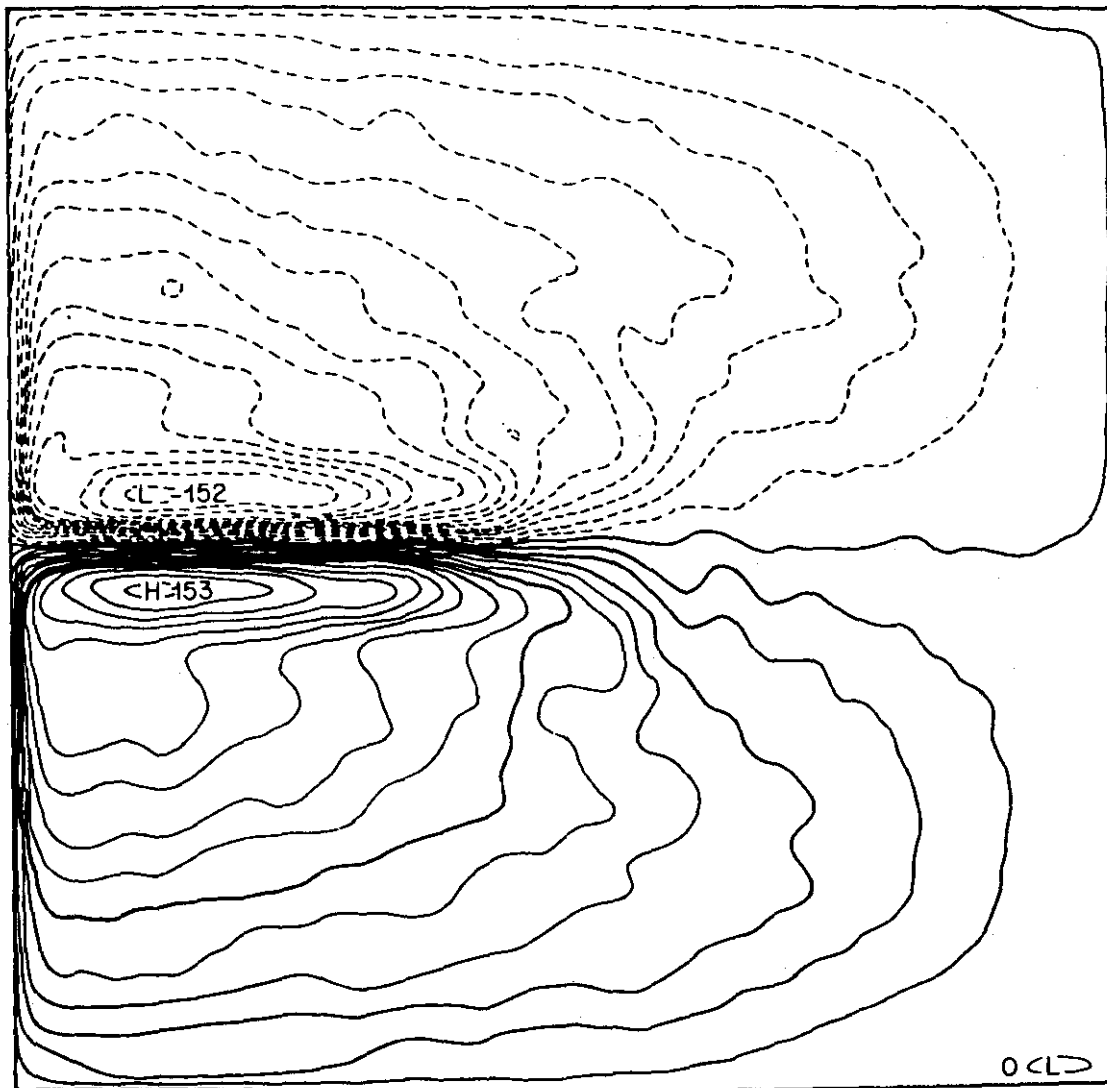
Figure 3.1b
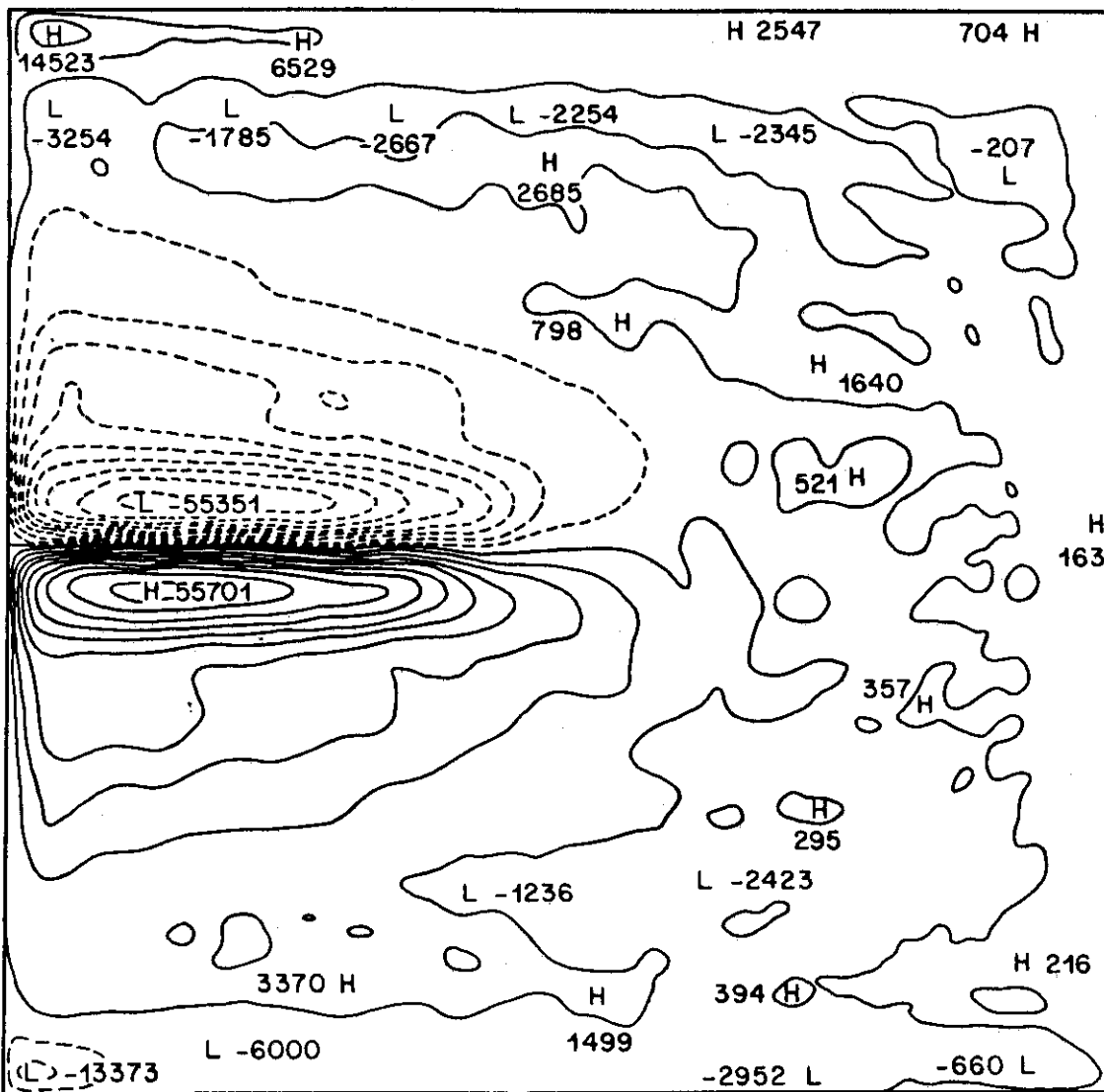
Figure 3.1c
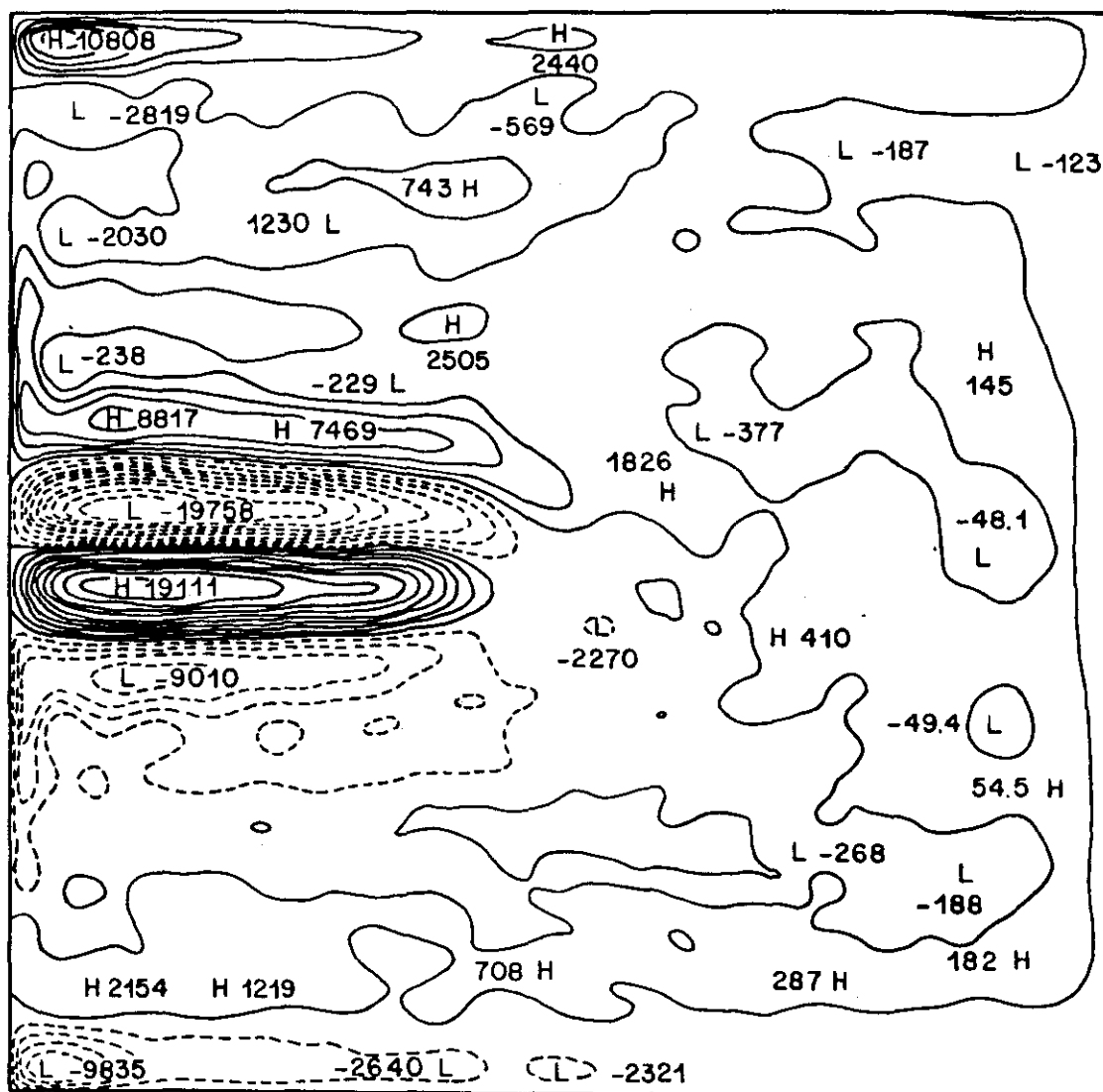
square basin. Three layers appear to be sufficient for capturing the proper degree of non-linearity in the free jet; moreover, in a three-layer as opposed to the two-layer models, there is a layer shielded from both surface and bottom effects, which displays vast regions of homogenized potential vorticity. Since such regions are predicted by theory (Rhines and Young, 1982) and found observationally (McDowell et al., 1982), it seems important to work with a model reproducing this feature. On the other hand, adding still more layers appears to do little more than enrich the vertical resolution of structures already observed in three-layer models.

In the remainder of the chapter, first the equations for mean and eddy kinetic energy are derived for a three-layer quasi-geostrophic system, starting either with the momentum equations or the potential vorticity equation. Next the calculations from the numerical data are described briefly. Finally, the results are presented, in which essentially six different energetic regions are identified and described.

3.2 Equations

In formally deriving the equations governing a quasi-geostrophic flow regime, it is useful to scale the dimensions out of most of the variables; then one or more nondimensional parameters govern the relative importance of terms in any equation, and consistency is achieved without confusion. However, when evaluating terms of an equation from a data set, it is less awkward and physically more intuitive to work with a dimensional set of equations, applying the results of quasi-geostrophic theory directly.

Thus, in this text, such results will be cited frequently without rigorous derivation; anyone unfamiliar with quasi-geostrophic theory is referred to Pedlosky (1979). Notation is kept as much as possible like Holland's (1984) notation, but in addition, expansion of variables in terms of a small parameter -- usually the Rossby number ε -- will be allowed for. Then subscripts refer to layers, superscripts to the order of a variable in its Rossby number expansion. Table 3-2 gives other notation and conventions.

In a three-layer system, there are five variables to solve for, u, v, w, p, and h; the governing equations are as follows:

a) In each layer, there are two horizontal momentum equations and a continuity equation:

$$\varepsilon(\frac{\partial u_k}{\partial t} + u_k \frac{\partial u_k}{\partial x} + v_k \frac{\partial u_k}{\partial y}) - fv_k = \frac{-1}{\rho_0} \frac{\partial p_k}{\partial x} + \delta(k-1) \frac{\varepsilon \tau^x}{\rho_0 H_k} - \delta(k-3)\varepsilon\gamma u_k - A\varepsilon\nabla^4 u_k \tag{3-1a}$$

$$\varepsilon(\frac{\partial v_k}{\partial t} + u_k \frac{\partial v_k}{\partial x} + v_k \frac{\partial v_k}{\partial y}) + fu_k = -\frac{1}{\rho_0} \frac{\partial p_k}{\partial y} - \delta(k-3)\varepsilon\gamma v_k - A\varepsilon\nabla^4 v_k \tag{3-1b}$$

$$\frac{\partial u_k}{\partial x} + \frac{\partial v_k}{\partial y} = \frac{-\partial w_k}{\partial z} = \frac{w_{k+1/2} - w_{k-1/2}}{H_k} \qquad k = 1, 2, 3 \tag{3-1c}$$

b) At each interface, a "thermodynamic" equation for evaluating w, and a relation between interface height and pressure:

$$w_{k+1/2} = \frac{\partial h_{k+1/2}}{\partial t} + u_{k+1/2} \frac{\partial h_{k+1/2}}{\partial x} + v_{k+1/2} \frac{\partial h_{k+1/2}}{\partial y} \tag{3-1d}$$

$$h_{k+1/2} = \frac{1}{\rho_0 g'_{k+1/2}} (p_{k+1} - p_k) \qquad k = 1, 2 \tag{3-1e}$$

(x,y)	$=$ (east, north) coordinates
(u_k, v_k)	$=$ (east, north) velocity in layer k
$h_{k+\frac{1}{2}}$	$=$ deviation of interface between layers k, $k+1$ from rest state; $h > 0$ for upward displacement
H_k	$=$ (constant) thickness of layer k in rest state
$W_{k+\frac{1}{2}}$	$=$ vertical velocity of interface $h_{k+\frac{1}{2}}$
ρ_o	$=$ basic density of fluid
ρ_k	$=$ actual density of fluid in layer k
$\Delta\rho_{k+\frac{1}{2}}$	$= \rho_{k+1} - \rho_k$
p_k	$=$ deviation of pressure from basic state, where basic state is in hydrostatic balance
$g'_{k+\frac{1}{2}}$	$= \dfrac{g\Delta\rho_{k+\frac{1}{2}}}{\rho_o}$, $g = 9.81$ m/s^2
γ	$=$ linear (bottom) friction coefficient
A	$=$ biharmonic (lateral) friction coefficient
K_k	$= KE_k =$ kinetic energy in layer k
K'_k	$= \frac{1}{2} H_k (u_k'^2 + v_k'^2)$
$\overline{K'_k}$	$= \frac{1}{2} H_k (\overline{u_k'^2} + \overline{v_k'^2})$
$\overline{K}_k$	$= \frac{1}{2} H_k (\overline{u}_k^2 + \overline{v}_k^2)$
P	$=$ available potential energy
EKE	$=$ eddy kinetic energy
MKE	$=$ mean kinetic energy
RHS	$=$ right hand side
LHS	$=$ left hand side

Table 3-2. Definitions for noatation used in Chapter 3.

Boundary conditions at top and bottom are that $w = 0$ there. The Kronecker delta function is used to include forcing and dissipation occurring only in particular layers. Wind stress and bottom friction act as body forces on a layer. Each variable will be expanded in terms of the Rossby number ε, which must be $<< 1$ for quasi-geostrophic theory to be valid.* Then, for example,

$$u_k = u_k^{(o)} + u_k^{(1)}\varepsilon + u_k^{(2)}\varepsilon^2 + \ldots$$ Rarely will more than two terms of any expansion be required here.

In a quasi-geostrophic regime, the flow field is horizontally non-divergent at lowest order so that a streamfunction ψ_k can be introduced -- in fact, $\psi_k = \dfrac{p_k}{\rho_0 f_0}$, and

$$u_k = \frac{-\partial \psi_k}{\partial y}, \quad v_k = \frac{\partial \psi_k}{\partial x}, \quad h_{k+1/2} = \frac{f_0}{g_{k+1/2}} (\psi_{k+1} - \psi_k) \tag{3-2}$$

Inserting the ε-expansion for each variable, cross-differentiating (3-1a,b), substituting from (3-1d) and (3-2), and retaining only lowest order quantities, one can derive a vorticity equation:

$$\frac{\partial}{\partial t} \nabla^2 \psi_k + J(\psi_k, f + \nabla^2 \psi_k) = \frac{f_0}{H_k} (w_{k-1/2} - w_{k+1/2})$$

$$- \delta(k-1) \frac{\rho_0}{H_k} \frac{\partial \tau^x}{\partial y} - \delta(k-3) \gamma \nabla^2 \psi_k - A \nabla^6 \psi_k \tag{3-3}$$

which may be further rearranged using (3-1) and (3-2) to obtain the potential vorticity equation as given in Holland and Schmitz (1984):

---

* It is also required that forcing and dissipation not enter the lowest order momentum balances (3-1a,b).

$$\frac{dQ_k}{dt} = T_k + F_k, \quad Q_k = \nabla^2 \psi_k + f_0 + \beta y + \frac{f_0}{H_k}(h_{k+1/2} - h_{k-1/2}) \tag{3-4}$$

and

$$\frac{d}{dt} = \frac{\partial}{\partial t} + J(\psi_k, \quad). \quad \text{Here, of course,} \quad T_k = -\delta(k-1)\frac{1}{\rho_0 H_k}\frac{\partial \tau^x}{\partial y},$$

while $F_k = -\delta(k-3) \gamma \nabla^2 \psi_k - A\nabla^6 \psi_k$.

Now consider the derivation of energy equations. Of primary interest here is the kinetic energy, which to lowest order is just

$$KE_k = \frac{1}{2} H_k \left| \nabla \psi_k \right|^2 = H_k \frac{(u_k^{(0)2} + v_k^{(0)2})}{2}$$

since at this order the vertical velocity makes no contribution. Although in the end the equations are integrated over depth, separate equations for each layer are derived first to show how energy is exchanged vertically between layers. An energy equation for each layer is obtained by multiplying (3-4) by $-\psi_k H_k$, then rearranging terms to obtain:

$$\frac{\partial}{\partial t}\frac{H_1}{2}(\psi_{1x}^2 + \psi_{1y}^2) - f_0\psi_1 \frac{\partial h_{3/2}}{\partial t} - H_1\frac{\partial}{\partial x}\left\{\frac{1}{2}\beta\psi_1^2 + u_1\psi_1(\nabla^2\psi_1 + \frac{f_0}{H_1}h_{3/2}) + \psi_1\psi_{1xt}\right\}$$

$$-H_1\frac{\partial}{\partial y}\left\{v_1\psi_1(\nabla^2\psi_1 + \frac{f_0}{H_1}h_{3/2}) + \psi_1\psi_{1yt}\right\} = -\frac{\psi_1}{\rho_0}\frac{\partial \tau^x}{\partial y} - AH_1\psi_1\nabla^6\psi_1 \tag{3-5a}$$

$$\frac{\partial}{\partial t}\frac{H_2}{2}(\psi_{2x}^2 + \psi_{2y}^2) - f_0\psi_2\frac{\partial}{\partial t}(h_{5/2} - h_{3/2}) - H_2\frac{\partial}{\partial x}\left\{\frac{1}{2}\beta\psi_2^2 + u_2\psi_2(\nabla^2\psi_2 + \frac{f_0}{H_2}(h_{5/2} - h_{3/2}))\right.$$

$$\left. + \psi_2\psi_{2xt}\right\} - H_2\frac{\partial}{\partial y}\left\{v_2\psi_2(\nabla^2\psi_2 + \frac{f_0}{H_2}(h_{5/2} - h_{3/2})) + \psi_2\psi_{2yt}\right\} = -AH_2\psi_2\nabla^6\psi_2 \tag{3-5b}$$

$$\frac{\partial}{\partial t}\frac{H_3}{2}(\psi_{3x}^2 + \psi_{3y}^2) + f_0\psi_3\frac{\partial h_{5/2}}{\partial t} - H_3\frac{\partial}{\partial x}\left\{\frac{1}{2}\beta\psi_3^2 + u_3\psi_3(\nabla^2\psi_3 - \frac{f_0}{H_3}h_{5/2}) + \psi_3\psi_{3xt}\right\}$$

$$-H_3 \frac{\partial}{\partial y}\left\{v_3 \psi_3(\nabla^2\psi_3 - \frac{f_o}{H_3} h_{5/2}) + \psi_3 \psi_{3yt}\right\} = -\gamma H_3 \psi_3 \nabla^2 \psi_3 - AH_3 \psi_3 \nabla^6 \psi_3 \qquad (3\text{-}5c)$$

In Appendix A.1 is derived the useful identity

$$\frac{\partial}{\partial x}(u_k \psi_k \nabla^2\psi_k) + \frac{\partial}{\partial y} (v_k \psi_k \nabla^2\psi_k) =$$

$$\frac{\partial}{\partial x}(\psi_k \hat{u}_k \cdot \nabla_H v_k) + \frac{\partial}{\partial y} (-\psi_k \hat{u}_k \cdot \nabla_H u_k) - \frac{\partial}{\partial x} (u_k \frac{KE_k}{H_k}) - \frac{\partial}{\partial y} (v_k \frac{KE_k}{H_k}) \qquad (3\text{-}6)$$

In layer k, the total derivative following the fluid is

$$\frac{d_k}{dt} = \frac{\partial}{\partial t} + u_k \frac{\partial}{\partial x} + v_k \frac{\partial}{\partial y} = \frac{\partial}{\partial t} + J(\psi_k, \quad)$$

while at an interface $k + 1/2$ it is

$$\frac{d_{k+1/2}}{dt} = \frac{\partial}{\partial t} + u_{k+1/2} \frac{\partial}{\partial x} + v_{k+1/2} \frac{\partial}{\partial y} = \frac{\partial}{\partial t} + J(\psi_{k+1/2}, \quad)$$

where the streamfunction at the interface is defined following Holland's

(1978) convention as $\psi_{k+1/2} = \dfrac{H_k \psi_{k+1} + H_{k+1} \psi_k}{H_k + H_{k+1}}$. In fact, as shown in

Appendix A.2,

$$J(\psi_{k+1/2}, h_{k+1/2}) = J(\psi_k, h_{k+1/2}) = J(\psi_{k+1}, h_{k+1/2})$$

so that in future the subscript on the total derivative is omitted, since

it is evident what is meant by $\frac{d}{dt}$.

Using the above, equations (3-5) can now be written as

$$H_1\left[\frac{d}{dt}\ \frac{1}{2}(\psi^2_{1x}+\psi^2_{1y})\ \right] = f_0\psi_1\frac{dh_{3/2}}{dt} + H_1\frac{\partial}{\partial x}(\frac{1}{2}\beta\psi^2_1+\psi_1\frac{dv_1}{dt}) + H_1\frac{\partial}{\partial y}(-\psi_1\frac{du_1}{dt})$$

$$+\ \frac{\psi_1}{\rho_0}\frac{\partial\tau^x}{\partial y}\ +\ AH_1\ \psi_1\nabla^6\psi_1 \tag{3-7a}$$

$$H_2\frac{d}{dt}\left[\frac{1}{2}(\psi^2_{2x}+\psi^2_{2y})\ \right] = f_0\psi_2\frac{d}{dt}(h_{5/2}-h_{3/2}) + H_2\frac{\partial}{\partial x}(\frac{1}{2}\beta\psi^2_2+\psi_2\frac{dv_2}{dt})$$

$$+\ H_2\frac{\partial}{\partial y}(-\psi_2\frac{du_2}{dt})\ +\ AH_2\psi_2\nabla^6\psi_2 \tag{3-7b}$$

$$H_3\frac{d}{dt}\left[\frac{1}{2}(\psi^2_{3x}+\psi^2_{3y})\right] = -f_0\psi_3\frac{dh_{5/2}}{dt} + H_3\frac{\partial}{\partial x}(\frac{1}{2}\beta\psi^2_3+\psi_3\frac{dv_3}{dt})$$

$$+H_3\frac{\partial}{\partial y}(-\psi_3\frac{du_3}{dt})\ +\ \gamma H_3\psi_3\nabla^2\psi_3\ +\ AH_3\psi_3\nabla^6\psi_3 \tag{3-7c}$$

Finally, it is useful to break down the first term on the RHS of (3-7a) as

$$f_0\psi_1\frac{dh_{3/2}}{dt} = f_0\psi_1w_{3/2} = f_0\frac{H_1\psi_2+H_2\psi_1}{H_1+H_2}w_{3/2} + \frac{f_0H_1}{H_1+H_2}(\psi_1-\psi_2)\ w_{3/2}$$

$$= f_0\psi_{3/2}w_{3/2}\ -\ \frac{H_1}{H_1+H_2}\ h_{3/2}\ w_{3/2}\ g'_{3/2} \tag{3-8}$$

Similar treatment for the other two layers gives the final versions of these energy equations:

$$\frac{d}{dt}KE_1 = f_0\psi_{3/2}w_{3/2}\ -\ \frac{H_1}{H_1+H_2}\ g'_{3/2}h_{3/2}w_{3/2} + H_1\frac{\partial}{\partial x}(\frac{1}{2}\beta\psi^2_1+\psi_1\frac{dv_1}{dt}) + H_1\frac{\partial}{\partial y}(-\psi_1\frac{du_1}{dt})$$

$$+\ \frac{\psi_1}{\rho_0}\frac{\partial\tau^x}{\partial y}\ +\ AH_1\psi_1\nabla^6\psi_1 \tag{3-9a}$$

$$\frac{d}{dt}KE_2 = f_0(\psi_{5/2}w_{5/2}-\psi_{3/2}w_{3/2})-(\frac{H_2}{H_1+H_2}\ g'_{3/2}h_{3/2}w_{3/2}+\ \frac{H_2}{H_2+H_3}\ g'_{5/2}h_{5/2}w_{5/2})$$

$$+ H_2 \frac{\partial}{\partial x}(\frac{1}{2}\beta \psi_2^2 + \psi_2 \frac{dv_2}{dt}) + H_2 \frac{\partial}{\partial y}(-\psi_2 \frac{du_2}{dt}) + AH_2 \psi_2 \nabla^6 \psi_2 \qquad (3\text{-}9b)$$

$$\frac{d}{dt}KE_3 = -f_0 \psi_{5/2} w_{5/2} \frac{-H_3}{H_2 + H_3} g'_{5/2} h_{5/2} w_{5/2} + H_3 \frac{\partial}{\partial x}(\frac{1}{2}\beta \psi_3^2 + \psi_3 \frac{dv_3}{dt}) + H_3 \frac{\partial}{\partial y}(-\psi_3 \frac{du_3}{dt})$$

$$+ \gamma H_3 \psi_3 \nabla^2 \psi_3 + AH_3 \psi_3 \nabla^6 \psi_3 \qquad (3\text{-}9c)$$

The first term on the RHS of each equation is like a vertical pressure work term, which transfers energy between the layers. The second term is the conversion in that layer of available potential to kinetic energy, where the total available potential energy is

$$P = \frac{1}{2}\frac{f_0^2}{g'_{3/2}}(\psi_2 - \psi_1)^2 + \frac{1}{2}\frac{f_0^2}{g'_{5/2}}(\psi_3 - \psi_2)^2 = \frac{1}{2}g'_{3/2}h_{3/2}^2 + \frac{1}{2}g'_{5/2}h_{5/2}^2 .$$

The total conversion, summed over the three layers, is $-g'_{3/2}w_{3/2}h_{3/2} - g'_{5/2}w_{5/2}h_{5/2}$. To obtain this result directly, multiply (3-1d) by $g'_{k+1/2}h_{k+1/2}$ and sum over the two interfaces. The result is

$$\frac{dP}{dt} = g'_{3/2}w_{3/2}h_{3/2} + g'_{5/2}w_{5/2}h_{5/2}.$$

The interpretation of the other terms on the RHS of (3-9a-c) remains ambiguous, so consider now the horizontal momentum equations (3-1a,b). To form a kinetic energy equation, multiply (3-1a) by $(H_k + h_{k-1/2} - h_{k+1/2})u_k$, (3-1b) by $(H_k + h_{k-1/2} - h_{k+1/2})v_k$, and add. Note that whereas before it was understood that u_k, v_k were the lowest order portions in the ε-expansions, now one must be careful to include enough orders in each variable's expansion so as not to miss any part of the balance (hence the

retention of $h_{k+1/2}$ in the layer depths). Omitting the forcing terms in layer 1, which are straightforward to include, noting that

$$u \frac{du}{dt} = \frac{d}{dt}(\frac{1}{2}u^2), \quad \text{and writing} \quad h_{3/2} = \varepsilon H_1 \eta_{3/2} \quad (\eta_{3/2} \text{ is } O(1)$$

and non-dimensional) yields for that layer:

$$\varepsilon H_1(1-\varepsilon\eta_{3/2}) \frac{\partial}{\partial t} \frac{1}{2}[(u_1^{(o)}+\varepsilon u_1^{(1)})^2+(v_1^{(o)}+\varepsilon v_1^{(1)})^2]+(u_1^{(o)}+\varepsilon u_1^{(1)})\frac{\partial}{\partial x} \frac{1}{2}[(u_1^{(o)}+\varepsilon u_1^{(1)})^2$$

$$+(v_1^{(o)}+\varepsilon v_1^{(1)})^2]+(v_1^{(o)}+\varepsilon v_1^{(1)})\frac{\partial}{\partial y} \frac{1}{2}[(u_1^{(o)}+\varepsilon u_1^{(1)})^2+(v_1^{(o)}+\varepsilon v_1^{(1)})^2] \quad -$$

$$f_o H_1(1-\varepsilon\eta_{3/2})u_1 v_1 + f_o H_1(1-\varepsilon\eta_{3/2})u_1 v_1 = -H_1(1-\varepsilon\eta_{3/2})(u_1^{(o)}+\varepsilon u_1^{(1)})\frac{\partial}{\partial x} \frac{1}{\rho_o}$$

$$(p_1^{(o)}+\varepsilon p_1^{(1)})-H_1(1-\varepsilon\eta_{3/2})(v_1^{(o)}+\varepsilon v_1^{(1)}) \frac{\partial}{\partial y} \frac{1}{\rho_o}(p_1^{(o)}+\varepsilon p_1^{(1)}) \qquad (3\text{-}10).$$

The lowest order balance is degenerate:

$$0 = -H_1 u_1^{(o)} \frac{\partial}{\partial x} \frac{p_1^{(o)}}{\rho_o} -H_1 v_1^{(o)} \frac{\partial}{\partial y} \frac{p_1^{(o)}}{\rho_o}$$

since $u_1^{(o)}p_{1 \ x}^{(o)} + v_1^{(o)}p_{1 \ y}^{(o)} = 0.$ The next order yields the equation

for the lowest order kinetic energy:

$$\varepsilon H_1 \frac{\partial}{\partial t} \frac{1}{2}(u_1^{(o)2}+v_1^{(o)2})+\frac{1}{2}u_1^{(o)}\frac{\partial}{\partial x}(u_1^{(o)2}+v_1^{(o)2})+\frac{1}{2}v_1^{(o)}\frac{\partial}{\partial y}(u_1^{(o)2}+v_1^{(o)})^2 \quad =$$

$$\frac{-\varepsilon H_1}{\rho_o}(u_1^{(o)} \frac{\partial p_1^{(1)}}{\partial x}+v_1^{(o)} \frac{\partial p_1^{(1)}}{\partial y})- \frac{H_1}{\rho_o}(\varepsilon u_1^{(1)} \frac{\partial p_1^{(o)}}{\partial x}+\varepsilon v_1^{(1)} \frac{\partial p_1^{(o)}}{\partial y}) \qquad (3\text{-}11)$$

or

$$\frac{d}{dt}(KE_1) = -H_1(\vec{u}_1^{(o)}+\varepsilon \vec{u}_1^{(1)}) \cdot \nabla \frac{(p_1^{(o)}+\varepsilon p_1^{(1)})}{\rho_o \varepsilon} \frac{u_1^{(o)} \tau^x}{\rho_o} -$$

$$AH_1(u_1^{(0)}\nabla^4 u_1^{(0)} + v_1^{(0)}\nabla^4 v_1^{(0)})$$

when forcing is included. The first term on the RHS can be written

$$\frac{-H_1}{\rho_0\varepsilon}\bar{\nabla}\cdot(p_1^{(0)}+\varepsilon p_1^{(1)})(u_1^{(0)}+\varepsilon u_1^{(1)}) +\frac{H_1}{\rho_0\varepsilon}(p_1^{(0)}+\varepsilon p_1^{(1)})\nabla\cdot(u_1^{(0)}+\varepsilon u_1^{(1)}) =$$

$$\frac{-H_1}{\rho_0\varepsilon}\nabla\cdot(p\vec{u})+\frac{H_1}{\rho_0}p_1^{(0)}\frac{w_{3/2}^{(1)}}{H_1} = \frac{-H_1}{\rho_0\varepsilon}\nabla\cdot(p\vec{u})+f_0\psi_1 w_{3/2}^{(1)}$$

Similar treatment of all three layers yields:

$$\frac{d}{dt}(KE_1)=f_0\psi_1 w_{3/2}-\frac{H_1}{\rho_0\varepsilon}\nabla\cdot(p_1\vec{u}_1)-\frac{\psi_{1y}\tau^x}{\rho_0}-AH_1(\psi_{1y}\nabla^4\psi_{1y}+\psi_{1x}\nabla^4\psi_{1x}) \qquad (3\text{-}12a)$$

$$\frac{d}{dt}(KE_2)=f_0\psi_2(w_{5/2}-w_{3/2})-\frac{H_2}{\rho_0\varepsilon}\nabla\cdot(p_2\vec{u}_2)-AH_2(\psi_{2y}\nabla^4\psi_{2y}+\psi_{2x}\nabla^4\psi_{2x}) \qquad (3\text{-}12b)$$

$$\frac{d}{dt}(KE_3)=-f_0\psi_3 w_{5/2}-\frac{H_3}{\rho_0\varepsilon}\nabla\cdot(p_3\vec{u}_3)-AH_3(\psi_{3y}\nabla^4\psi_{3y}+\psi_{3x}\nabla^4\psi_{3x})-rH_3(\psi_x^2+\psi_y^2) \qquad (3\text{-}12c).$$

The first term on the RHS of each equation is the same one that was rewritten in (3-9) as the sum of a vertical transfer of energy and a conversion between potential and kinetic energies. The second term is the divergence of the horizontal pressure work, a term that ultimately will be calculated directly. The remaining terms are input and extraction of energy by wind and lateral and bottom friction.

The next step is to note the following identities:

$$\psi_1\frac{\partial\tau^x}{\partial y} = \frac{\partial}{\partial y}(\psi_1\tau^x) - \frac{\partial\psi_1}{\partial y}\tau^x;$$

$$\psi_3 \nabla^2 \psi_3 = \frac{\partial}{\partial x}(\psi_3 \psi_{3x}) + \frac{\partial}{\partial y}(\psi_3 \psi_{3y}) - (\psi_{3x}^2 + \psi_{3y}^2);$$

$$\psi_k \nabla^6 \psi_k = \frac{\partial}{\partial x}(\psi_k \nabla^4 \psi_{kx}) + \frac{\partial}{\partial y}(\psi_k \nabla^4 \psi_{ky}) - \psi_{kx}\nabla^4 \psi_{kx} - \psi_{ky}\nabla^4 \psi_{ky}$$

If these are put into equations (3-9) then a comparison of terms between the resultant forms and equations (3-12) shows, finally:

$$\frac{-H_1}{\rho_0 \varepsilon}\nabla\cdot(p_1\vec{u}_1) = H_1\frac{\partial}{\partial x}(\frac{1}{2}\beta\psi_1^2 + \psi_1\frac{dv_1}{dt} + A\psi_1\nabla^4\psi_{1x}) + H_1\frac{\partial}{\partial y}(-\psi_1\frac{du_1}{dt} + \psi_1\frac{\tau^x}{\rho_0 H_1} + A\psi_1\nabla^4\psi_{1y})$$

$$\frac{-H_2}{\rho_0 \varepsilon}\nabla\cdot(p_2\vec{u}_2) = H_2\frac{\partial}{\partial x}(\frac{1}{2}\beta\psi_2^2 + \psi_2\frac{dv_2}{dt} + A\psi_2\nabla^4\psi_{2x}) + H_2\frac{\partial}{\partial y}(-\psi_2\frac{du_2}{dt} + A\psi_2\nabla^4\psi_{2y})$$

$$\frac{-H_3}{\rho_0 \varepsilon}\nabla\cdot(p_3\vec{u}_3) = H_3\frac{\partial}{\partial x}(\frac{1}{2}\beta\psi_3^2 + \psi_3\frac{dv_3}{dt} + A\psi_3\nabla^4\psi_{3x} + \gamma\psi_3\psi_{3x}) + H_3\frac{\partial}{\partial y}(-\psi_3\frac{du_3}{dt} + A\psi_3\nabla^4\psi_{3y}$$

$$+ \gamma\psi_3\psi_{3y}). \tag{3-13}$$

Thus, the <u>divergence</u> of horizontal pressure work is calculable entirely in terms accessible from the numerical model data.

It is clear that in the mean the Gulf Stream weakens as it flows eastward into the North Atlantic (Fofonoff and Hall, 1983); the same is true of its analog, the free jet, in the numerical model. Yet the possibility must be anticipated that variations from the mean are important in determining the mean distribution of energy in the ocean basin. Thus, all quantities are separated into time-averaged and time-varying components where

$$\overline{(\quad)} = \frac{1}{T}\int_0^T (\quad)dt, \quad (\quad)' = (\quad) - \overline{(\quad)}$$

and T is the total length of the time series being analyzed. Thus, by definition $\frac{\partial(\ )}{\partial t} = 0$. Time-varying or "eddy" terms are not restricted in magnitude relative to the mean. It is evident from Fig. 3.1 that because the model forcing and equations are symmetric about the mid-latitude of the model domain, the time-mean jet flows directly eastward. Notice that this energetic analysis treats the jet as the Eulerian average flow of a particular region, not as a feature changing position and orientation constantly. There are two reasons for having taken this approach: first, it was not technically feasible to take the latter approach due to computing limitations; second, energetic analyses have traditionally been conducted in an Eulerian frame, so for comparison it makes sense to use that approach here.

Bryden (1982) discusses the derivation of equations describing the change of kinetic energy of the mean flow,

$\frac{1}{2}(\overline{\psi}_x^2 + \overline{\psi}_y^2)$, and of the mean value of the kinetic energy of the eddies,

$\frac{1}{2}(\overline{\psi'^2_x} + \overline{\psi'^2_y})$. Integrated over all three layers, the equations are respectively,

$$\sum_{k=1}^{3} H_k \ (\overline{u}_k \frac{\partial}{\partial x} + \overline{v}_k \frac{\partial}{\partial y})(\frac{\overline{u}_k^2 + \overline{v}_k^2}{2}) = -\sum_{k=1}^{3} \frac{H_k}{\rho_0 \varepsilon} \nabla_H \cdot \overline{p}_k \overline{u}_k - \sum_{k=1}^{2} g'_{k+1/2} \overline{W}_{k+1/2} \overline{h}_{k+1/2}$$

$$+\frac{\overline{u_1 \overline{\tau}^x}}{\rho_0} - \gamma H_3 (\overline{u}_3^2 + \overline{v}_3^2) - \sum_{k=1}^{3} A(\overline{u}_k \nabla^4 \overline{u}_k + \overline{v}_k \nabla^4 \overline{v}_k)$$

$$-\sum_{k=1}^{3} H_k \bar{u}_k [\frac{\partial}{\partial x}(\overline{u_k'^2}) + \frac{\partial}{\partial y}(\overline{u_k' v_k'})] - \sum_{k=1}^{3} H_k \bar{v}_k [\frac{\partial}{\partial x}(\overline{u_k' v_k'}) + \frac{\partial}{\partial y}(\overline{v'^2})] \qquad (3\text{-}14a)$$

$$\sum_{k=1}^{3} H_k [(\bar{u}_k \frac{\partial}{\partial x} + \bar{v}_k \frac{\partial}{\partial y})(\overline{\frac{u_k'^2 + v_k'^2}{2}}) + u_k' \frac{\partial}{\partial x} \overline{\frac{u_k'^2 + v_k'^2}{2}} + v_k' \frac{\partial}{\partial y} \overline{\frac{u_k'^2 + v_k'^2}{2}}] =$$

$$-\sum_{k=1}^{3} \frac{H_k}{\rho_0 \varepsilon} \overline{\nabla_H \cdot p_k' \vec{u}'}_k - \sum_{k=1}^{2} g_{k+1/2} \overline{w_{k+1/2} h_{k+1/2}} - \overline{H_3(u_3'^2 + v_3'^2)} - \sum_{k=1}^{3} A(\overline{u_k' \nabla^4 u_k'} +$$

$$\overline{v_k' \nabla^4 v_k'}) - \sum_{k=1}^{3} H_k [\overline{u_k'^2} \frac{\partial \bar{u}_k}{\partial y} + \overline{u_k' v_k'}(\frac{\partial \bar{u}_k}{\partial y} + \frac{\partial \bar{v}_k}{\partial x}) + \overline{v_k'^2} \frac{\partial \bar{v}_k}{\partial y}] \qquad (3\text{-}14b).$$

Several comments are in order here. First, superscripts denoting the ε-expansion order of variables have been dropped: in all cases save the pressure work term, only lowest order quantities are required. Since the calculation of $-\nabla \cdot (p\vec{u})$ actually is made from (3-13), which involves only lowest order variables, the superscripts are omitted for neatness. Second, it should be noted that the time-varying field obeys quasi-geostrophic dynamics as well, whence $u'_k = -\psi'_{ky}$, $v_k = \psi'_{kx}$. As a result, _any_ term of the sort $\vec{u} \cdot \nabla[(\quad)]$ can be written $\nabla \cdot [\vec{u}(\quad)]$ regardless of how time-averaging enters the term. This last point will be useful in interpreting the equations in terms of kinetic energy fluxes.

The equation for the time average of the total kinetic energy is obtained either by adding (3-14a and b) or directly by time-averaging the sum of equations (3-12). The result is:

$$\sum_{k=1}^{3} \frac{\partial}{\partial x}[(\overline{u}_k\overline{K}_k + \overline{u}_k\overline{K'}_k + \overline{u'_k K'_k}) + H_k(\overline{u_k u'^2_k} + \overline{v_k}\ \overline{u'_k v'_k})] + \frac{\partial}{\partial y}[(\overline{v}_k\overline{K}_k + \overline{v}_k\overline{K'}_k + \overline{v'_k K'_k})$$

$$+ H_k(\overline{u_k u'_k v'_k} + \overline{v_k v'^2_k})] = -\sum_{k=1}^{3}\frac{H_k}{\rho_0 \epsilon}\overline{\nabla}_H \cdot \overrightarrow{p_k \vec{u}_k} - \sum_{k=1}^{2} \overline{g'_{k+1/2}w_{k+1/2}h_{k+1/2}}$$

$$+ \frac{\overline{u_1 \tau}^x}{\rho_0} - \gamma H_3(\overline{u^2_3} + \overline{v^2_3}) - \sum_{k=1}^{3} H_k A(\overline{u_k \nabla^4 u_k} + \overline{v_k \nabla^4 v_k}) \tag{3-15}$$

where $\overline{K} = \frac{1}{2}(\overline{u}^2 + \overline{v}^2)H$, $K' = \frac{1}{2}(u'^2 + v'^2)H$. In (3-14a), the mean advection of mean kinetic energy is balanced by the pressure work term due to the mean field, conversions to and from mean potential energy, input of energy by the wind, removal of energy by bottom and lateral stresses acting on the mean field, and a term which represents the conversion of eddy to mean kinetic energy. In (3-14b), the mean plus eddy advection of eddy kinetic energy is balanced by the horizontal pressure work due to the eddy field, conversions to and from eddy potential energy, losses to friction due to the eddy field, and a term giving the conversion of mean to eddy kinetic energy. When the two equations are added, as Bryden (1982) has pointed out, the conversion terms between mean and eddy kinetic energy do not cancel, but give rise to the peculiar-looking part of the divergence on the LHS of (3-15), i.e.,

$\frac{\partial}{\partial x}(\overline{u}\ \overline{u'^2} + \overline{v}\ \overline{u'v'}) + \frac{\partial}{\partial y}(\overline{u}\ \overline{u'v'} + \overline{v}\ \overline{v'^2})$. The mystery of this term disappears when it is observed that the LHS of (3-15) is just the total divergence of the total kinetic energy flux, time-averaged:

$$\text{LHS of (3-15)} = \sum_{k=1}^{3} (\frac{\partial}{\partial x} u_k H_k \overline{\frac{u_k^2+v_k^2}{2}} + \frac{\partial}{\partial y} v_k H_k \overline{\frac{u_k^2+v_k^2}{2}}).$$

The kinetic energy budget will be considered over volumes of ocean with open side boundaries at $x = (x_w, x_E)$ to west and east, $y = (y_s, y_N)$ to south and north. Integrating (3-15) over the area yields:

$$\sum_{k=1}^{3} \left\{ \int_{y_s}^{y_N} dy (\overline{u}_k \overline{K}_k + \overline{u}_k \overline{K}_k' + \overline{u_k' K_k'} + H_k (\overline{u}_k \overline{u'^2_k} + \overline{v_k \overline{u_k'v_k'}})) \Big|_{x_w}^{x_E} + \int_{x_w}^{x_E} dx (\overline{v}_k \overline{K}_k + \overline{v}_k \overline{K}_k' + \right.$$

$$\left. \overline{v_k' K_k'} + H_k (\overline{u}_k \overline{u_k'v_k'} + \overline{v}_k \overline{v_k'^2})) \Big|_{y_s}^{y_N} \right\} = \sum_{k=1}^{3} \left\{ H_k \int_{y_s}^{y_N} dy (\frac{1}{2} \beta \overline{\psi_k^2} + \overline{\psi_k \frac{dv_k}{dt}} + \right.$$

$$A \overline{\psi_k \nabla^4 \psi_k} + \delta(k-3)\gamma \overline{\psi_k \psi_{kx}} \Big|_{x_w}^{x_E} + H_k \int_{x_w}^{x_E} dx (-\overline{\psi_k \frac{du_k}{dt}} + \delta(k-1)\overline{\frac{\psi_k \tau^x}{\rho_o H_k}} + A \overline{\psi_k \nabla^4 \psi_{ky}} +$$

$$\left. \delta(k-3)\overline{\psi_k \psi_{ky}} \Big|_{y_s}^{y_N} \right\}$$

$$- \sum_{k=1}^{2} \int_{x_w}^{x_E} dx \int_{y_s}^{y_N} dy (g'_{k+1/2} \overline{w}_{k+1/2} \overline{h}_{k+1/2} + \overline{g'_{k+1/2} w'_{k+1/2} h'_{k+1/2}}) + \int_{x_w}^{x_E} dx \int_{y_s}^{y_N} dy \frac{\overline{u_1 \tau^x}}{\rho_o}$$

$$- \gamma H_3 \int_{x_w}^{x_E} dx \int_{y_s}^{y_N} dy (\overline{u}_3^2 + \overline{v}_3^2 + \overline{u_3'^2} + \overline{v_3'^2}) - \sum_{k=1}^{3} H_k A (\overline{u_k \nabla^4 u_k} + \overline{v_k \nabla^4 v_k}) \qquad (3-16)$$

The following points are made regarding (3-16):

1) $(*)\Big|_{x_w}^{x_E}$ is the value of $(*)$ at x_E minus its value at x_w;

2) the divergence of pressure work has been replaced by the terms
    used to calculate it, but the individual fluxes across the
    boundaries are not necessarily equal to the fluxes of pu:
    only the net divergence over the volume has any meaning in this
    context;

3) those terms for which separate mean and eddy components have
    been calculated are broken down into those components in (3-16).

Before the kinetic energy budgets for the model are discussed, the model
data and calculations are briefly described.

3.3 Calculations

Important attributes of numerical model 3L-4 analyzed here are given
in Table 3-1. Little will be said concerning the actual numerics used to
run the model, as Chow and Holland (1985) describe this in detail. The
wind stress in 3L-4 is steady and drives two gyres with opposite vorticity
input. The circulation is spun up from a rest state, then run for a number
of years after reaching statistical equilibrium. Although the model time
step is a fraction of a day, instantaneous values of the streamfunction are
stored only every two days. The data treated here use streamfunction
values for every fourth day, extending over about four years of model time,
resulting in a total of 360 instantaneous values of streamfunction.

Due to limited resources, it was necessary to restrict the
calculations in several ways. First, only a subset of the entire domain
was investigated, extending from 820 km south of mid-basin to 780 km north,
and from the western boundary to the middle of the basin, 2000 km

eastward. (It was originally intended to go from 800 km south to 800 km north of mid-basin, but the data were accidentally offset by 20 km.) Equation (3-16) was evaluated by first calculating all the necessary time-averages at every grid-point, then using the resulting data sets to examine budgets of various volumes. While it seemed useful to break down some terms into mean and eddy contributions, there would simply

be too many moments to evaluate in a term like $\overline{\psi_k \dfrac{dv_k}{dt}}$,

so that only the overall time-average has been calculated. Also, initial calculations of terms involving the biharmonic friction proved very noisy and very small: indeed, in models of this type (see, .e.g., Holland, 1978) this term contributes negligibly to the dissipation of energy (but is important in dissipating enstrophy). Hence it is not included in the budgets.

Evaluation of terms in the instantaneous vorticity equation using the model data yields relatively large imbalances. Evidently that is due to the poor estimate of local time change of vorticity afforded by the sampling interval of four days (Holland, personal communication). Similarly, calculations of "instantaneous" kinetic energy budgets show that on a short time scale there are apparent imbalances, but again,

$\dfrac{\partial}{\partial t} KE$ would be poorly estimated. On the other hand, once the averages of terms have been formed, the well-defined meridional structure of individual quantities suggests the time-averaged budgets give a reliable assessment of the energetics in the domain. Also, due to the strength of flow right at

the western boundary, the instantaneous values may be extremely noisy; thus

for examining the budgets, the western wall itself has not been used, but

rather the data from the first grid-point in (20 km east of the boundary).

First and second derivatives have been calculated using ordinary

centered finite-difference schemes. Any term involving a Jacobean has been

evaluated using an Arakawan scheme. Time-differences were also evaluated

using a centered scheme, and in terms where they are part of an average,

such as in $\overline{\psi \frac{\partial u}{\partial t}}$, the poor estimate of local time change may be partly res-

ponsible for the residuals that are found in the energy budgets.

Straightforward trapezoidal integrations have been used in the horizontal

in these calculations.

3.4 Results

Once the tools are at hand to evaluate kinetic energy budgets for any

volume of the domain, it is important to consider carefully the choice of

volumes to be investigated. Sometimes one is interested in the exchanges

of energy between the mean and eddy flows; Harrison (1979), for example,

investigated the interaction between the mean and eddy kinetic energy

fields of a variety of numerical experiments by integrating over the entire

basin. He points out that local budgets of open-bounded regions may be

quite different from the basin-averaged budgets, however. Harrison and

Robinson (1978) have in fact done some analysis of this sort, which will be

discussed later. Here the point is to investigate the very strong

convergence or divergence of kinetic energy in the vicinity of a free jet

like the Gulf Stream, and to determine which, if any, of the mechanisms on the RHS of (3-16) is dominant in producing a balance.

First a number of volumes were examined, chosen according to experience with the Gulf Stream '60 data. These volumes were of small enough size to prevent extensive overlap of energetically different regions, until the gross energetic patterns emerged. A comparison of the areas suggested by this search with the mean streamlines in all three layers helped to refine the horizontal boundaries of the volumes and offered rigorous criteria for selecting them. Essentially six types of energetic regimes have been identified, but since the model is symmetric about mid-latitude, four regimes appear on each side of the jet, so that there are actually ten different physical volumes for which budgets have been calculated. The criteria for determining the latitudinal and meridional boundaries of these volumes are as follows:

1) Of paramount importance is delimiting the north-south extent of the jet. Throughout the jet, the deep-layer zonal velocities nearly always change sign between the grid-points corresponding to $y = 140$ km and $y = 160$ km north and south of the jet axis at $y = 0$. This also turns out to be the latitude at which upper layer zonal velocity has dropped off to approximately $1/e^2$ times its maximum value for any given section. Thus, the jet's boundaries are chosen to be $y = \pm 140$ km.

2) Although the motivation for this work was the weakening of the free jet, there is a significant accelerating portion starting at the western boundary. The jet is considered to change from accelerating

to decelerating where the mean zonal flux of mean kinetic energy attains a maximum, 660 km from the western boundary.

3) From Fig. 3.1, it is clear that in the top and middle layers there is both a broad Sverdrup circulation and a tighter inertial recirculation, while in the deep layer only the latter is visible. Holland and Rhines (1980) have found that the exact Sverdrup balance $\beta v = f w_z$ obtains over a relatively small area of numerical models, but in that work it was found that it did describe the region in the top layer that appears in Fig. 3.1a as broadly spaced streamlines with a primarily meridional orientation. The latitude at which the deep-layer mean streamfunction goes to zero, defining the meridional extent of the recirculation, is very close to the latitude where the mean vertical heat flux $gw\rho$, integrated over the eastern part of the domain, changes sign. The latitude midway between the two is chosen as the boundary for this regime. The last region, referred to as the Sverdrup regime, extends from the edge of the recirculation to the open boundaries of the domain, at $y = -820$ km and $y = +780$ km.

4) For each of the latitude bands defined in 3), an east-west division is also made at $x = 660$ km, to correspond to the division made in the jet regions. As will be seen, the eastern and western portions of the recirculation and Sverdrupian regimes are characterized by different energetic budgets.

In Fig. 3.2, the obvious feature common to all six volumes is that there is a dominant balance between just two of the many terms included in

Figure 3.2. Summary of depth-integrated energy budgets for six regions (described in text). Arrows show direction of fluxes into or out of boxes; numbers are terms integrated over the volume. Pattern is given in upper left box and is same for others. Sign is appropriate to LHS of energy equation for all terms. Key: KE = total kinetic energy flux and its divergence over the volume; PW = pressure work terms; HF = heat flux, or conversions between potential and kinetic energy; WW = work done on volume by wind stress; FR = dissipation due to bottom friction. Residual imbalance is shown in box.
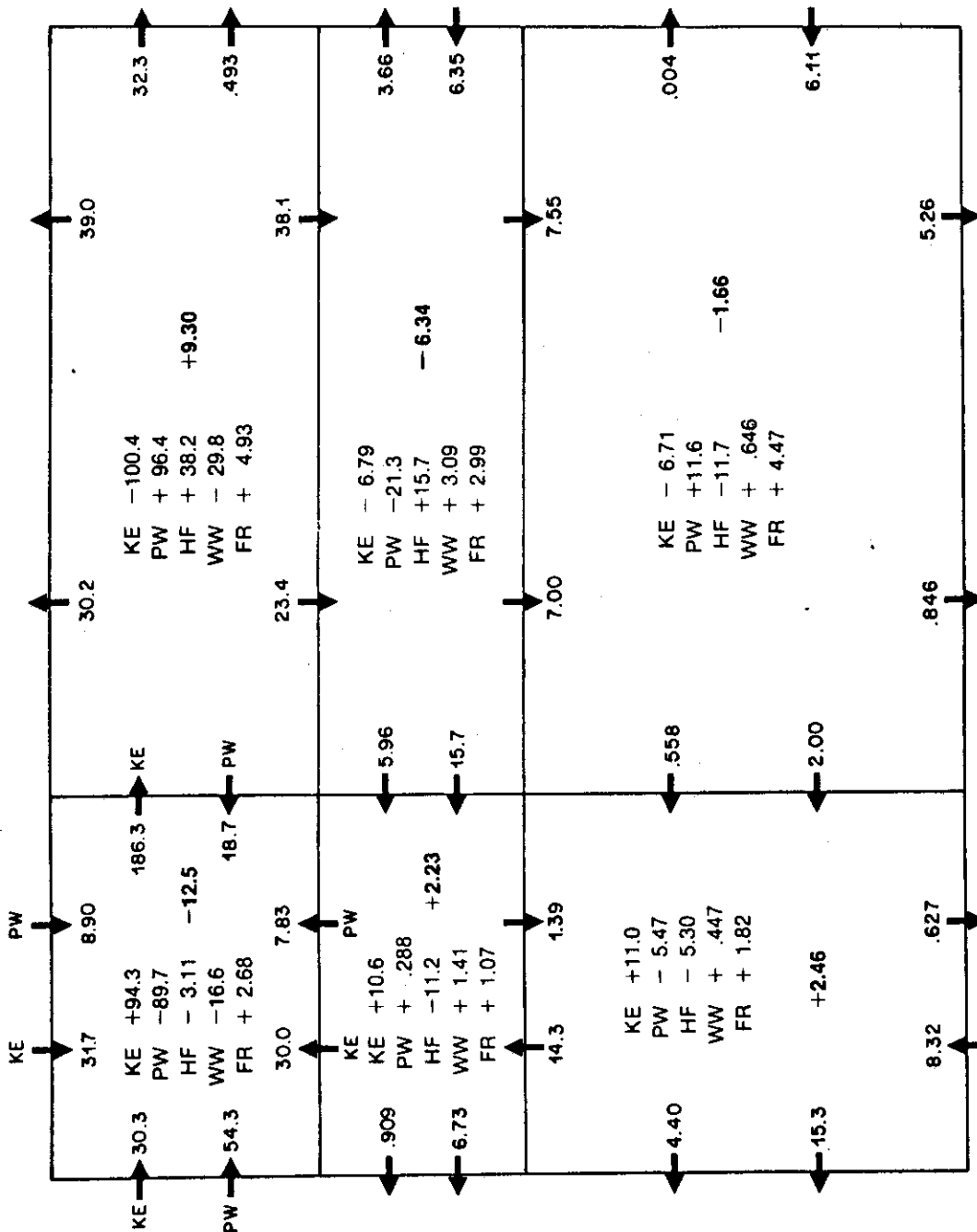
the budget. (Notice that the residuals never exceed about 1/3 the magnitude of the dominant terms.) In the accelerating portion of the jet, the total flux of kinetic energy out of the region is nearly double that coming in. This divergence appears to be balanced by a net amount of work being provided by pressure-velocity correlations; of secondary importance is the fact that the wind stress tends to accelerate the flow throughout the jet region. In the decelerating jet, the roles of kinetic energy flux and pressure work are reversed: the former provides a tremendous convergence of energy which is radiated mostly north and south via the pressure work. The secondary terms in this region, which are a third the size of the dominant ones, are a net input of energy by the wind stress and a net conversion of kinetic to available potential energy. Because they are so similar in magnitude, it is tempting to suggest that all the wind work is going directly into potential energy, but of course there is no real basis for drawing this conclusion. It is possible that the overall conversions in this region are quite complicated.

The balances in the recirculation regions are of a different nature, for here conversions to and from potential energy play a dominant role. In the eastern portion of the recirculation region, south of the decelerating jet, there is a substantial amount of pressure work exerted on the region, which is primarily balanced by a sizable conversion of kinetic to potential energy. Of secondary importance in this region is a convergence of kinetic energy flux, due primarily to a large flux coming across the northern boundary from the jet. In the western recirculation pressure work

is unimportant, and there is a conversion from potential to kinetic energy, which is returned to the accelerating jet region as it fluxes across the northern boundary of this area. In all the regimes, of course, bottom friction extracts energy from the system; everywhere except in the jet regions, wind stress acts to remove energy as well, usually on a small scale comparable to or less important than friction.

The Sverdrup regimes depart from strict two-term balances. In the western portion, kinetic energy is fed into the jet to the west and north, resulting in a divergence that is balanced half by the pressure work exerted on the region and half by a conversion of potential to kinetic energy. The eastern Sverdrup region also sees a conversion of potential to kinetic energy, which it appears to export to surrounding areas via pressure work. The secondary terms in this region, however, are nearly 50 percent as large as the dominant ones: there is a convergence of kinetic energy roughly equal in magnitude to the net loss of energy to bottom friction.

An examination of the individual energy fluxes across the boundaries of all the regions (Figure 3.3) reveals several interesting asymmetries, for example, that the accelerating and decelerating jet regimes are not "mirror images" in an energetic sense. In the west, mean flux of mean kinetic energy accounts for only about half the net divergence, the deficit being made up mostly by the terms $\frac{\partial}{\partial x}(\bar{u}\,\overline{u'^2} + \bar{v}\,\overline{u'v'}) + \frac{\partial}{\partial y}(\bar{u}\,\overline{u'v'} + \bar{v}\,\overline{v'^2})$. Because of the role these terms play in the individual mean and eddy equations, they will be referred to as the mean/eddy exchange terms. In
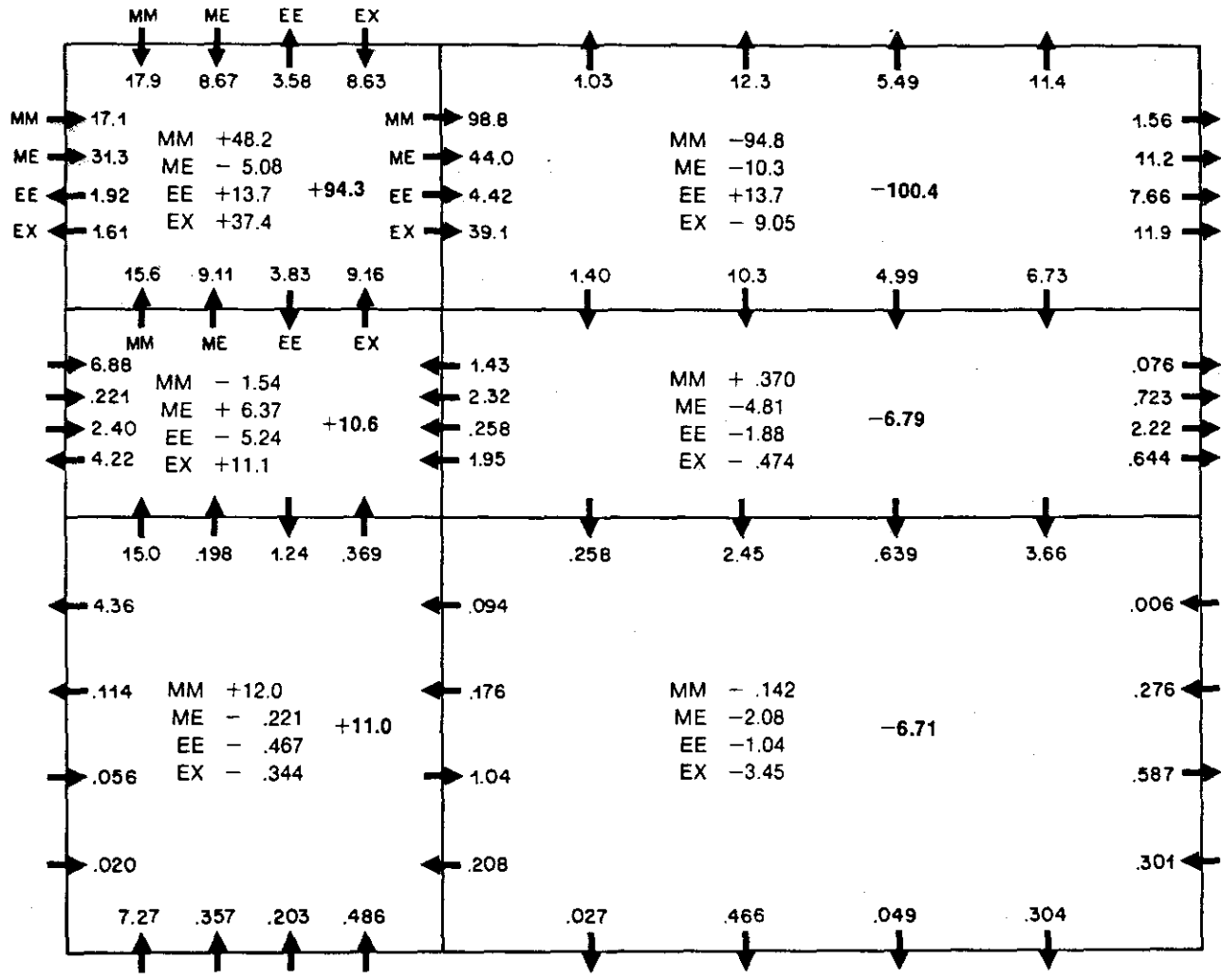
Figure 3.3. Summary of independent components of depth-integrated kinetic energy flux. Arrows show directions of fluxes into or out of boxes. Key: MM = mean flux of MKE; ME = mean flux of EKE; EE = eddy flux of EKE; EX = flux of mean/eddy exchange terms (see text). Divergence of various fluxes are listed, and total divergence is in heavy type. Left to right, top to bottom, are: accelerating and decelerating jet; western and eastern recirculation; western and eastern Sverdrup.

MM ME EE EX
17.9 8.67 3.58 8.63   1.03 12.3 5.49 11.4

MM 17.1   MM 98.8   1.56
ME 31.3   ME 44.0   11.2
EE 1.92   MM +48.2   +94.3   EE 4.42   MM −94.8   −100.4   7.66
EX 1.61   ME − 5.08   EX 39.1   ME −10.3   11.9
           EE +13.7   EE +13.7
           EX +37.4   EX − 9.05

15.6 9.11 3.83 9.16   1.40 10.3 4.99 6.73

MM ME EE EX

6.88   1.43   .076
.221   2.32   .723
2.40   MM − 1.54   +10.6   .258   MM + .370   −6.79   2.22
4.22   ME + 6.37   1.95   ME −4.81   .644
       EE − 5.24   EE −1.88
       EX +11.1   EX − .474

15.0 .198 1.24 .369   .258 2.45 .639 3.66

4.36   .094   .006

.114   .176   .276
       MM +12.0   MM − .142
.056   ME − .221   +11.0 1.04 ME −2.08   −6.71   .587
       EE − .467   EE −1.04
.020   EX − .344   .208 EX −3.45   .301

7.27 .357 .203 .486   .027 .466 .049 .304

the east, the convergence of kinetic energy flux is 95 percent due to the mean fluxes. The eddy flux of EKE is divergent in the decelerating as well as accelerating part of the jet, so that it acts as another, smaller scale "radiation agent" in the eastern portion, while the mean flux of EKE is everywhere convergent in the jet. This opposition of the tendencies for mean and eddy fluxes of EKE extends to other parts of the domain and is interesting because the two terms are similar in magnitude, while any linear or small-amplitude non-linear theory would completely ignore the eddy fluxes of EKE.

Still more insight may be gained by examining separately the budgets for mean and eddy kinetic energies. In this context, one must be careful in the interpretation of the mean/eddy exchange terms. Harrison and Robinson (1978) have discussed at some length the interpretation of these terms in open regions. They classify three types of regions, which may be summarized as follows: 1) those regions in which the conversion of mean to eddy kinetic energy implied by the equation for $\overline{K}$ is approximately equal and opposite to the conversion of eddy to mean kinetic energy implied by the equation for $\overline{K'}$: in other words, the divergence of the mean/eddy exchange terms over the volume is nearly zero; 2) regions in which the two conversions are small compared to other processes and may be ignored in the energy budgets; 3) regions in which the two conversions are large, but equal and opposite: in other words, the devergence of the mean/eddy exchange terms over the volume is considerable. Only in regions of type 1 or 2 is there a clear interpretation of the energy budget for the region in terms of mean to eddy conversion processes. Here a different interpre-

tation is adopted. The budget for EKE over a region, for example, may indicate that eddy energy is increasing at the expense of MKE; yet over the same region, the budget for MKE may suggest that there is a conversion of eddy to mean kinetic energy. The region is of type 3 according to Harrison and Robinson. Indeed, the exchange terms as they appear in the two equations are not equal and opposite, but differ by a divergence of the mean/eddy exchange fluxes across the boundary, which redistribute eddy and mean kinetic energy regionally, where it may then appear as a conversion from one type to the other. Because the major thrust of this work is to examine the divergence of fluxes across the open boundaries, rather than to evaluate the conversions between eddy and mean kinetic energies as in Harrison and Robinson (1978), a type 3 region is not considered a "problem" in the present work.

Figures 3.4 through 3.6 display the interdependent budgets for mean and eddy kinetic energy in the six regimes, and are to be interpreted as follows. Consider Fig. 3.4a as an example. Here, in the accelerating jet, the net divergence of MKE fluxes over the area, equal to 48.2 x 10^9 J/s, implies that mean kinetic energy must be supplied to the region at this rate by other mechanisms in order to maintain the budget. Moreover, there is a constant conversion to EKE of 32.0 x 10^9 J/s, which is interpreted as being fluxed out of the region, and a net loss to dissipation of 1.4 x 10^9 J/s. On the supply side, mean potential energy is being converted to MKE at the rate of 5.5 x 10^9 J/s and wind is supplying eneregy at 16.6 x 10^9 J/s. There is still a net deficit of 59.5 x 10^9 J/s, which must be supplied by the pressure work divergence, the only term remaining in the

91

Figure 3.4. Schematic of interconnected mean and eddy energy budgets in
a)western; b)eastern jet region. See text for explanation of how to
interpret. Key: $\overline{K}$ = MKE; K' = EKE; $\overline{P}$ = mean potential energy; P' =
eddy potential energy; τ = work done by wind stress; $\overline{D}$ = dissipation due
to bottom friction acting on mean flow; D' = dissipation due to bottom
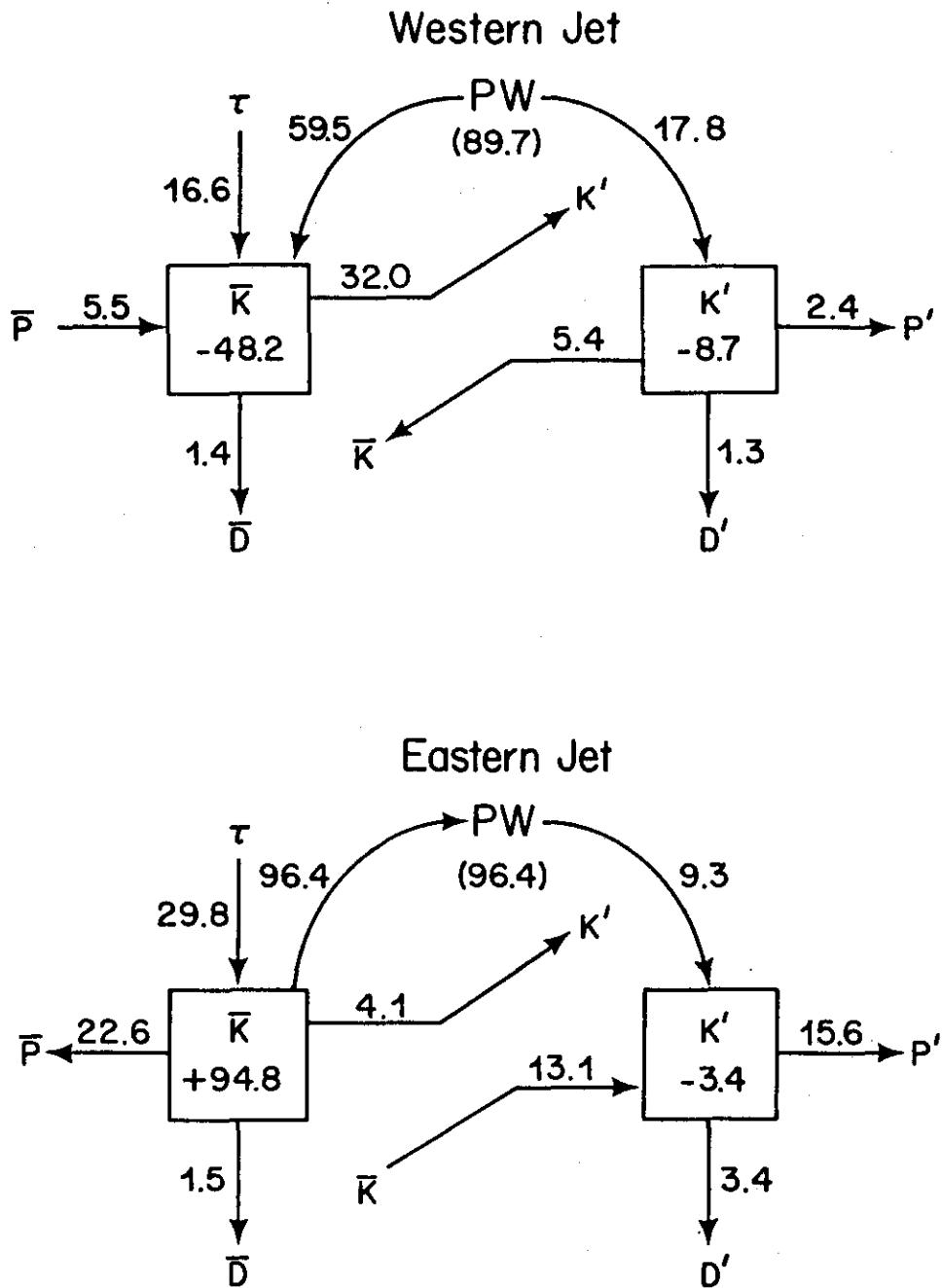friction acting on eddy terms; PW = pressure work.

Western Jet

Eastern Jet

Figure 3.5. Same as Figure 3.4, but for recirculation region.

Western Recirculation
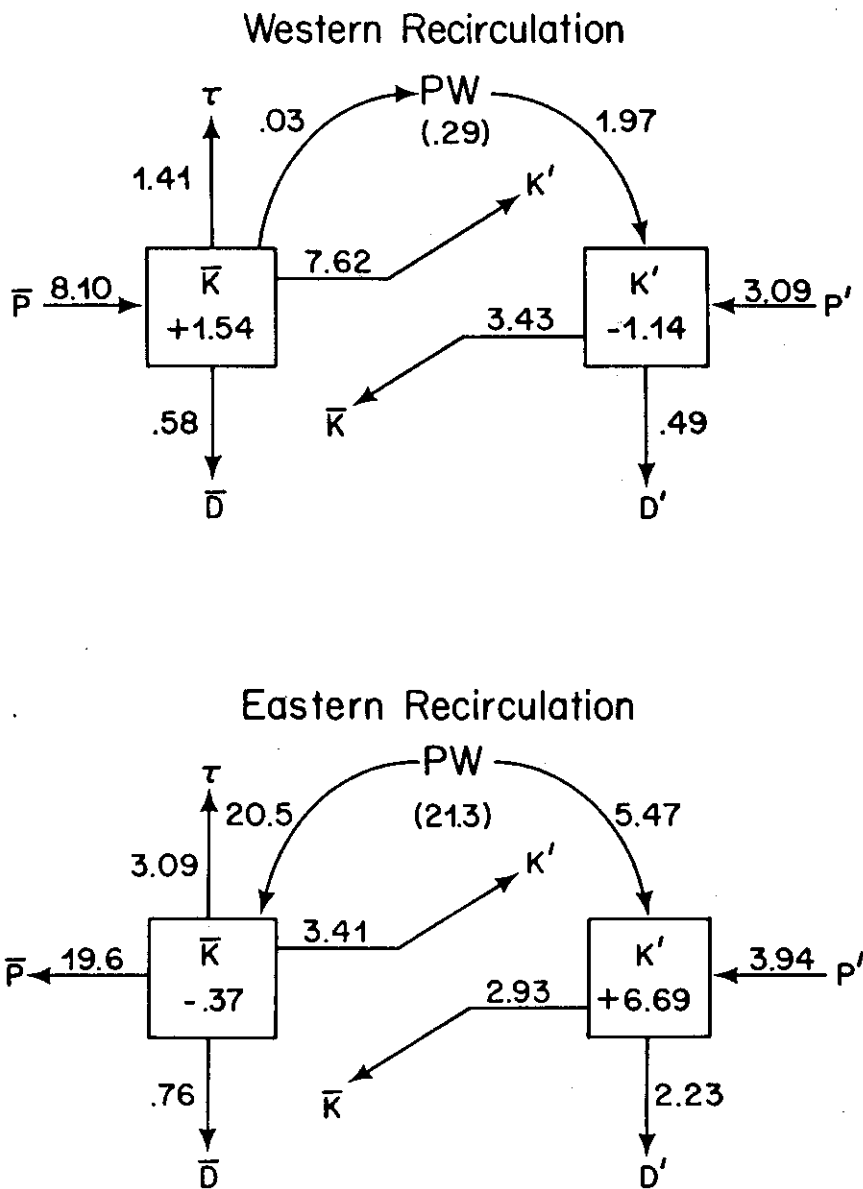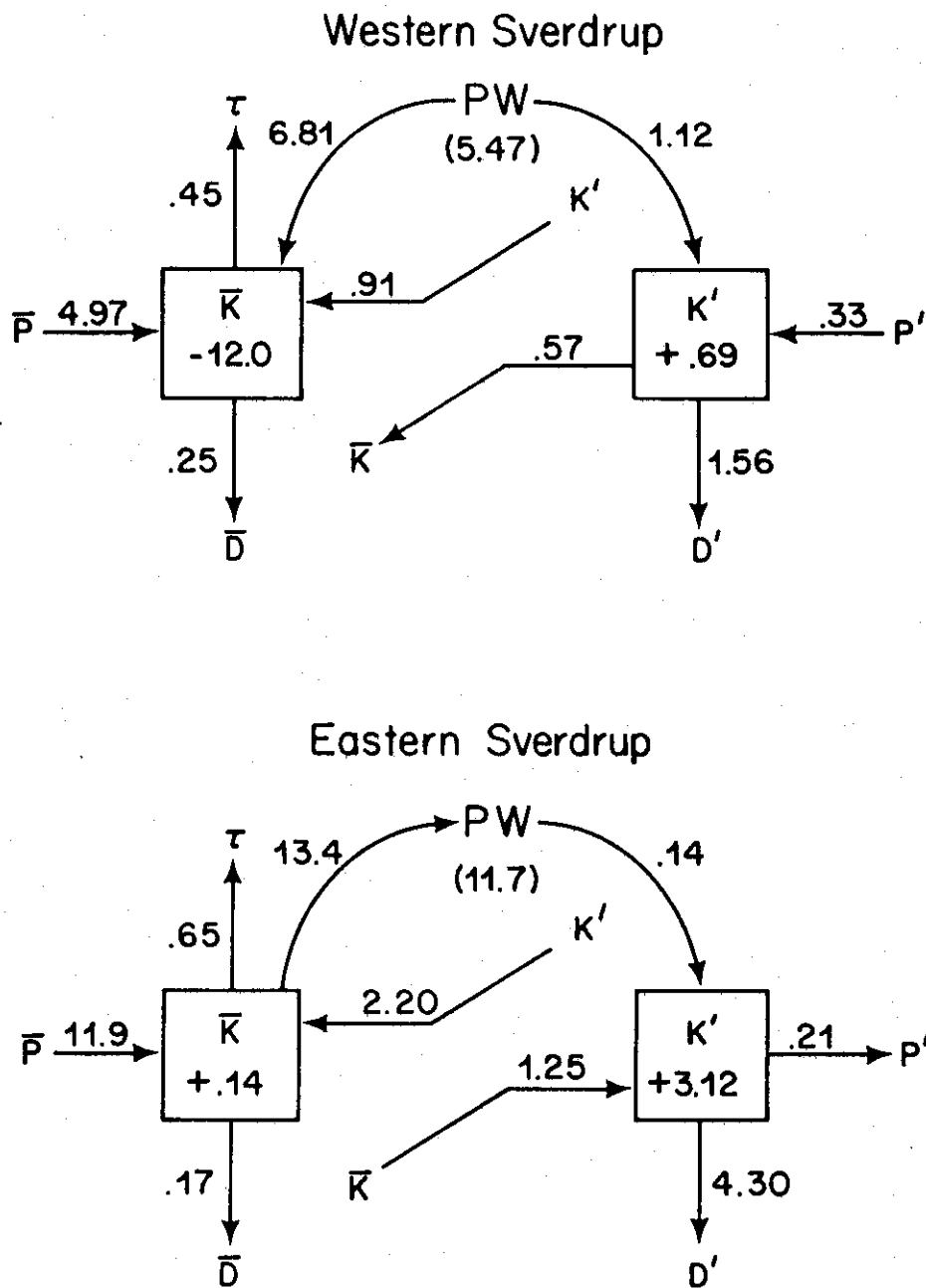

Eastern Recirculation

Figure 3.6. Same as Figure 3.4, but for Sverdrup region.

budget for MKE. Similar analysis of the eddy budget suggests the pressure work is supplying 17.9 x 10^9 J/s, for a total of 77.3 x 10^9 J/s. In parentheses is the calculated pressure work divergence of 89.7 x 10^9 J/s, and the two values differ by the residual imbalance shown in Fig. 3.2.

Still concentrating on the jet region, observe that the fluxes and exchanges involved in maintaining the MKE budget are nearly an order of magnitude larger than those in the EKE budget. In particular, one is forced to interpret most of the pressure work divergence as being due to the correlations between the mean pressure field and a mean ageostrophic velocity field. That interpretation runs counter to the notion that the pressure work is radiating energy via wavelike structures, through terms like p'u'. However, recall that the mean ageostrophic velocity field depends on time-dependent quantities arising from inertial accelerations in the momentum equations. In the decelerating jet (Fig. 3.4b), going beyond the dominant balance, there are two more interesting features. First, there is a sizable conversion of mean kinetic to potential energy, the mechanism proffered by Fofonoff and Hall (1983) to account for downstream decreases in kinetic energy flux. Second, in the eddy budget, there is an energy pathway suggestive of barotropic instability, as MKE, interpreted as being fluxed into the region, is converted to EKE at a rate of 13.1 x 10^9 J/s. Meanwhile, the direction of energy flow between eddy kinetic and potential energies is opposite of what would be anticipated were baroclinic instability operative in this region.

The story told by the budgets in the recirculation regime is quite different (Figure 3.5). In the first place, mean and eddy fluxes and

exchanges are of like magnitude. In the east there is a continuation of the conversion of MKE to mean potential energy. However, eddy budgets throughout the recirculation now display an energy pathway implying baroclinic instability, where eddy potential energy is converted to EKE (at rates of 3-4 x 10^9 J/s), and EKE is converted to MKE (at rates of 3-3.5 x 10^9 J/s). Curiously, throughout the recirculation, the eddy budget implies that pressure work due to eddy terms radiates energy into, rather than out of, the region. The mean budget in the west shows the other half of the inertial recirculation of energy as potential energy -- that is, there is now a conversion of mean potential to mean kinetic energy, which helps to accelerate the flow.

Figure 3.6, showing the Sverdrup regions, reveals little more than has already been learned, save that the energy budgets here are dominated by mean fluxes and exchanges. In the west, there is again acceleration of the mean flow as mean potential energy is converted to MKE.

Comparison of these results with Harrison and Robinson's (1978) results is limited, for several reasons. In the first place, they analyzed a single gyre model with the eastward jet flowing along the northern wall rather than freely in mid-ocean, and the basin was only 2000 km by 2000 km. Second, they did not examine the accelerating and decelerating portions of the eastward jet separately, so the very large fluxes of mean kinetic energy in the jet are of no importance in their budgets. Volume-averaged magnitudes of the mean to eddy conversion are roughly comparable for the two investigations, but because of the importance of the mean flow terms in the budgets presented here, most of the regions in this

Figure 3.7. Same as Figure 3.4, but for total domain.
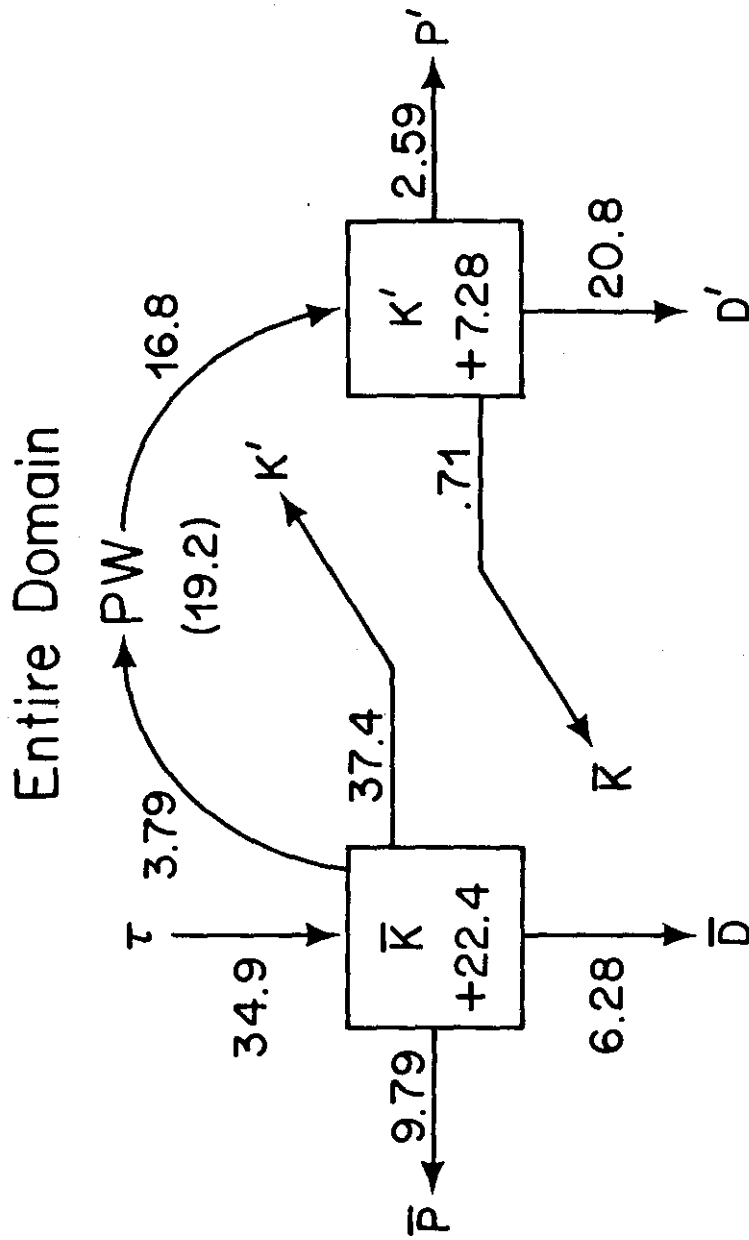
analysis would be considered type 2 (with the exception of the western recirculation and possibly the western jet). Notice that if the regions had not been divided into their eastern and western portions, conversions in the mean energy equations would tend to cancel out, and the mean/eddy conversions would become relatively more important; then most of the regions would be type 3.

Finally, it is worth considering the energy picture for the entire domain, shown in Figure 3.7. Although there may still be fluxes across the open boundaries, the very strong internal fluxes and exchanges tend to cancel out, and forcing and dissipation assume much more important roles. In the complete absence of fluxes across the boundaries of the domain, the two would necessarily be found equal and opposite. Even in this open domain, that balance is the most obvious part of the budget, as bottom friction removes energy at a rate of 27.1×10^9 J/s while wind puts energy in at 34.9×10^9 J/s. Also note that most of the energy is dissipated through eddy terms: in spite of the dominance of mean terms in the localized budgets, ultimately the total system depends on the eddies in a direct way to balance the energy budget. The fact that the system is entirely forced by the wind stress, which directly affects only the mean kinetic energy budget, means that there is an inescapable coupling between mean and eddy fields, as Harrison (1979) concluded.

Individually, the mean and eddy kinetic energy fluxes over the domain appear to be convergent. However, taking into account the mean/eddy exchange terms, it is found that the total energy fluxes are in fact divergent; there is also a net conversion of kinetic to potential energy.

Although the excess of forcing over dissipation makes up part of the deficit, notice that energy must still be imported via pressure work terms -- curiously, this occurs in the eddy field, so that waves from regions outside this domain evidently radiate energy into it!

This discussion of energy budgets in the numerical model must be concluded with several warnings. As pointed out at the beginning of this chapter, the analysis has treated the time-averaged flows in the vicinity of an intense jet which meanders strongly on an instantaneous basis. Thus, this analysis addresses not so much the energetics of the jet as the energetics of that region in which the jet is usually found. The jet itself may have some average "structure" that it carries about as it meanders. The deviations from such an average are lumped together with the meandering to comprise the eddy portion in an Eulerian time-average of the flow field. Without separating various effects, one cannot carry out a phenomenological investigation of the energetics, identifying time and space scales, energy sources, and propagation characteristics of those features most important to maintaining the energy budgets.

Rather, a zeroth order evaluation of the budgets has been presented, with the idea that it can provide guidelines for future work of this type either on numerical models or in the ocean. Of the six energetic regimes that have been identified, balances in both the accelerating and decelerating jet regions are dominated by mean quantities. In particular the downstream convergence of kinetic energy in the decelerating jet is balanced primarily by a mean ageostrophic flow against the pressure gradient, which in turn implies some conversion of kinetic to available

potential energy. Mean and eddy quantities are of equal importance in the recirculation regimes, but the mean flow again dominates energetic balances in the Sverdrup regions. That so much energy is exported from the jet region implies that the jet is not energetically isolated from its environs, so channel models probably are not a good means for investigating the jet's dynamics and energetics. Indeed, Harrison (1979) has pointed out the necessity for local energetic analyses of regions with open boundaries in numerical models. The conversions between kinetic and potential energy in both the jet and recirculation regions are consistent with Fofonoff and Hall's (1983) conclusions regarding energy conversions evaluated from the Gulf Stream '60 data. Finally, the energetic budgets suggest that barotropic instability may be occurring in the jet itself, while baroclinic instability energy pathways appear only in the recirculation regime. Energetically, the jet and recirculations are evidently parts of an inseparable whole; further observational and numerical investigations should be designed with that result in mind.

Chapter 4. Cross-sections of potential vorticity in the Gulf Stream

4.1 Introduction

Potential vorticity of a fluid is a dynamically important quantity because it is nearly conserved following fluid parcels if forcing, dissipation, and mixing are sufficiently small. Fofonoff (1962) and Stommel (1965), among others, have suggested modelling the Gulf Stream as a layer of water with uniform potential vorticity , which corresponds to q being constant on temperature (or density) surfaces, and simplifies the mathematics of the problem. On the other hand, if potential vorticity is not constant on surfaces of constant temperature, then if temperature is also conserved following fluid parcels, paths of flow may be determined from the intersection of surfaces of constant potential vorticity and constant temperature. Thus it is important to determine how potential vorticity is distributed on isothermal surfaces. Recent investigators mapping large scale potential vorticity fields in the oceans (McDowell et. al., 1982; McCartney, 1982) have recognized this point, but their work has been restricted to regions of relatively quiet flow, where q can be approximated by $f\theta_z$. From the GUSTO data set it is possible also to calculate the relative vorticity contributions $-u_y\theta_z$ and u_zT_y. The resulting potential vorticity section, when compared with the temperature structure in the Stream, should offer some insight as to whether a uniform potential vorticity model of the Gulf Stream is indeed appropriate.

The mean potential vorticity field of a quasi-geostrophic flow regime also determines the instability properties of the flow. In particular, the

following constitute a necessary condition for instability of the flow to
infinitessimal perturbations (see Pedlosky, 1979, for a good discussion):

In a zonally bounded flat-bottomed channel in which a basic flow
$U = U(y,z)$ only exists, then if:

1)The potential vorticity gradient q_y changes sign within the
flow; or

2)q_y is somewhere the opposite sign of U_z at the surface, or the
same sign as U_z at the bottom; or

3)U_z at the surface is the same sign as at the bottom, then the
flow may be unstable.

The easiest of these to test from data is whether or not q_y changes sign
somewhere in the flow; if it does, then the flow under consideration is
potentially unstable. Because isothermal surfaces depart markedly from
horizontal surfaces, the gradient of q on both will be examined, and the
results compared.

One test for the validity of a numerical model is how well it
reproduces the observed potential vorticity distribution of the real
ocean. Since the model jet is highly energetic, it is especially important
that this region be reproduced realistically. Thus, it is useful to
compare the observed potential vorticity distribution with that found in
the numerical model jet. Because the layers in the model are isopycnal, q
in each layer should again be compared with q along isothermal surfaces in
the data.

4.2 Potential vorticity section from the mooring data

It was established in Chapter 2 that the appropriate form for potential vorticity at the mooring site is

$$q = (f - u_y) \theta_z + u_z T_y.$$

To construct an average potential vorticity section, the mooring data were first divided into temperature bins determined by T_{575}. From $T_{575} = 4.5°C$ to $7.5°C$, and from $T_{575} = 13.5°C$ to $17°C$, the bins are $.5°C$ wide; from $T_{575} = 7.5°C$ to $13.5°C$, they are $1°C$ wide, giving a total of 19 bins. The average along stream velocity shear between the 400 and 700 m instruments was then calculated for each bin, and from these values, an average T_y was obtained for each bin. (Since only rotated velocities will be discussed, hat notation will be dropped for this chapter.) This average function $T_y(T)$ at 575 db was then integrated across all values of T_{575} to obtain y as a function of T_{575}. This procedure was completely analogous to that used in Chapter 2 to obtain a continuous function $y(T)$, only there the function $T_y(T)$ was determined continuously, as two best fit lines, rather than discretely. The values obtained both ways are compared in Table 4-1, where the origin for y is at $13.0°C$. Except at the very coldest estimate, the comparison is excellent. Next along-stream velocities at all depths were sorted into temperature bins and an average velocity for each bin at each depth was obtained: these values were assigned to the mid-points of the bin. In order to assure that along-stream velocity could go to zero at the edges of the average profile, average eastward (rather than along-stream) velocity was calculated in the warmest and coldest bins. The along-stream velocities were center

T_{575} (°C)	y(analytical) (km)	y(from average) (km)
4.5	97.5	123.5
5.0	78.9	82.2
5.5	66.1	65.3
6.0	56.4	55.0
6.5	48.5	46.6
7.0	41.9	40.9
7.5	36.3	35.7
8.5	26.8	27.5
9.5	19.2	20.5
10.5	12.7	13.8
11.5	7.2	8.3
12.5	2.3	2.6
13.5	-2.4	-2.6
14.0	-5.3	-5.4
14.5	-8.7	-8.9
15.0	-13.1	-13.0
15.5	-19.0	-19.8
16.0	-28.3	-30.7
16.5	-51.1	-50.8

Table 4-1. Intercomparison of horizontal coordinate values obtained analytically from equations 2-5, 2-6 with values obtained from averaging procedure described in Chapter 4. In both cases, y is set equal to zero at T_{575} = 13°C.

T_{575} Bin (°C)	Y_{center} (km)	$\hat{U\hat{y}}(575)$	$\hat{U\hat{y}}(875)$	$\hat{U\hat{y}}(1175$	$\hat{U\hat{y}}(2000)$	$\hat{U\hat{y}}(4000)$
		(All shears have units of $10^{-5}\ s^{-1}$)				
4.593						
4.997	85.9	-.688	-.398	-.391	-.403	-.387
5.340	79.1	-.814	-.459	-.415	-.455	-.469
5.899	62.2	-.623	-.199	-.147	-.235	-.262
6.400	51.9	-.351	.447	.064	.296	.427
6.982	44.5	-1.138	-.145	-.402	-.143	-.046
7.658	37.7	-1.181	-.292	-.384	-.325	-.241
8.463	31.1	-1.737	-.626	-.250	-.174	.015
9.441	24.4	-1.394	-.783	-.307	-.109	.271
10.405	17.5	-1.196	-.228	.111	.270	.324
11.475	11.3	-1.917	-1.100	-.191	-.140	-.218
12.410	5.5	-1.615	-1.303	-.414	-.215	-.149
13.276	0.7	-.799	-.826	-.231	.016	.069
14.013	-3.6	1.950	-.261	.140	-.207	-.314
14.590	-7.5	2.726	.117	.547	.065	-.214
15.142	-11.8	2.720	.170	.720	.442	.371
15.663	-18.1	2.700	.952	.852	.507	.374
16.113	-28.6	1.312	.647	.264	.156	-.039
16.374	-41.9	1.383	.927	.209	.200	.003
16.775	-49.6	1.958	1.496	.452	.388	.801

Table 4-2. Temperature bins arrived at for averaging procedure described in text, along with the value of y halfway between the end point values for each bin. Horizontal shear of long-stream velocity is from center-differencing average $\hat{u}$ values from Hall and Bryden (1984), except first and last values, which could not be centered.

finite-differenced to obtain estimates of $\partial u/\partial y$; because the calculated values of u are not evenly spaced in y, this step required calculating the new values of y (and hence T_{575}) to which $\partial u/\partial y$ values applied. Correspondingly, new temperature bins were also defined, as shown in Table 4-2, along with values of $\partial u/\partial y$. In the new temperature bins, average values of vertical temperature gradient and vertical shear of along-stream velocity were calculated from the mooring data for the top three standard levels. Taken all together, it is then possible to obtain estimates of q at three points in the vertical and 19 in the horizontal, from

$$q = (f - \overline{u}_y)\, T_z - \frac{\rho_o f}{g\alpha_o}\, \overline{u}_z^2 \, .$$

Simple linear interpolation or extrapolation was used to obtain continuous values of q in the vertical which were then contoured to provide the map of dashed lines shown in Figure 4.1.

The solid lines in Figure 4.1 are isotherms. This average temperature cross section was obtained as follows. At each y, values of T_{575} are already known; average values of T_{875} and T_{1175} were calculated for the corresponding temperature bins. Then the analytic fits for $\partial \theta/\partial z$ at each level (Raymer, Spencer and Bryden, 1984) were used to integrate up or down to obtain nearly continuous vertical profiles at each y. (The vertical gradient functions change form at 700 and 1000 m.) The temperature values were then contoured to yield the map of solid lines in Figure 4.1.

Figure 4.1 requires careful consideration. Recall that the map of q was constructed from only 3 points in the vertical. Thus, for example,

Figure 4.1. Cross-section of potential vorticity (dashed lines) and temperature (solid lines) at 68°W in the Gulf Stream, derived from GUSTO data, as described in text. Isotherms are labeled to right in °C, isostrophes to left in units of 10^{-7}°C/m/s.
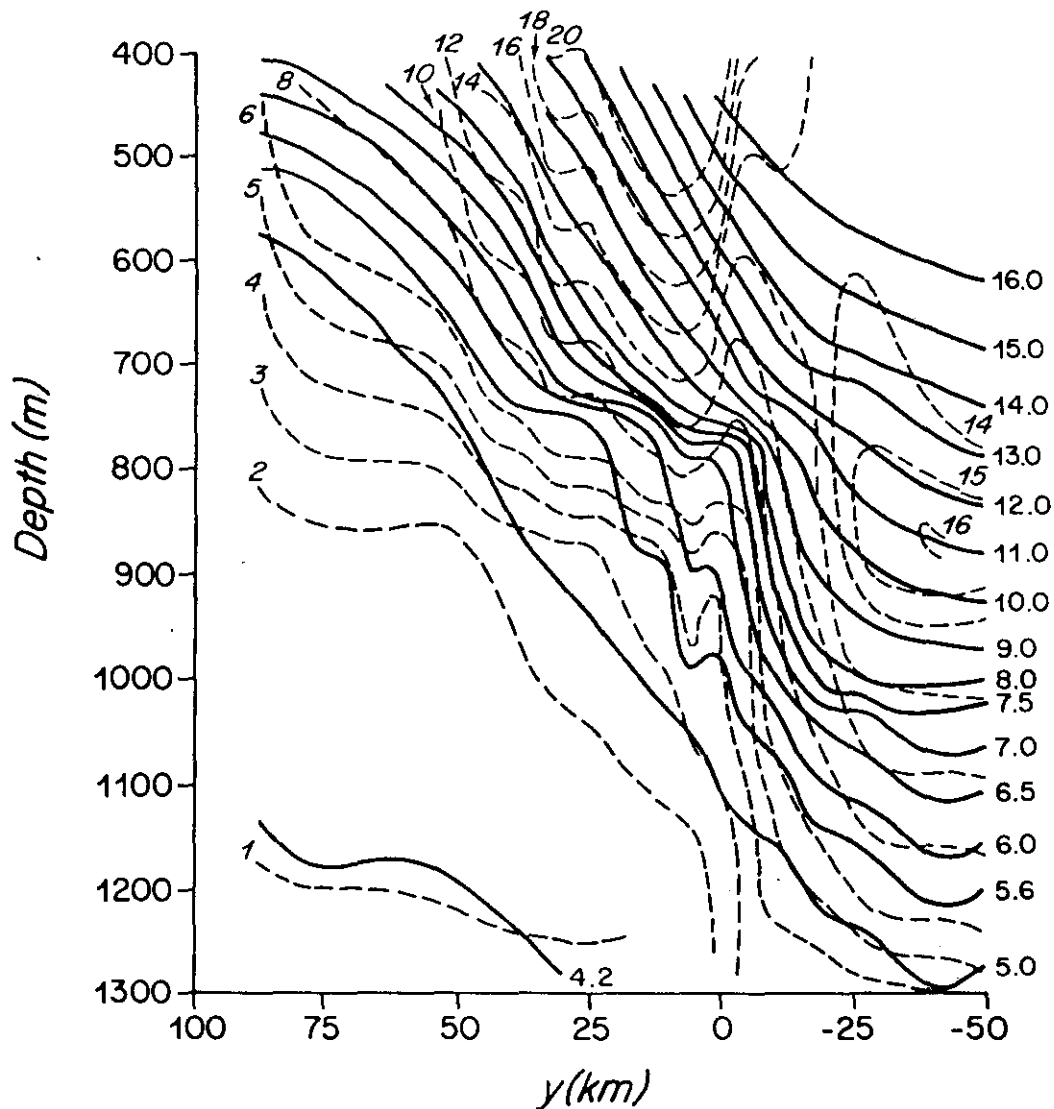
the mid-depth maximum at the southern edge is defined by nine points: at

the three southernmost values of y, estimates of q at 875 db are larger

than those above and below. The strong central maximum in the upper layer

results from estimates only at 575 db, but it is a well-defined trend at

this level. Comparison with a section from Watts (1983) as well as with

sections from the numerical model will show that certainly the latter

feature and probably the former feature are both real.

On the cold side of the Stream, for $T_{575} < 11^{\circ}C$, isotherms tend

to parallel isostrophes (lines of constant potential vorticity). Isotherms

for $T > 9^{\circ}C$ heading northward into the core of the Stream must cross

isostrophes almost perpendicularly, going from lower values in the south to

higher values in the north. In addition, most of these isotherms pass

through the weak relative minimum south of the core. Isotherms for

$T < 8^{\circ}C$, on the other hand, tend to lie on the same isostrophe at both the

southern and northern edges of the section; that they do not exactly

parallel isostrophes in between the endpoints may be due to the

uncertainties involved in creating the cross-section.

To complement Figure 4.1, q is shown as a function of y for

selected isotherms in Figure 4.2, which is derived simply by reading points

off Figure 4.1. These curves may be compared with the values derived from

the analytic expressions at 575 db and tabulated in Table 2-4: both

results display a strong "wall" in q near the jet axis, a minimum just

south of that, and an increase and subsequent leveling off as we head into

warmer waters, on isotherms $T = 11^{\circ}C$ and $14^{\circ}C$. The β-effect has not been

explicitly included in the estimates of q, and it is now shown that the

Figure 4.2. Values of potential vorticity q on various selected isotherms as a function of cross-stream distance y. Figure was derived directly from Figure 4.1.
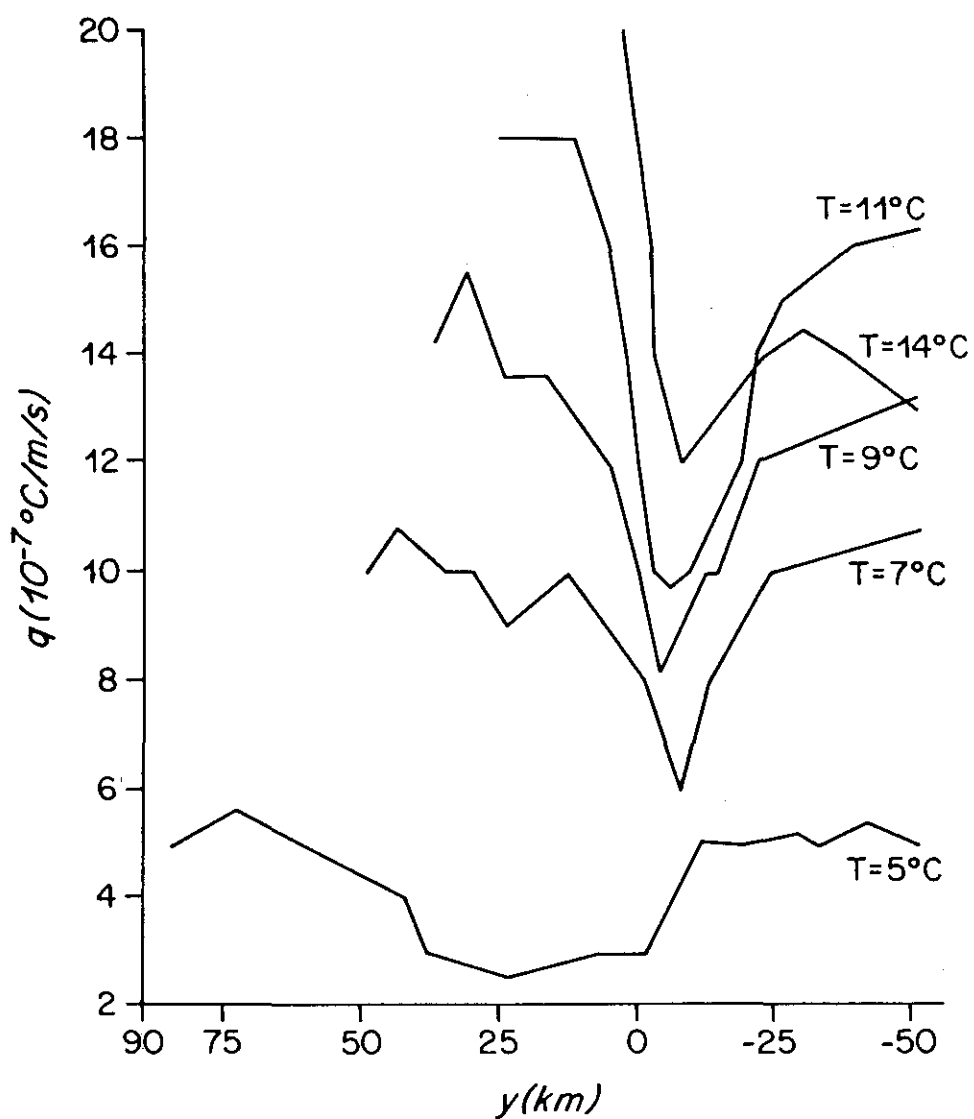
omission introduces very small errors. In the first place, $\beta y \ll f$ and even u_y: values of $\beta = 2 \times 10^{-11} m^{-1} s^{-1}$ and $y = 100$ km yield maximum values of $\beta y = 2 \times 10^{-6} s^{-1}$. The β-effect could still be important to the gradient of q. If β were included in the definition of q, two extra terms βT_z and $\beta y \, T_{zy}$ would appear in q_y. Estimates of q_y from Figure 4.2 are compared with estimates of βT_z in Table 4-3 (scale analysis suggests that $\beta y \, T_{zy}$ would be the same order as βT_z). The latter tends to be one to two orders of magnitude smaller than $\partial q / \partial y$, and clearly would not alter the major features displayed in Figure 4.1.

Values of q on the remaining isotherms are less easily interpreted. Endpoints of the 5, 7, and 9°C isotherms tend to lie on equal values of q, but all three exhibit a minimum near $y = 0$. Inspection of Fig. 4.1 shows that while the relative minimum between $y = 0$ and -25 km is well-defined above 800 m depth or so, it decays considerably below that, so that the appearance of a minimum on the 5°C and 7°C isotherms in Fig. 4.2 may be an artifact of the contouring in Fig. 4.1.

4.3 Comparison with past results

Watts (1983) discusses the potential vorticity distribution across the Gulf Stream, its relation to the general circulation, and its implications for instability. In particular, he points out the following important contrast: on the one hand, the uniformity of q in the gyre interior taken with conservation of q along streamlines, suggests that potential vorticity in the Gulf Stream ought to be uniform as well, since streamlines from the gyre feed the Stream. On the other hand, Watts says

T_{575}	y	z_T	T_z	q	q_y	βT_z
(°C)	(km)	(m)	(°C/m)	(10^{-7} °C/m/s)	(°C/m²/s)	(°C/m²/s)
				$T = 7°C$		
4.96	85.9	405	1.62×10^{-2}	6.45		3.1×10^{-13}
					-6.8×10^{-12}	
8.19	31.1	672	1.45×10^{-2}	10.17		2.8×10^{-13}
				$T = 11°C$		
12.86	0.7	659	2.51×10^{-2}	13.47		4.8×10^{-13}
					4.4×10^{-11}	
14.30	-7.5	715	2.30×10^{-2}	9.86		4.4×10^{-13}
					-1.4×10^{-11}	
16.47	-49.6	880	2.15×10^{-2}	15.91		4.1×10^{-13}
				$T = 14°C$		
12.86	0.7	532	2.33×10^{-2}	18.86		4.4×10^{-13}
					8.2×10^{-11}	
14.30	-7.5	597	1.99×10^{-2}	12.15		3.8×10^{-13}
					-1.1×10^{-11}	
15.90	-28.6	698	1.90×10^{-2}	14.48		3.6×10^{-13}

Table 4-3. Comparison of β effect with total potential vorticity gradient. Values of q for isotherms come essentially from Figure 4.1. Values of T_z are from analytic fits of Raymer et al. (1985). β is taken as 1.9×10^{-11} m^{-1} s^{-1}.

that "for all isopycnal layers in and above the main thermocline, $q \sim f\, T_z$ is several times higher in the Slope Water than in the Sargasso Sea;" hence, a strong jump in potential vorticity must occur across the Stream. The same features were noted much earlier by Stommel (1965), who demonstrated the uniformity of potential vorticity across the Stream, from the Sargasso Sea to the inshore edge of the Stream, where there is a sharp discontinuity in q.

Two of Watts' (1983) figures may be compared with Figures 4.1 and 4.2. His Figure 12 is a section of potential vorticity across the Gulf Stream near 73°W, from the surface to 800 m depth, with isotherms superimposed. Curiously, below 400 m in this figure, isotherms tend to parallel isostrophes consistently, while above 400 m features very similar to those seen in Figure 4.1 may be found. In particular there is a strong maximum in q lying just around the axis of the Stream, with q increasing upward. This feature corresponds to the high q values lying between y = 0 and 25 km, at depths of 400-700 m in Fig. 4.1. Just south of the maximum is an intermediate minimum reaching down from above, much like the minimum in Figure 4.1 lying between y = 0 and -25 km, at depths of about 500-800 m. In general, the highest values Watts finds for q below 400 m are in the range $2 - 3 \times 10^{-6}\,°C\ m^{-1}\ s^{-1}$, slightly higher than the values calculated here.

Watts' Figure 15, which shows potential vorticity across the Stream for the 12°-17°C layer near 69°W, may be compared with the 14°C isotherm in Figure 4.2. The latter shows this isotherm rising from its minimum value of $q = 1.2 \times 10^{-6}\,°C\ m^{-1}\ s^{-1}$ to its maximum value (below 400 m) of

$2 \times 10^{-6}°C \ m^{-1} \ s^{-1}$ about 10 km northward; Watts' Figure 15 shows an increase from a similar minimum of $1 - 1.2 \times 10^{-6}°C \ m^{-1} \ s^{-1}$ to a maximum of around $4 \times 10^{-6}°C \ m^{-1} \ s^{-1}$ some 40 km northward (where this layer lies well above 400 m). Moving southward, both figures show a slight increase and subsequent decrease in q over similar horizontal scales (50-60 km). Watts' figures were constructed partly from recent hydrographic data and partly from a section taken by Warren and Volkmann (1968), when deep reference velocities were measured by floats. The present evaluation has the advantage of direct velocity measurements throughout the water column, as well as greater coverage in time, so that Fig. 4.1 may be considered an average and not a synoptic section.

Now consider the issues raised in the introduction to this chapter. A two-layer model for a free zonal inertial jet with uniform potential vorticity is governed by the following equations:

$$\frac{f - u_y}{h} = \frac{f}{h_0} \qquad fu = - g \frac{\partial h}{\partial y} \qquad y \leq 0$$

$$h = 0 \text{ at } y = 0; \quad h \longrightarrow h_0 \text{ as } y \longrightarrow -\infty$$

$$h = u = 0 \qquad\qquad\qquad y > 0$$

where h is the upper layer depth, h_0 is the quiet upper layer depth far to the south, and the lower layer is at rest. These may be solved to obtain:

$$h = h_0(1 - e^{\lambda y}), \qquad u = (gh_0)^{1/2} e^{\lambda y}, \qquad \lambda = (f_0)/(gh_0)^{1/2}$$

Thus, the zonal velocity jumps discontinuously from zero to its maximum value where the upper layer depth goes to zero, then decreases exponentially across the jet towards the interior, and the flow in the jet

is everywhere anti-cyclonic, so that this model cannot be expected to describe the cyclonic portion of the observed jet. In isothermal layers at temperatures lying above those observed at the mooring, there evidently is a tendency towards uniform q in the anti-cyclonic portion of the Stream (Watts, 1983; Stommel, 1965); between y = -25 and -50 km in Fig. 4.1, there is a suggestion that the isotherms for T = 10 to 13 $^\circ$C may be starting to parallel isostrophes as the interior is approached. Thus it is likely that the two-layer inertial jet model gives a reasonable rendition of the steady (average) cross-stream structure of velocity in that portion of the Stream.

Investigation of the potential vorticity gradient q_y can lead to a fuller understanding of the dynamics of the Stream, beyond the prediction of average cross-stream structure. Two features of q_y are of predominant importance. One is the possibility that q_y changes sign across the Stream; the other is the strength of the gradient near the Stream axis. Each point will be addressed in turn.

It has been noted that a necessary condition for the baroclinic instability of a zonal flow under certain conditions is that q_y change sign somewhere in the basic flow. This condition can be easily tested with data, but one must be cautious in applying these criteria to the potential vorticity and velocity fields at the mooring site, for various reasons. The criteria are meant to apply to quasi-geostrophic flow, and although the Rossby number of flow at the mooring site is generally ≤ 0.3, the non-quasi-geostrophic term $u_z T_y$ is as much as 25 percent the size of q, and its gradient may be as large as q_y.

Figure 4.3. Values of potential vorticity q on the 575 db surface as a function of cross-stream distance y at the mooring site, and individual components making up total potential vorticity. Key: dashed line = total q; solid line = $f\theta_z$; dash-dotted line = relative vorticity $(-u_y\theta_z)$; dotted line = $u_z T_y$.
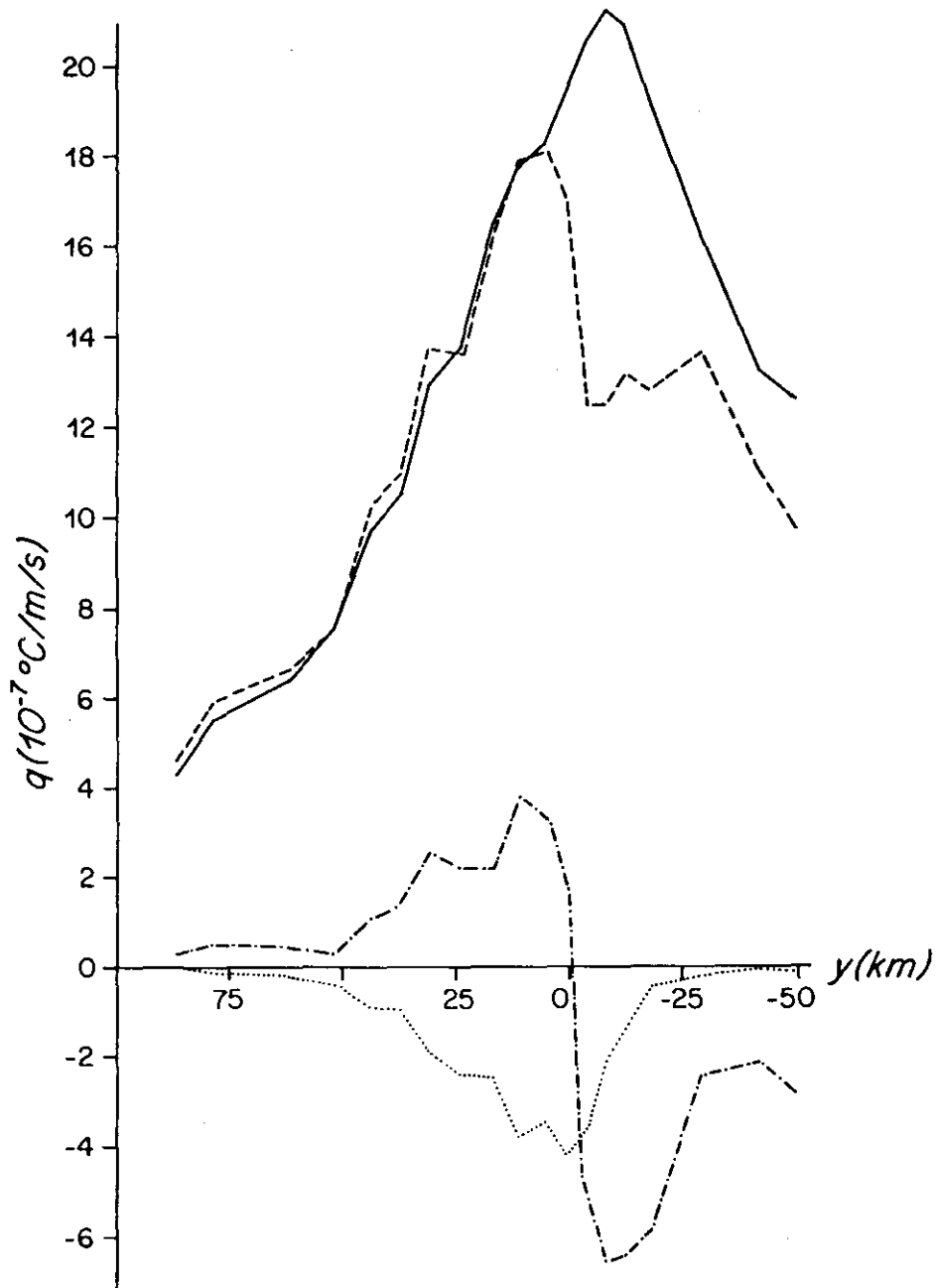
Figure 4.3 shows potential vorticity and its components at a
horizontal level, 575 dbar. There is a pronounced maximum near the core of
the Stream, as in Fig. 4.1, and moving southward, a rather weak relative
minimum between $y = -25$ and -50 km. Notice that $q_y < 0$ to the north of
the maximum is misleading in this figure; a glance at Figure 4.1 shows
that q tends to become uniform on isotherms in this region. The vertical
and horizontal relative vorticity contributions combine to affect the
potential vorticity profile in two ways. North of the maximum, they very
nearly offset each other so that $q \sim f T_z$. However, passing through the
Stream axis, where u_y changes sign, the combined strongly negative
values of $-u_y T_z$ and $u_z T_y$ are enough to offset significantly the
maximum in q from that in $f T_z$, and to produce the weak minimum just
south of there. In the region where q_y is slightly negative, its
average value is -4.5×10^{-12} °C m^{-2} s^{-1}; over the same region, β would
contribute to the gradient a term of the size $(2.8-4.5) \times 10^{-13}$ °C m^{-2} s^{-1},
an order of magnitude smaller. Moreover, recall that isotherms are sloping
downward to the south, thus passing through the minimum and into higher
values of q than appear at $y = 22$ km in Figure 4.3 (see Figure 4.1). It
would appear that q_y changes sign on a horizontal surface as well as on
isothermal surfaces. Deeper down, q_y tends to be of one sign
($q_y > 0$; see Figure 4.1), so it is only in the upper part of the water
column $(T > 9°C)$ south of the core that $q_y < 0$ somewhere in the
Stream. If the Gulf Stream can be modeled as a quasi-geostrophic zonal
flow confined to a channel (or at least restricted from exchanging energy
with its environs), then linear baroclinic instabilities could arise in the

current. So many qualifications are required in drawing this conclusion that it should be considered a guideline to further studies rather than a concrete result.

Inspection of a potential vorticity section constructed from the GUSTO velocity and temperature data establishes that isostrophes generally parallel isotherms north of $y = 10$ km; south of that, there are two distinct regimes according as T is greater or less than about $10°C$. For $T < 10°C$, isostrophes and isotherms remain parallel. For $T > 10°C$, there are strong changes in potential vorticity on isotherms, including reversals in the sign of q_y when $T \geq 12°C$, or on horizontal surfaces above 700 m. Relative vorticity contributions to q are as large as 25 percent, and their gradients may be as large as q_y itself, which has typical values an order of magnitude greater than the β-effect. Finally, there is a very striking change from low to high values of q on isotherms $T \geq 10°C$ near $y = 0$, which appears as a "wall" of potential vorticity when $q(T = \text{constant})$ is plotted as a function of y, as in Fig. 4.2.

This strong "wall" in potential vorticity across the Gulf Stream has immediate implications. The sharp transition from low to high values suggests that the thermocline Gulf Stream is a potential vorticity front and can be modeled as an interface between two types of water of different potential vorticity. Pratt and Stern (1985), using such a model, have been examining the time growth of large amplitude meanders on the interface, including the "wave-breaking" of the meanders. The study should be more relevant to the development of Gulf Stream rings and meanders than linearized instability models (Talley, 1982, e.g.), because it includes

large amplitude non-linear effects.

The other immediate implication is for the motion of water parcels in the Gulf Stream. In the absence of strong forcing, dissipative or mixing mechanisms, water parcels tend to conserve their temperature (density) and potential vorticity. It is anticipated that over long downstream distances, the potential vorticity of a water parcel may be modified due to relatively weak processes, though quantifying these changes is a difficult problem. On the other hand, it is unlikely that a water parcel on the $12°$ isotherm, for example, encounters processes sufficiently strong to change its potential vorticity from 12 to 20 x $10^{-7}°C\ m^{-1}\ s^{-1}$, the change in potential vorticity on that surface over just 50 km. (Even if θ_z had values as strong as $.02°C/m$, as it does only at 575 dbar in the core of the Stream, a change in q of 8 x $10^{-7}\ °C/m/s$ would correspond to increasing f by 0.4 x $10^{-4}s^{-1}$ -- in other words, a water parcel from $37°N$ would have to go to about $63°N!$) Thus, for all water with T > $9°C$, there is a strong constraint against cross-stream excursions of water parcels, due to the potential vorticity wall there. Deeper down, where isotherms and isostrophes tend to be parallel, this constraint is relaxed, suggesting that water parcels should have little trouble in crossing the Stream. This conclusion is entirely in accord with what has been observed numerous times in data from SOFAR floats: namely, that floats tracked at 700 m always seem to get caught by the Gulf Stream once they encounter it, while tracks from floats at 2000 m hardly reveal the existence of the Stream above, and apparently have no difficulty in crossing from one side to the other. Although they are isobaric rather than isopycnal floats, the same reasons

for their behavior can be expected to apply, since (as we have seen) the potential vorticity wall exists on horizontal surfaces as well.

Owens (1984) has recently discussed the tracks of 17 such floats deployed at 700 and 2000 m in or near the Gulf Stream. He concludes that the difference in float trajectories could be attributed to the relation between particle speeds and the propagation speed of meanders: "At shallow depths, the particles are advected along the meandering flow field while at depth, parcels of water cannot move sufficiently fast enough to stay with the meander patterns." He further suggests that the difference between isobaric and isopycnal surfaces could induce an "artificial dispersion" beneath the thermocline Gulf Stream. The results presented here, however, suggest that an isopycnal float could behave in much the same way, as there is no apparent dynamical constraint against cross-stream movement.

4.4 Comparison with numerical model results

Lastly cross-sections of potential vorticity in the jet of Holland's numerical model 3L-4 are examined. Because the density is constant in each layer, a cross-section of potential vorticity in a model layer corresponds to that on an isothermal surface in the data. Also, since the numerical model has been constructed in a quasi-geostrophic framework, just the quasi-geostrophic potential vorticity has been examined. Temperature does not appear explicitly as a variable in the numerical model formulation, but rather implicitly in the variation of layer thicknesses from their rest depths. Then, the quasi-geostrophic potential vorticity for layer k

$$q_k = \frac{f_0 + \beta y + \nabla^2 \psi_k}{H_k + h_{k-1/2} - h_{k+1/2}} \approx \frac{1}{H_k}(f_0 + \beta y + \nabla^2 \psi_k + \frac{f_0}{H_k}(h_{k-1/2} - h_{k+1/2}))$$

+ (order Rossby number terms), since $\frac{h}{H} = O(\epsilon)$.

Then, because the H_k are constant, q_k is more simply defined as in (3-4), repeated here for individual layers:

$$q_1 = f_0 + \beta y + \nabla^2 \psi_1 + \frac{f_0 h_{3/2}}{H_1} = f_0(1 + \frac{h_{3/2}}{H_1}) + \beta y + \nabla^2 \psi_1 \qquad (4-1a)$$

$$q_2 = f_0 + \beta y + \nabla^2 \psi_2 + \frac{f_0(h_{5/2} - h_{3/2})}{H_2} = f_0(1 + \frac{h_{5/2} - h_{3/2}}{H_2}) + \beta y + \nabla^2 \psi_2 \qquad (4-1b)$$

$$q_3 = f_0 + \beta y + \nabla^2 \psi_3 - \frac{f_0 h_{5/2}}{H_3} = f_0(1 - \frac{h_{5/2}}{H_3}) + \beta y + \nabla^2 \psi_3 \qquad (4-1c)$$

The units of potential vorticity in this system are not the same as shown in Fig. 4.1, but the terms are analogous. (Multiplying (4-1) by some value θ_z yields the same units.) The first term of the far RHS will be referred to as the stretching term, and corresponds to $f\theta_z$ in the form used for the mooring data.

The limited vertical resolution of the numerical model and the mooring data demands that care be taken in comparing the two. The top layer of the model reaches to only 300 meters' depth, while the mooring data extends no farther up than 400 m. However, it will be found that the structure of potential vorticity in the top layer is comparable to that at thermocline levels at the mooring site. In the downstream direction, there is little qualitative change in the model q profiles over many hundreds of kilometers; the section examined has been chosen for computational reasons, and is 20 km downstream from the boundary between accelerating and

decelerating jet flow.

Figure 4.4 (a through c) shows the potential vorticity profile for
each of the three layers, with f_0 subtracted out, and with the various
components plotted as well. (Subtracting out f_0 would be comparable to
subtracting out a value of $f\bar{\theta}_z$ from the form used on the data, where $\bar{\theta}_z$
at a level was a spatial average over the whole domain.) First consider
the potential vorticity cross-section for the top layer, Figure 4.4a.
Throughout the domain, variations in q are dominated by the stretching
term, while β makes a very small contribution, and relative vorticity is
important only in the jet. There is a strong gradient of q in the jet,
with a weak minimum and secondary maximum to the south. Although these
latter features are present in the stretching term alone, they are
accentuated by the contribution of relative vorticity to the profile. The
comparison with Figure 4.3, showing q at 575 dbar, is quite remarkable.
Absolute magnitudes of potential vorticity may be compared by dividing q
in Figure 4.3 by a typical value of θ_z at 575 dbar of .015 °C/m, then
subtracting out $f_0 = .89 \times 10^{-4}\text{s}^{-1}$. Then, for example, the peak
value of q in Fig. 4.3, $q = 18 \times 10^{-7}$°C/m/s, becomes $q' = (q/\theta_z) -$
$f_0 = 3.1 \times 10^{-5}\text{s}^{-1}$, which is somewhat less than the maximum values of
q in Fig. 4.4a. In both profiles the stretching term is dominant; the
ratio of relative vorticity to stretching is about 25 percent where
attains its maximum value in both figures; and the β-effect is an order of
magnitude smaller than the stretching terms. The qualitative resemblance
between Figure 4.4a and one of the isothermal profiles of q shown in
Figure 4.2, such as $T = 14$°C, is equally important: there is the potential

Figure 4.4. Values of quasi-geostrophic potential vorticity Q from Holland numerical model 3L-4. Sections are 720 km east of western boundary. Individual components are indicated directly on figure. Horizontal lines in lower half mark off boundaries between energetic regions referred to in Chapter 3. a)Layer 1; b)layer 2; c)layer 3.
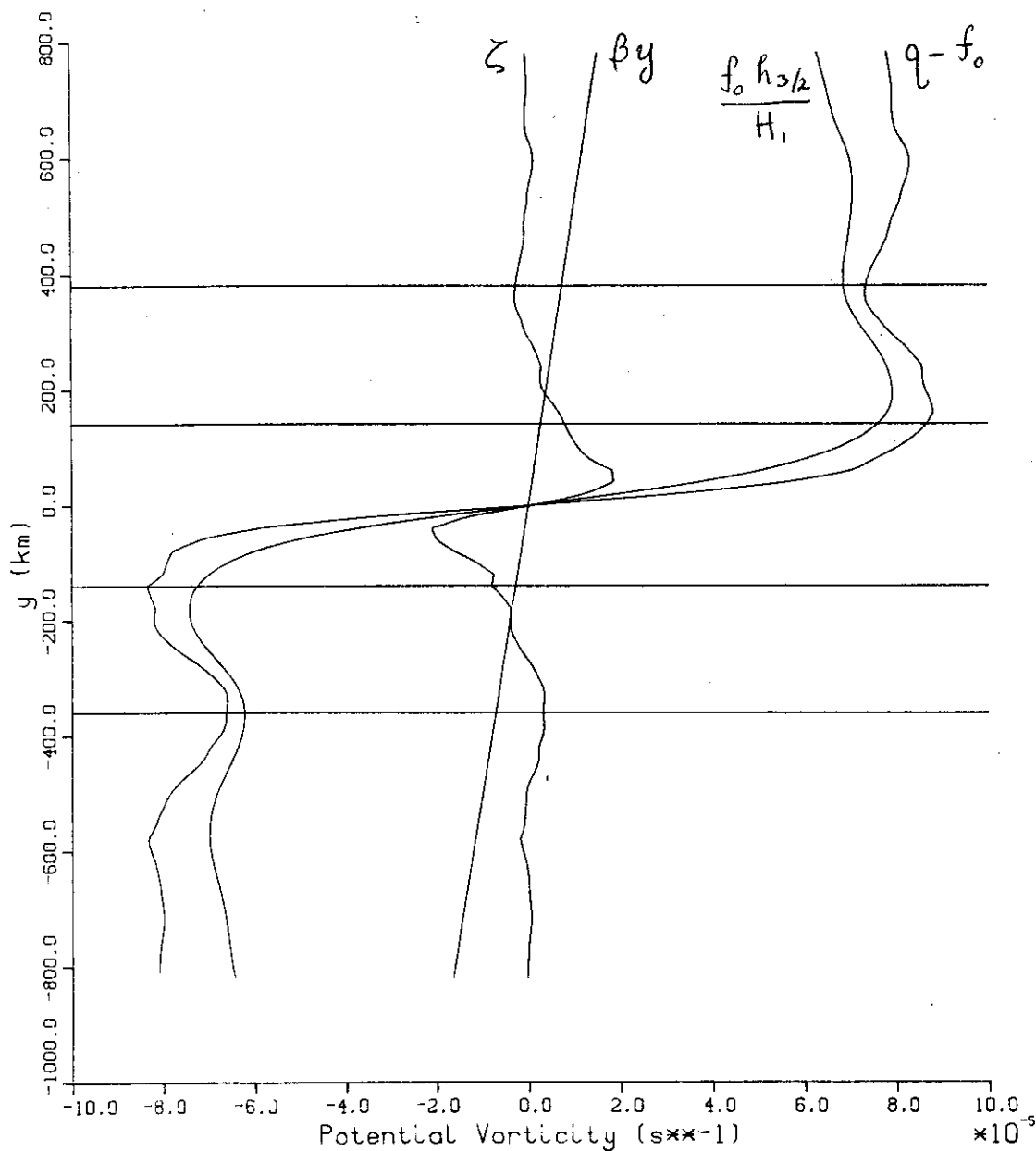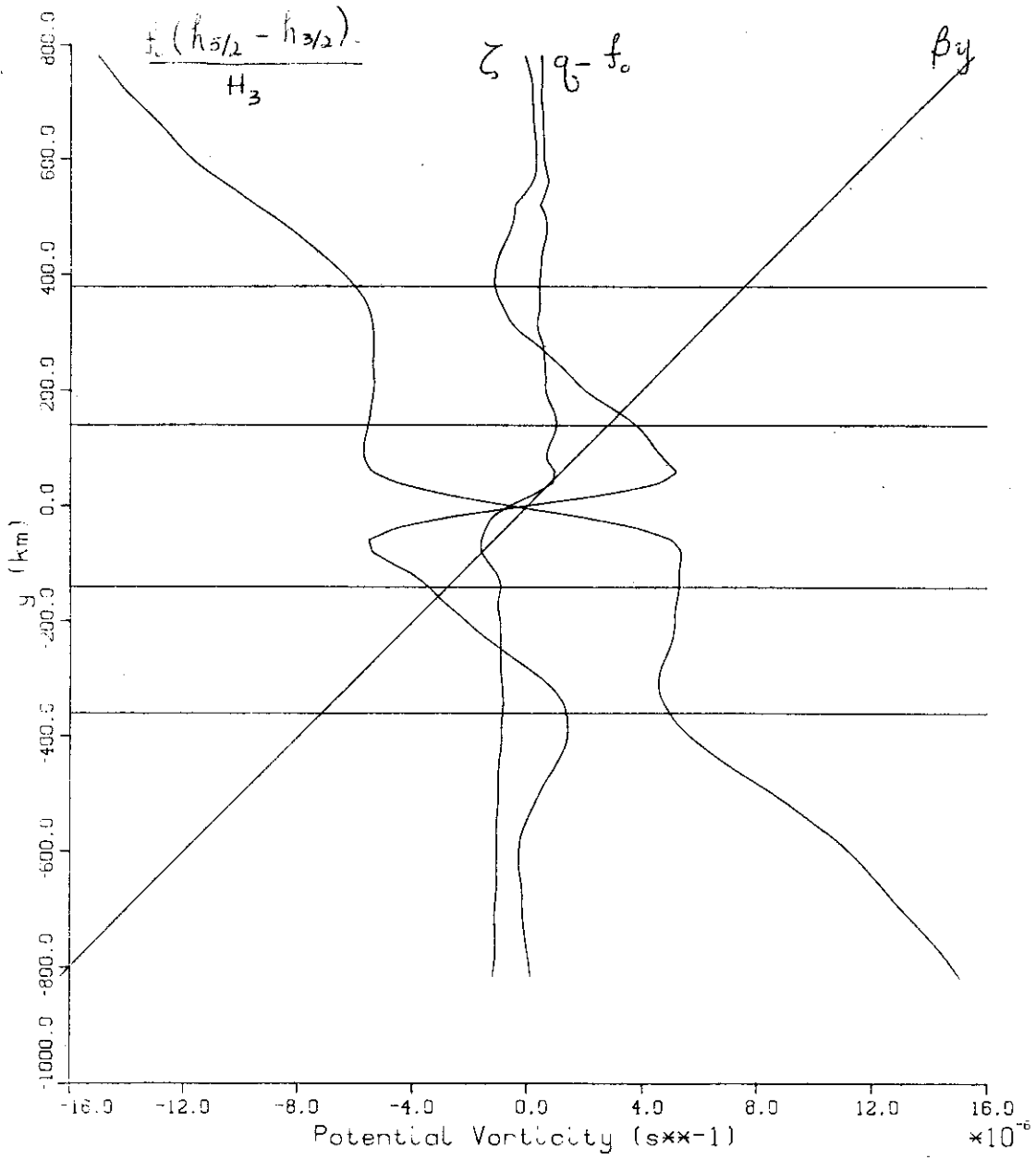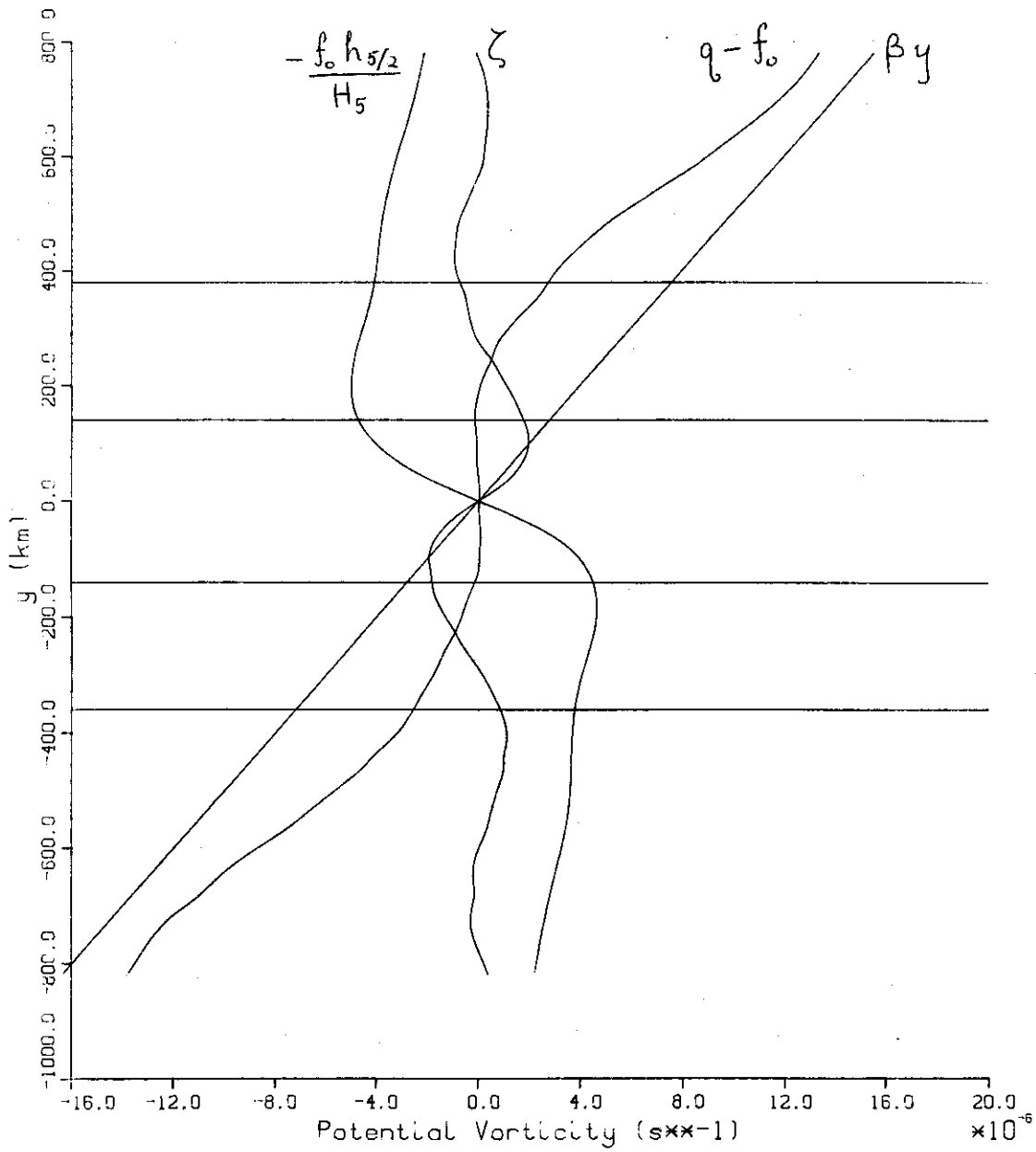
Figure 4.4b

Figure 4.4c

vorticity wall at or near the jet axis, a minimum to the south, and a secondary maximum south of that. The potential vorticity to the north of the wall in Fig. 4.4a does not decrease as does q at 575 dbar, but again that is due to the difference in evaluating q on isothermal and horizontal surfaces.

Notice in Figure 4.4a that the jet region, as characterized by the energetic analysis, corresponds almost exactly to the region over which q forms the strong wall: in other words, the gradient of q does not change sign in the jet in this layer, though Figures 4.4b and c show very weak reversals in q_y deeper down. On the basis of these features, it might be anticipated that baroclinic instability would not emerge as a major energetic component in the jet region; indeed in Chapter 3 that was found to be the case. On the other hand, the recirculation region of layer 1 shows $q_y < 0$ for the most part, so that if the jet and recirculation areas are considered together q_y indisputably changes sign just within the top layer. In Chapter 3 it was found that all the regions are coupled energetically, particularly these two, so that trying to apply a channel model to the model jet is unrealistic; clearly the recirculation region needs to be considered, especially if one anticipates the existence of baroclinic instability. Talley (1982) drew a similar conclusion from a study of two-layer jets flanked by "westward recirculations."

Now consider Figures 4.4b and c more closely. The abscissa scale on these two figures is different than that of Figure 4.4a, as is evident by the rather dominant contribution of βy in each case. The middle layer profile shows nicely the homogenization of potential vorticity mentioned in

Chapter 3, and how it arises for the various regions. In the Sverdrup region, stretching and β offset one another; this same balance between layer thickness and the planetary vorticity tendency has been documented numerous times for mid-depth subtropical gyre flow in the North Atlantic (see, e.g., Luyten et al., 1983; or McDowell et al., 1982). In the jet region the primary balance is between stretching and relative vorticity, with a slight net increase in q going northward through the jet. In the recirculation region, the layer thickness is nearly uniform, and it is the relative vorticity offsetting β that produces uniform q. It is difficult to make close comparisons between the middle layer profile and mooring data, except to note that in the latter there was a tendency for q to be constant on isotherms for $T < 8°C$, that is, below the thermocline.

Finally, Fig. 4.4c shows the deep layer profile, though comparison with the mooring data is tenuous at best. Potential vorticity variations are dominated by βy in that layer, except in the jet region where the profile is fairly flat. Not only is there no suggestion of a potential vorticity "wall" in this layer, but q_y is actually slightly negative underneath the jet. The 5°C isotherm in Figure 4.3 shows that while q tends to be constant on deep isotherms, possibly q_y is slightly negative beneath the Stream axis (and positive again farther north), according to the mooring data. However, the similarity between these results is probably fortuitous, for the values of q at 1175 dbar are dominated by changing T_z, rather than by βy as in the deep layer of the numerical model. The dominance of βy in that layer is a signature of

the absence of thermohaline forcing in the model, which could produce meridional flow in the deep layer, thus requiring isostrophes to depart significantly from latitude circles. The structure of $\partial T/\partial z$ (or $\partial \rho/\partial z$) in the ocean -- prescribed as density jumps in the model -- may in fact be determined to some extent by thermohaline processes.

4.5 Summary

There are a number of ubiquitous features which appear in the observed structure of the Gulf Stream and its analog in theoretical and numerical models. First of all, there is a tendency towards uniform potential vorticity in the shallower part of the anti-cyclonic portion of such jets. Second, the core of the thermocline jets is characterized by a strong gradient in q, or a potential vorticity wall, along isothermal surfaces. In a way, even the two-layer inertial jet model contains this feature, for where the interface of the top layer surfaces there is a discontinuity in potential vorticity. Finally, below the thermocline, the observational and numerical data suggest that potential vorticity is uniform on isothermal (isopycnal) surfaces.

The implications of these features have been discussed at length, but are reiterated here for emphasis. A uniform potential vorticity model is at best appropriate for describing the cross-stream structure of the anti-cyclonic part of the jet. Modeling the thermocline Gulf Stream as a potential vorticity front is better for investigating large amplitude meandering, while linearized instability models have dubious application even though q_y changes sign across the Stream. Finally, the difference

in shallow and deep potential vorticity structure may be largely
responsible for the difference in the Lagrangian flow patterns observed in
different parts of the water column.

Chapter 5. Speculative results and interpretations of mooring data

5.1 Introduction

In Chapters 2 and 4 it was demonstrated that by using an inferred horizontal coordinate, it was possible to describe the average velocity and potential vorticity of the Stream, or calculate fluxes of mass, momentum and kinetic energy for four separate events when the Gulf Stream passed across the mooring site. Moreover, the results obtained are in good agreement with past results, obtained primarily from hydrographic, float, and current profiler data all the way across the Stream.

In this chapter, the energetics and dynamics at the mooring site are examined. In particular, the year-long time series of data ought to provide new insight into the energetic exchanges between mean and eddy flows, since for the first time there are concurrent records at thermocline and abyssal depths. It has proven difficult to address the dynamics governing this complicated flow, but a kinematical picture may be deduced. Finally, in view of what has been been possible with the GUSTO data set and what questions remain unanswered, suggestions are presented for the directions future programs might fruitfully pursue.

5.2 Energetics at the mooring site

In order to discuss energy exchanges between mean and eddy flow, it is necessary to be able to define the two. Although it has been possible to describe an average Gulf Stream profile with horizontal and vertical structure, it is unlikely that there is sufficient data to discuss deviations from that average. Yet if the strict time average of flow at

each depth is examined, the horizontal information pertinent to a discussion of the role of barotropic instability is lost.

Two compromises are made in discussing the eddy kinetic and potential energy equations. First, they are considered in the unrotated frame rather than the rotated because the time-averaging involved in obtaining the equations introduces an interpretative problem; in addition, this approach is more traditional and is more readily compared with past results as well as the numerical results of Chapter 3. Second, horizontal resolution is limited to two bins, corresponding to $T_{575} <$ 13°C (north of the Stream axis) or $T_{575} > 13°C$ (south of the axis).

The equation for eddy kinetic energy $\overline{K'} = (1/2)\rho(\overline{u'^2} + \overline{v'^2})$ has been discussed in some detail already; it is obtained by adding u'x(u-momentum equation) + v'x(v-momentum equation) and then time-averaging:

$$(\frac{\partial}{\partial t} + \bar{u}\frac{\partial}{\partial x} + \bar{v}\frac{\partial}{\partial y})\overline{K'} = -\nabla_H \cdot \rho(\vec{u}_H x \frac{\overline{u'^2} + \overline{v'^2}}{2}) - \overline{u'v'}(\bar{v}_x + \bar{u}_y) - \rho\overline{u'^2}\bar{u}_x$$

$$- \rho\overline{v'^2}\bar{v}_y - \overline{\vec{u}_H' \cdot \nabla_H p'} \tag{5-1}$$

where the subscript H is used to mean the horizontal components only. Similarly, the equation for eddy potential energy $\overline{P'} = \frac{1}{2}(g\alpha_0\overline{T'^2})/(\bar{\theta}_z)$ obtained by multiplying equation (2-15) by $g\alpha_0 T'/\bar{\theta}_z$ and time-averaging is:

$$(\frac{\partial}{\partial t} + \bar{u}\frac{\partial}{\partial x} + \bar{v}\frac{\partial}{\partial y})\overline{P'} = \frac{-g\alpha_0}{\bar{\theta}_z}(\overline{u'T'}\,\bar{T}_x + \overline{v'T'}\,\bar{T}_y) - g\alpha_0\overline{w'T'} -$$

$$\nabla_H \cdot (\overline{\vec{u}'T'^2}\, g\alpha_0/2\bar{\theta}_z) \tag{5-2}.$$

Recalling that $-\vec{u}'_H \cdot \nabla_H p' = -\nabla_H \cdot p'\vec{u}'_H - p'w'_z = -\nabla_3 \cdot p'\vec{u}'_3 + w'p'_z =$

$-\nabla_3 \cdot p'\vec{u}'_3 - g\rho'w' = -\nabla_3 \cdot p'\vec{u}'_3 + g\alpha_0 w'T'$, (5-1) and (5-2) can be added to get the equation for the total eddy energy:

$$(\frac{\partial}{\partial t} + \bar{u}\,\frac{\partial}{\partial x} + \bar{v}\,\frac{\partial}{\partial y})(\overline{K'} + \overline{P'}) = -\nabla_H \cdot \overline{\vec{u}'(K'+P')} - \overline{\rho u'v'}(\bar{v}_x + \bar{u}_y) -$$

$$\frac{g\alpha_0}{\bar{\theta}_z}(\overline{u'T'}\,\bar{T}_x + \overline{v'T'}\,\bar{T}_y) - \rho\bar{u}_x(\overline{u'^2} - \overline{v'^2}) - \overline{\nabla_3 \cdot p'\vec{u}'_3} \qquad (5-3).$$

The total eddy energy may be modified by essentially two types of terms that appear on the RHS of equation (5-3): 1)exchanges between the mean and eddy flows, represented by up- or down-gradient momentum and heat fluxes; and 2)"radiating" terms, which appear as divergences of quantities depending only on the eddy field. From (5-1) and (5-2) it is clear that the exchange between eddy kinetic and potential energies is given by the term $\pm\ g\alpha_0 \overline{w'T'}$, which appears with opposite sign in the two equations.

To assess the relative importance of terms on the RHS of (5-3) in a gross rather than localized sense, one ought to integrate over a volume, as in Chapter 3. Integration in z is possible because of the mooring's vertical resolution; to achieve integration in y, two separate temperature bins, corresponding to regions north and south of the Stream axis, have been used for the time-averaging process; integration in x poses some difficulty and will simply be ignored, since only a rough qualitative picture is sought. Furthermore, it is useful to recognize that even in unrotated coordinates, it is true that $\bar{v}_x << \bar{u}_y$, and $\overline{v'^2} << \overline{u'^2}$, so that the net mean-to-eddy momentum exchange is

approximately given by $-\rho\overline{u'v'}\bar{u}_y - \rho\overline{u'^2}\bar{u}_x$. To calculate the

Reynolds stress u'v', all the data were divided into two bins according

to whether T > 13°C. or T < 13°C (where u_y changes sign). Then, for

each of the new data sets, mean and eddy velocities were computed, as was

the product $\overline{u'v'}$. These values are given in Table 5-1. The accompanying

values of $\bar{u}_y$ were obtained by taking $\bar{u}_y$ at 575 dbar equal to

e^{-1} times the maximum value attained analytically from (2-8,9). The

magnitude is assumed to decay with depth on an e-folding scale of 1000

m. The width of the anticyclonic side is taken as 50 km, the distance

from $T_{575} = 13°C.$ to 16.5°C.; on the cyclonic side, $\Delta y = 80$ km (T_{575}

= 5°C. to 13°C.).

Previous long time-series from measurements in the deep water (4000

m) beneath the Gulf Stream (Schmitz, 1977) have suggested that $\overline{u'v'}$

changes sign across the axis (geographical average) of the Stream over

perhaps 2-3 degrees of latitude, such that there is a flux of eddy to

mean kinetic energy ($\overline{u'v'} > 0$ south of the Stream); directly under the

axis, $\overline{u'v'} < 0$ and has magnitudes of 5-15 $cm^2 s^{-2}$. The Reynolds

stresses in the deep part of the water column here are not terribly

different for the two bins, but they do not change sign across the Stream

axis. In addition, $(\overline{u'v'})_y > 0$ across the Stream, the opposite sense

of Schmitz's findings. However, the results in the upper 1000 m, which

will make the greatest contribution to the net momentum exchange because

$\bar{u}_y$ is strongest there, are remarkably different from all the deep water

values. For both bins (i.e., on both "sides" of the Stream), $\overline{u'v'}$ is

large and negative, and $(\overline{u'v'})_y > 0$, so the more negative values

Depth (db)	Δz (db $\sim$ m)	$T_{575} < 13°C$			$T_{575} > 13°C$		
		$\overline{u'v'}$ (cm^2/s^2)	C	$\overline{u}_y$ (10^{-5} s^{-1})	$\overline{u'v'}$ (cm^2/s^2)	C	$\overline{u}_y$ (10^{-5} s^{-1})
575	725	-321.52	-.34	-.952	-424.70	-.49	2.234
875	300	-45.40	-.25	-.706	-115.28	-.38	1.655
1175	563	-34.56	-.27	-.523	-11.44	-.16	1.226
2000	1412	-12.64	-.14	-.229	-5.83	-.13	.537
4000	1688	10.65	0.16	-.031	8.71	0.22	.073

$\rho = 1.027$ gm/cm^3

$\Delta y = 80$ km $\qquad\qquad\qquad\qquad \Delta y = 50$ km

$- \sum_{T<13} \overline{u'v'} \, \overline{u}_y \rho = -251.9$ gm/s^3 $\qquad$ $- \sum_{T>13} \overline{u'v'} \, \overline{u}_y = 776.6$ gm/s^3

$$- \int dy \int dz (\rho \, \overline{u'v'} \, \overline{u}_y) = 1.867 \times 10^4 \text{ kg m/s}^3$$

Table 5-1. Reynolds stresses and shear for two temperature bins. $\overline{u'v'}$ is calculated from data, with 128 (242) data points contributing to averages for $T_{575} < 13°C$ ($T_{575} > 13°C$). $\overline{u}_y$ obtained as described in text. Integration is trapezoidal, gives estimate of energy exchange due to down-gradient momentum flux. Correlation co-efficients are listed in columns headed 'C'.

occur on the warm side, $T > 13°C$, where also $\bar{u}_y$ has the greater

magnitude. The net effect is that of a down-gradient eddy momentum flux

(see Table 5-1), which implies a growth of eddy energy at the expense of

the mean kinetic energy via this mechanism. Furthermore, while the

result from deep measurements cited above suggests some symmetry of

energetics across the Stream, the shallow measurements show there is net

southward eddy transport of eastward momentum across the Stream. The

mean contribution $\bar{uv}$ indicates a similarly directed flux, an order of

magnitude smaller; $\overline{u'v'} < 0$ may be related to the fact that the average

flow was south of east. Fofonoff and Hall (1983) found that eastward

momentum flux of the Gulf Stream is decreasing in this region; $(\overline{u'v'})_y$

> 0 is one mechanism that can account for such a decrease but was not

calculable in that work.

The effect of the other exchange term is hard to determine from the

mooring. Some historical data (Worthington, 1976; or Knauss, 1969)

suggest that Gulf Stream transport may still be increasing at 68°W, and

if $\bar{u}_x > 0$ as well, then $-\rho\overline{u'^2}\bar{u}_x$ would offset the effect of the

Reynolds stresses in this region. Fofonoff and Hall (1983) found

$\bar{u}_x < 0$ at this longitude, however, so that $-\rho\overline{u'^2}\bar{u}_x$ might enhance

the Reynolds stresses.

Both similarities and differences exist between the data and

numerical results. On the average, in the decelerating portion of the

numerical jet, the Reynolds stresses are positive rather than negative in

the upper layer, about one-fifth the size of those at the mooring site at

575 dbar, and $(\overline{u'v'})_y > 0$. In the deep layer $\overline{u'v'}$ changes sign across

the jet, but in this layer $(\overline{u'v'})_y < 0$. However, because the horizontal shear is so much stronger in the top layer, there is a net transfer of mean to eddy kinetic energy once the budgets are integrated over a volume; half of the transfer is due to a contribution from the term $-\rho \overline{u'^2} \bar{u}_x$. To compare absolute magnitudes, suppose that the exchange estimated from Table 5-1 occurs over a width of 130 km (T_{575} = 5°-16.5° C) and downstream for 1000 km. Then the net transfer would be:

$$(777 \ \frac{gm}{s^3} \times 50 \text{ km} - 252 \frac{gm}{s^3} \times 80 \text{ km}) \times 10^3 \text{km} \simeq 19 \times 10^9 \text{ J/s},$$

which is very close to the value of 14.0×10^9 J/s calculated for the same mechanism in the decelerating jet of the numerical model.

From the data the mean to eddy potential energy flux at the mooring, $\overline{u'T'} \ \bar{T}_x + \overline{v'T'} \ \bar{T}_y$, can be estimated without the necessity of separating the data into bins. This flux is down-gradient as well, with an integrated magnitude less than half as large as the barotropic conversion, dominated by values from the upper 1500 m or so of the water column (see Table 5-2). As expected, $\overline{v'T'} > 0$, but all the correlation coefficients for the heat flux calculations are small. The vertical eddy heat flux term $g\alpha_0 \overline{w'T'}$ is positive (although again the correlation coefficients are very small), and may be estimated from values at 575 dbar alone, since its magnitude falls off rapidly to negligible values. At 575 db, $\overline{w'T'} = 24.979 \times 10^{-3}$ °C cm/s; taking $\Delta z = 725$ m, $\Delta y = 130$ km:

$$\int dy \int dz (g\alpha_0 \overline{w'T'}) = (130 \text{ km})(725 \text{ m})(9.81 \ \frac{m}{s^2})(10^{-4} \ \frac{gm}{cm^3 \cdot C}) \times$$

$$(24.979 \times 10^{-3} \text{°C cm/s}) = 2.310 \times 10^4 \text{ kg m/s}^2.$$

Depth	Δz	$\bar{u}_z$	$\bar{T}_y$	$\overline{v'T'}$	$\bar{v}_z$	T_x	$\overline{u'T'}$	$\bar{\theta}_z$
(db)	(db $\sim$ m)	(cm/s/m)	$(10^{-5}\,°C/m)$	(°C cm/s)	$(10^{-3}\,cm/s/m)$	$(10^{-5}\,°C/m)$	(°C cm/s)	(°C/m)
575	725	.0710	-6.61	1.547	.303	.0282	31.039	.0178
875	300	.0262	-2.44	3.284	2.76	.257	5.000	.0127
1175	475	.0262	-2.44	.055	2.76	.257	-.539	.00348

$$-\,\Sigma\,\frac{g\alpha}{\bar{\theta}_z}\,(\overline{u'T'}\,\bar{T}_x + \overline{v'T'}\,\bar{T}_y)\,\Delta z \qquad\qquad = 56.65 \text{ gm/s}^3$$

$$-\int dy \int dz\,\{\frac{g\alpha}{\bar{\theta}_z}\,(\overline{u'T;}\,\bar{T}_x + \overline{v'T'}\,\bar{T}_y)\} \qquad\qquad = 7.365 \times 10^3 \text{ kg m/s}^3$$

$$\alpha = 10^{-4} \text{ gm/cm}^3/°C \qquad \Delta y = 130 \text{ km}$$

Table 5-2. Estimate of mean to eddy potential energy conversion. Temperature gradients are estimated geostrophically from shear. Shear at 575 db is calculated from top 2 instruments; at 875 and 1175 db, from instruments at 700 and 1000 m (nominal). Variables are not rotated. $\bar{\theta}_z$ is from analytic fits of Raymer, Spencer and Bryden (1984). Integration is down to 1500 db only because contribution below is negligible. Correlation co-efficients for heat fluxes are all less than 0.1, except for $\overline{u'T'}$ at 575 db, where C = .20.

Since this term appears with a minus sign in (5-2), eddy potential energy evidently is being converted into eddy kinetic energy; moreover, it is much larger than the release of mean to eddy potential energy, so that the net tendency of eddy potential energy is to decrease. The energy pathway-- mean potential to eddy potential to eddy kinetic energy-- tantalizingly suggests the presence of baroclinic instability at the mooring site. Caution is warranted, however, for all of the calculations involved are rather noisy: the correlation coefficients are generally small and not significantly different from zero for the year long data record.

The net results are not unlike the numerical model findings in the decelerating jet and associated recirculation region: both types of instabilities appear to be present, with barotropic instability possibly dominating within the Stream. The difference in sign of the Reynolds stresses in the two cases (observational vs. numerical) is curious and may be related to the symmetry of the double gyre model. The energy transfer of mean to eddy fields implies local growth of eddy energy, mean or eddy advection of eddy energy away from the mooring site, or radiation of eddy energy away from the mooring site. The term $-(\partial/\partial y)(\overline{v'(K'+P')})$ may be estimated with the "two-bin method" used on the Reynolds stresses, and although it has the desired sign to balance the momentum and heat fluxes, it is at least an order of magnitude smaller than those terms. Moreover, $(\overline{v'K'})_y$ alone has the opposite effect as in the model, though it is relatively much smaller. All of the remaining radiation type terms are completely intractable. It is plausible that this region is one of

either temporal or spatial eddy growth, and corresponding time and space scales for the implied growth may be estimated from the numbers so far derived, along with an estimate of net eddy energy from values in Table 2-1. The average along-stream velocity u is an integrated value over the depth. Then:

$$\int dy \int dz \, \frac{1}{2} \, (\rho(\overline{u'^2} + \overline{v'^2}) + \frac{g\alpha_o \overline{T'^2}}{\overline{\theta}_z}) \simeq 8.06 \times 10^{10} \text{kg m/s}^2 \quad ;$$

$$-\int dy \int dz (\rho \, \overline{u'v'} \, \bar{u}_y) \simeq 1.87 \times 10^4 \text{ kg m/s}^3 \quad ;$$

$$-\int dy \int dz (\frac{g\alpha_o}{\overline{\theta}_z}) (\overline{v'T'} \, \overline{T}_y + \overline{u'T'} \, \overline{T}_x) \simeq 7.36 \times 10^3 \text{ kg m/s}^3 \quad ;$$

$$\bar{u} \simeq 9 \text{ cm/s}$$

The above values imply either a growth rate r (calculated from $\frac{\text{energy}}{\text{conversion}}$)

$$r \sim \frac{1.87 \times 10^4 + 7.36 \times 10^3}{8.06 \times 10^{10}} \text{ s}^{-1} = 3.23 \times 10^{-7} \text{s}^{-1} \implies \frac{1}{r} = 36 \text{ days}$$

or a downstream scale L_x for eddy energy growth (calculated from

$$L_x \sim \frac{\bar{u} \times \text{energy}}{\text{conversion}}) \text{ of}$$

$$L_x \sim \frac{(9 \text{ cm/s})(8.06 \times 10^{10} \text{ kg m/s}^2)}{(1.87 \times 10^4 + 7.36 \times 10^3) \text{kg m/s}^3} = 278 \text{ km.}$$

The time-averaging process over a 360-day period automatically obscures the implied 36-day growth rate. Although the predicted scale for downstream growth seems reasonable, it should be noted that the mooring site is in a region that has been identified as a maximum in eddy kinetic and potential energies (Schmitz, 1984; Richardson, 1983).

The analysis of Chapter 3 showed that unlimited spatial and temporal coverage of the free jet does not resolve all possible questions concerning its energetics. On the other hand, diagnosis of numerical models needs to be pursued, since the streamfunction and hence the pressure work terms are known everywhere. However, the lack of parity between the accumulation of data and yield of results suggests that a few well placed moorings might be as valuable as a large, dense array for addressing questions of the type discussed here.

5.3 A kinematic framework for interpreting the flow

Because the equations for mean and eddy energies do not depend on small amplitude expansions, different terms in them may be examined for signatures of familiar processes such as barotropic or baroclinic instabilities. Analysis of dynamical balances is less tractable, however, because the relevant terms in the vorticity equation, for example, involve so many derivatives. Moreover, with Rossby numbers of about 0.3, it may be necessary to search for a new dynamical framework that explains the flow. Although such a dynamical framework has not been fully developed, a kinematic framework has been explored that is consistent with the data. It is just one interpretation of what is occurring at the mooring site, and is not necessarily unique.

Once the data from the mooring had been scrutinized, a number of peculiarities emerged. The barotropicity of the cross-stream velocity field was not anticipated, nor were the large magnitudes of the vertical velocities. The latter feature usually resulted from the difference

between the apparent translational velocity of the Stream (as indicated by $\partial T/\partial t$) and the measured cross-stream velocities. Additionally, there is the lack of symmetry in details of the four individual Gulf Stream crossings. An interpretation is sought to relate these unusual features.

The scenario is based on the supposition that primarily the lower layer of a two-layer system is observed, as suggested by the vertical structure of vertical velocity in Chapter 2. In the discussion of the vorticity equation, it was found that the vertical and cross-stream velocities were better correlated than v and w_z; that was ascribed to the linear (two-layer) structure of w and the fact that w_z would be a noisy time-series. It was also pointed out that the correlation can be explained by the following argument: vertical velocities are induced at the bottom by flow up or down the bottom slope; higher in the water column, water parcels moving vertically must also move horizontally -- primarily cross-stream -- to remain on isotherms. Given that cross-stream velocities are nearly barotropic, as has been shown empirically, then the vertical velocities will be greatest where the isotherm slopes are greatest, that is, in the thermocline or at its equivalent, the interface in the two-layer model. The orientation of isotherm slopes may be quite different from the direction of the bottom slope, whence the bottom vertical velocity appears as an independent forcing mechanism.

So far, of course, all that has really been said is that $w = \vec{u} \cdot \nabla z_T = \hat{v} \, \partial z_T/\partial \hat{y}$, where z_T is the depth of an isotherm, and since $\hat{v}$ is barotropic $\partial z_T/\partial \hat{x}$ is assumed to be zero. The local
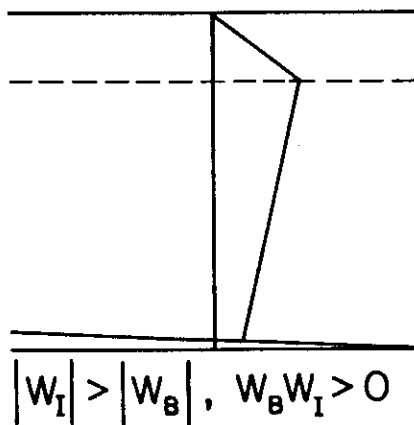
temperature change is important too, however, and may be represented as $T_t = -V T_{\hat{y}}$, where V is then related to the cross-stream translational velocity, so that $w = (\hat{v}-V)\partial z_T/\partial \hat{y}$. It has been noted that there are events for which the apparent translational and cross-stream velocities are opposite in sign; then $|\hat{v} - V| > |\hat{v}|$ and w is larger in magnitude. On the one hand, the EOF cross-stream velocity amplitude is highly correlated with w_B (vertical velocity at 4000 m), but not at all with $\partial T/\partial t$ at 575 dbar. One way to interpret these results is to assume that the barotropic cross-stream velocity arises in response to w_B. The size of the vertical velocities throughout the remainder of the water column depends on the Gulf Stream's translation: in the case of opposing translational and measured velocities, then w_z below the thermocline should have the same sign as w_B:

$$\frac{\partial w}{\partial z} \approx (\hat{v} - V)\left(\frac{\partial z_T}{\partial \hat{y}}(575) - \frac{\partial z_T}{\partial \hat{y}}(4000)\right); \quad (\hat{v}-V)w_B > 0; \quad \frac{\partial z_T}{\partial \hat{y}}\Big|_{4000}^{575} > 0$$

Thus, if $w_B > 0$ (whence $\hat{v} > 0$) then $T_t < 0$ should imply $w_z > 0$; while $w_B < 0$ ($\hat{v} < 0$) and $T_t > 0$ implies $w_z < 0$. In fact, $\partial T/\partial t$ at 575 dbar and $\Delta w = w_{575} - w_{4000}$ are negatively correlated with $C = -.75$, which is significant at the 95 percent confidence level. Since that result comes from using the entire time series, and since $vT_t < 0$ only about half the time, there are evidently two different flow regimes, that can be summarized as follows:

Figure 5.1. Vertical velocity amplitude structures for a two-layer system for cases discussed in text. Slight bottom slope allows $w \neq 0$ at the bottom. Interface (dashed line) represents thermocline of real ocean. w_B = vertical velocity at bottom; w_I = vertical velocity at interface. Case Ia or IIa occurs when given amplitude structure is negative, i.e., $w_B < 0$.

Case I

$$\left| W_I \right| > \left| W_B \right|, \; W_B W_I > 0$$

Case II

$$\left| W_B \right| > \left| W_I \right|, \; W_B W_I > 0 \qquad\qquad W_B W_I < 0$$
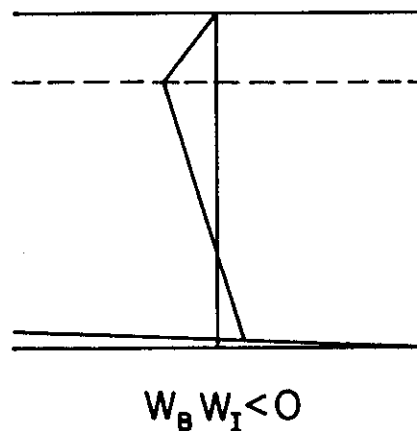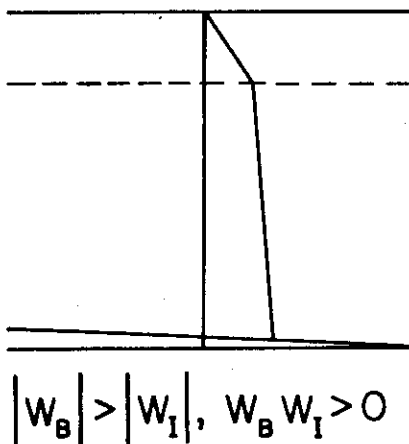
Case I	(Case Ia)		Case II	(Case IIa)
$w_B > 0$	$(w_B < 0)$		$w_B > 0$	$(w_B < 0)$
$\hat{v} > 0$	$(\hat{v} < 0)$		$\hat{v} > 0$	$(\hat{v} < 0)$
$T_t < 0$	$(T_t > 0)$		$T_t > 0$	$(T_t < 0)$
$w_z > 0$	$(w_z < 0)$		$w_z < 0$	$(w_z > 0)$

Figure 5.1 shows what the vertical velocity structure would be in the two-layer system for these two cases; in Case II, there are two possibilities, since w at the interface need not have the same sign as w at the bottom; but the data suggest the baroclinic response (shown on the right in Fig. 5.1 under Case II) is more typical. Johns and Watts (1985) present a linear analysis of the temperature equation, from data just downstream of Cape Hatteras, which yields results analogous to Case I described here; but in that study, Case I evidently described most of the data, and Case II was not considered at all. Their Fig. 11 depicts Case I very nicely.

The individual events are described rather well by the various cases, and all cases except IIa occur (in other words, Case II does not occur with negative bottom velocities). The March and early September crossings are examples of Case I: temperatures are decreasing, but $\hat{v} > 0$; examination of the vertical velocity time series shows that $w_B > 0$ and $w_z > 0$ (where w_z is taken between the thermocline and the bottom). The June event is a combination of two cases. Clearly $T_t < 0$ the whole time, but $\hat{v} < 0$ for the first 11 days and $\hat{v} > 0$ for the remainder of the crossing. Accordingly, w_B changes sign from negative to positive after 10 days; and w_z is generally less than zero

throughout (this statement will be qualified below). Finally, the late September event falls under Case II with $T_t > 0$.

That is just the beginning of the story, however. In the first place, $\partial w / \partial z$ has implications for the vorticity balance. Moreover, since ε for the flow has been estimated to be as large as 0.3, $\partial w / \partial z$ may be important to the mass balance. Finally, the above cases are really only a one-dimensional description of the flow: what is the associated three-dimensional picture Recall that in Section 2.5.2, it was suggested that curvature of the Stream could be important to the vorticity balance. To get at the curvature directly, consider vorticity in cylindrical (rather than rotated) coordinates. Figure 5.2 gives a definition sketch for the variables. Then

$$\zeta = \frac{1}{r}\frac{\partial}{\partial r}(vr) - \frac{1}{r}\frac{\partial u}{\partial \lambda} = \frac{v}{r} + \frac{\partial v}{\partial r} - \frac{1}{r}\frac{\partial u}{\partial \lambda}$$

$$\vec{u} \cdot \nabla \zeta = u\frac{\partial}{\partial r}(\frac{1}{r}\frac{\partial}{\partial r}(rv) - \frac{1}{r}\frac{\partial u}{\partial \lambda}) + \frac{v}{r}\frac{\partial}{\partial \lambda}(\frac{1}{r}\frac{\partial}{\partial r}(rv) - \frac{1}{r}\frac{\partial u}{\partial \lambda})$$

(Note that now v is long-stream velocity, and may be negative or positive according to the curvature of the Stream.) With $v \gg u$, $\frac{\partial}{\partial r} \gg \frac{1}{r}\frac{\partial}{\partial \lambda}$, then $\zeta \sim \frac{v}{r} + \frac{\partial v}{\partial r}$ and the vorticity equation becomes

$$\frac{\partial}{\partial t}(\frac{v}{r} + \frac{\partial v}{\partial r}) + \frac{u}{r}\frac{\partial v}{\partial r} - \frac{uv}{r^2} + u\frac{\partial^2 v}{\partial r^2} + \frac{v}{r^2}\frac{\partial v}{\partial \lambda} + \frac{v}{r}\frac{\partial^2 v}{\partial \lambda \partial r} +$$

$$\beta(u \sin \lambda + v \cos \lambda) = f\frac{\partial w}{\partial z} \qquad (5\text{-}4).$$

Now the local change of curvature explicitly appears, and its size can be estimated by referring to maps constructed from satellite data. Figure 5.3 shows schematically how the curvature changes from May 27 when r is

Figure 5.2. Definition sketch for variables in cylindrical coordinates.

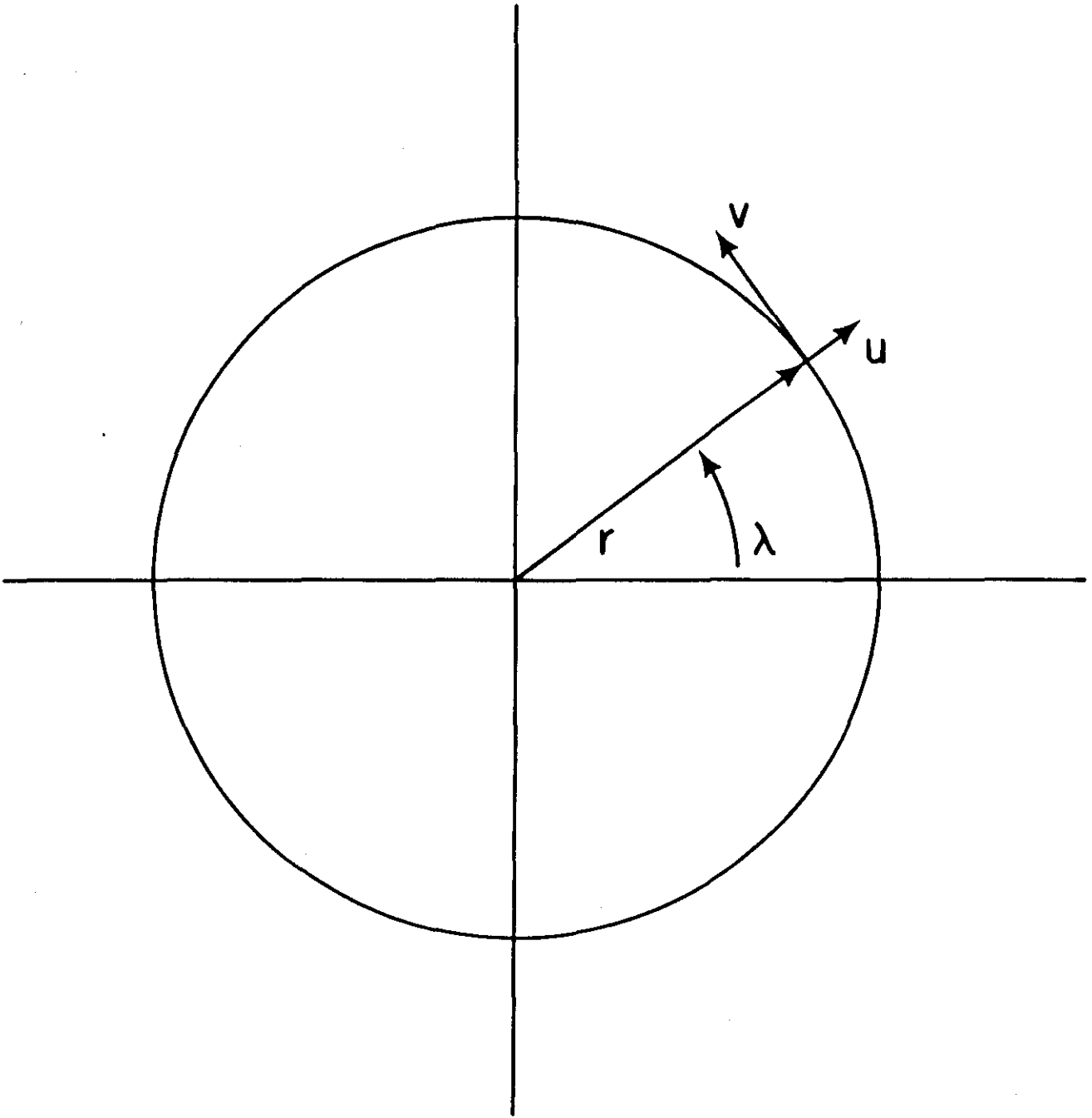Radius $r > 0$ always; $v > 0$ when motion is cyclonic.

Figure 5.3. Schematic showing change of curvature in Gulf Stream from
May 27, 1983 to June 1, 1983. Cross indicates mooring site.
Path is adapted from northern edge of front as shown on
satellite composites. Dotted circle has radius of about 70 km
and approximately matches curvature of Stream at mooring site
on May 27.

May 27   June 1
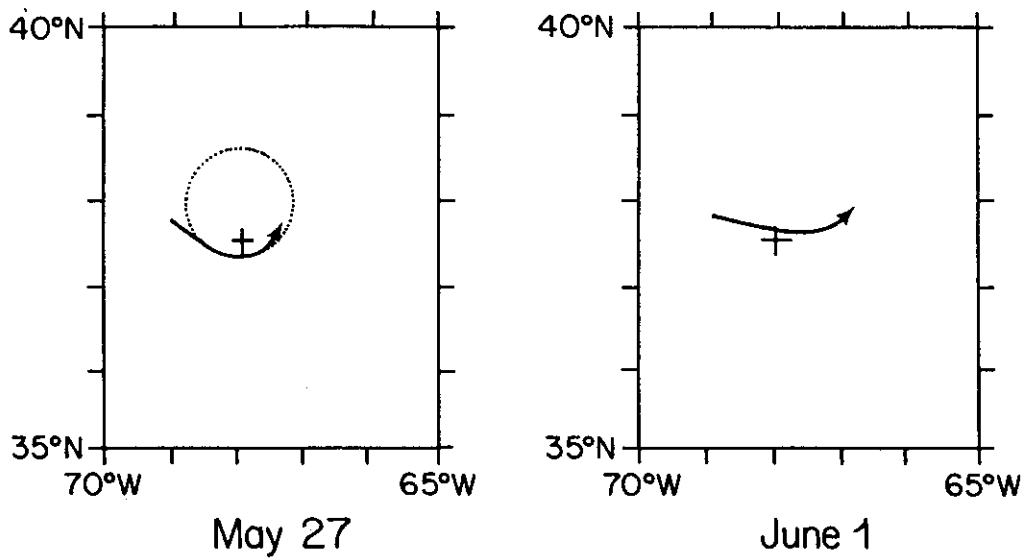
roughly 70 km, to June 1, when the flow has straightened out so r is essentially infinite. During this time, the along-stream velocity at 575 dbar $v \sim 30$ cm/s whence

$$\frac{\partial}{\partial t}(\frac{v}{r}) \sim \frac{0 - (30 \text{ cm/s})/(70 \text{ km})}{5 \text{ days}} = -.99 \times 10^{-11} \text{ s}^{-2}.$$
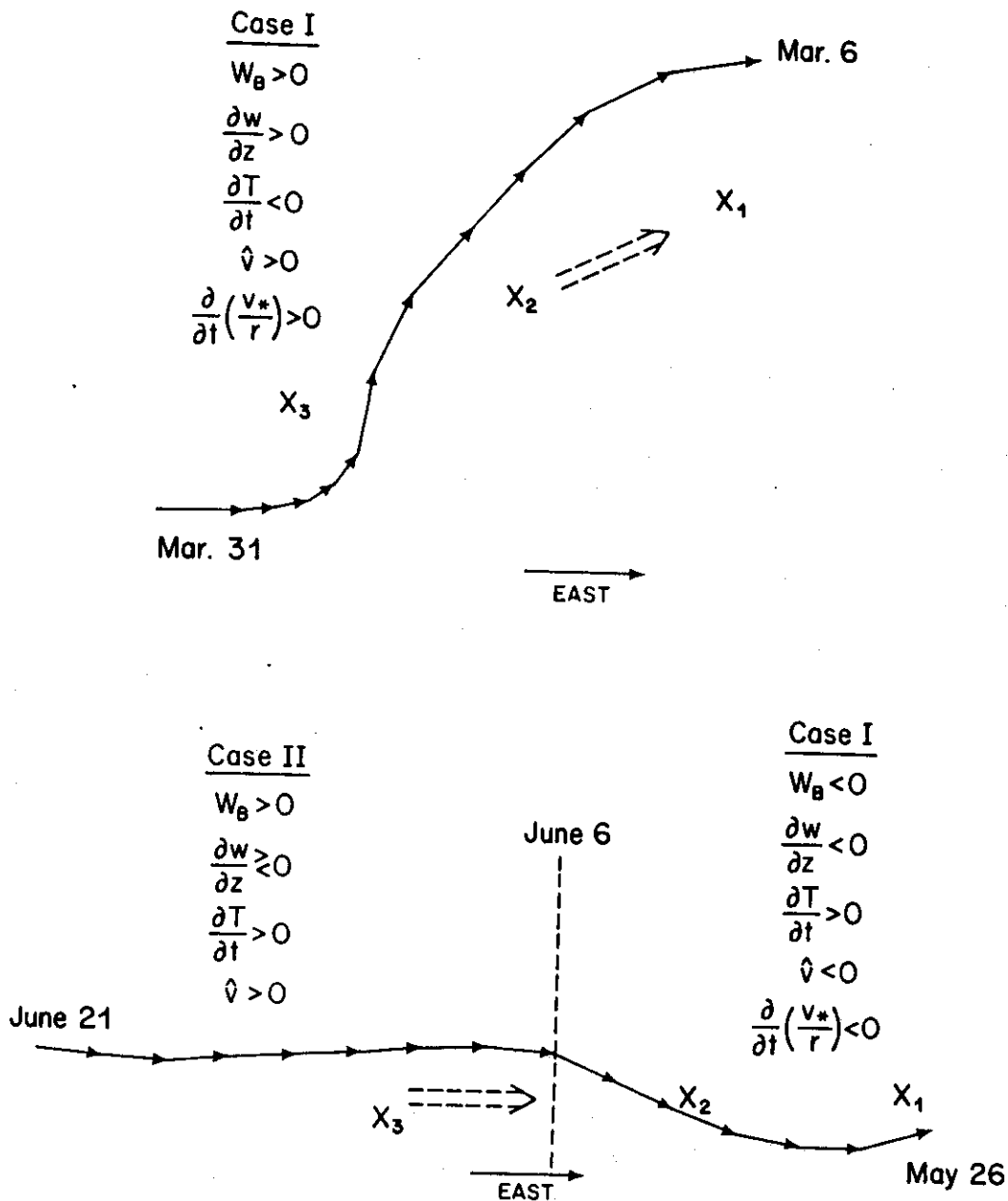
Meanwhile, $\frac{\partial w}{\partial z}$ between the bottom and thermocline is negative, and has an estimated magnitude:

$$f \frac{\partial w}{\partial z} \sim (.89 \times 10^{-4} \text{ s}^{-1}) \times \frac{(-30 \times 10^{-3} \text{ cm/s})}{3425 \text{ m}} = -.78 \times 10^{-11} \text{s}^{-2}$$

Thus, the effect of changing curvature is more than enough to balance the squashing in the lower part of the water column. (Notice that the same balance cannot obtain above the thermocline, where w_z must be < 0.)

Proceeding in a similar but qualitative manner for the four individual events suggests that the observed flow patterns can be accounted for by quasi-fixed spatial patterns like meanders being advected past the mooring site, or by patterns propagating past the site. There is qualitative agreement between the calculated long-stream direction of flow and the apparent direction from the satellite pictures, indicating that surface patterns broadly reflect structure in the deeper flow (Fofonoff, personal communication). Figure 5.4 shows how this idea of moving patterns is consistent with all the calculations from the data for those events. Single line arrows are selected daily long-stream directions, which when placed end to end suggest a spatial pattern which could account for flow direction at the mooring site if the feature passes over the mooring site in the general direction shown by the double dashed line arrows. The X's show successive positions of the mooring

Figure 5.4. Single line arrows point in direction of flow for selected successive dates during each Gulf Stream passage event; length is proportional to time between successive arrows. Double dashed lines are velocities of meanders with shapes outlined by single arrows, required to account for flow at mooring site. Successive qualitative positions of site are indicated by X's. Along-stream velocity in cylindrical coordinates is indicated by v_*. Relevant information on each event according to classification scheme discussed in text is listed with each feature.

Case I

$W_B > 0$

$\frac{\partial w}{\partial z} > 0$

$\frac{\partial T}{\partial t} < 0$

$\hat{v} > 0$

$\frac{\partial}{\partial t}\left(\frac{v_*}{r}\right) > 0$

X_1

X_2

X_3

Mar. 6

Mar. 31

EAST

Case II

$W_B > 0$

$\frac{\partial w}{\partial z} \gtrless 0$

$\frac{\partial T}{\partial t} > 0$

$\hat{v} > 0$

June 21

June 6

X_3

X_2

EAST

Case I

$W_B < 0$

$\frac{\partial w}{\partial z} < 0$

$\frac{\partial T}{\partial t} > 0$

$\hat{v} < 0$

$\frac{\partial}{\partial t}\left(\frac{v_*}{r}\right) < 0$

X_1

May 26

148

Figure 5.4, cont'd.

Case I

$W_B > 0$

$\dfrac{\partial w}{\partial z} > 0$

$\dfrac{\partial T}{\partial t} < 0$

$\hat{v} > 0$

$\dfrac{\partial}{\partial t}\left(\dfrac{v_*}{r}\right) > 0$

Aug. 29

X_1

X_2

X_3

EAST →

Sept. 10

Case II

$W_B > 0$

$\dfrac{\partial w}{\partial z} < 0$

$\dfrac{\partial T}{\partial t} > 0$

$\hat{v} > 0$

$\dfrac{\partial}{\partial t}\left(\dfrac{v_*}{r}\right)_{x_2 \to x_3} < 0$

X_1 Sept. 11

X_2

Oct. 5

X_3

EAST →
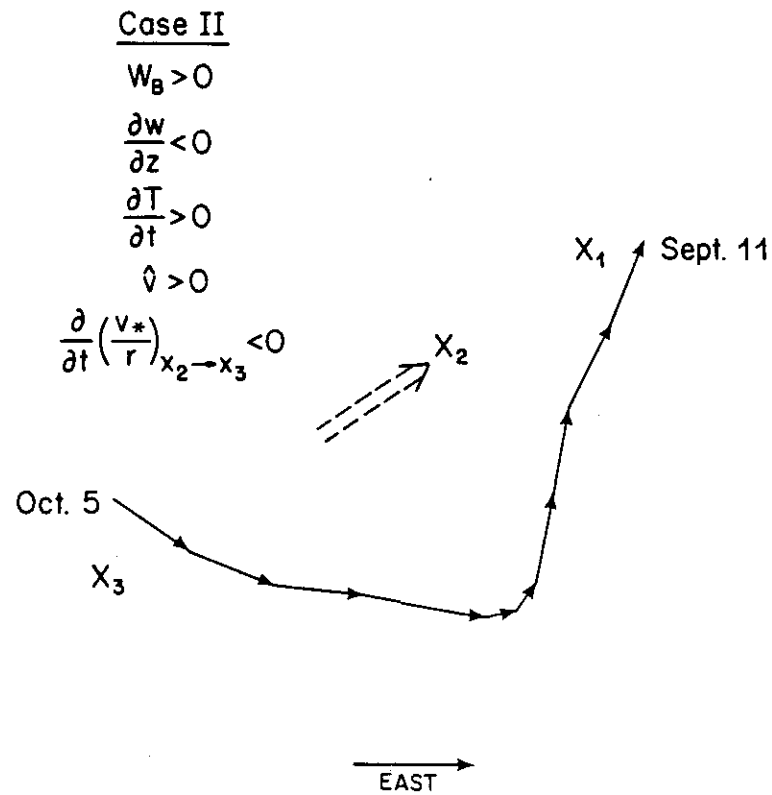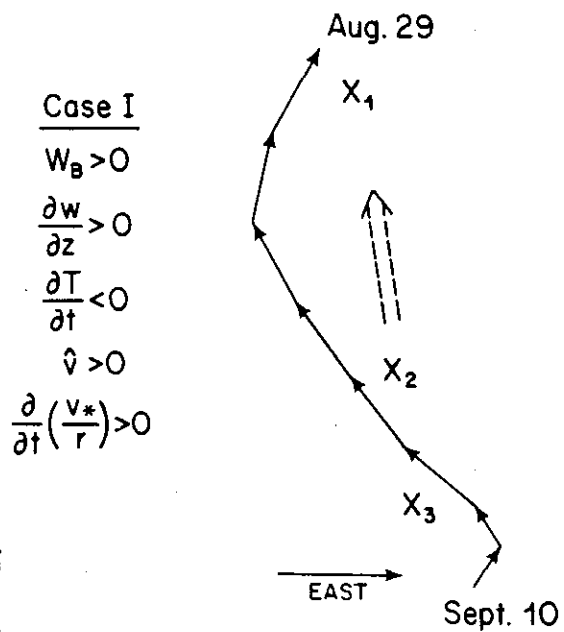
relative to the propagating features. With each feature is a summary of the behavior of relevant quantities during the event, and its classification according to the above cases. The June event, which changes character halfway through, has already been considered in detail. It was noted that in late May/early June, bottom vertical velocities were negative, and accordingly cross-stream velocities were negative as well. However, temperature was locally increasing so that evidently Case Ia is occurring. Consistent with this conclusion, $\partial w/\partial z < 0$ during that time frame, and (as calculated above) $\frac{\partial}{\partial t} \left(\frac{v}{r} \right) < 0$ as well. Between June 5 and 7, w_B and $\hat{v}$ change sign and the flow straightens out to a steady direction of about 90° true, while $\partial T/\partial t$ remains positive; this case is like II if $\partial w/\partial z$ is estimated from 575 to 4000 dbar, which yields negative or small positive values. However, $\partial w/\partial z$ between 875 dbar and the bottom is definitely positive for the remainder of the event.

March and early September are good examples of Case I, with the sign of $\partial/\partial t$ (v/r) consistent with the overall stretching between thermocline and bottom during those events. As the meanders propagate or are advected past the mooring site, there is a shift in each case from anti-cyclonic to cyclonic flow. In later September, Case II is observed, although a clear indication of the curvature tendency for this event is lacking. Going in detail through the data, one can find other isolated examples of shorter duration that are also consistent with the schematic interpretation presented and fall into one of the four cases enumerated above.

A distinction has been made above between meanders "propagating" and "being advected" past the mooring. There is a conceptual difference between the two possibilities, the latter occurring as a result of an ambient velocity field outside the Stream "pushing" the meander along. In this case, the transport estimates made from the current meter data can be altered substantially by the existence of the ambient field, because without explicit knowledge of what the ambient velocity is, it is impossible to separate it from the velocity structure of the Stream itself. The projection of the ambient velocity onto the along-stream direction can then augment the transport estimate for an event as follows: suppose the ambient field is zonal, while the Stream is directed at an angle α to due East. Then the apparent transport will exceed the actual Gulf Stream transport (which would be measured if one could move with the meander) by an amount

$$\Delta T = u_{amb} \cos\alpha \, \Delta y \, \Delta z$$

which for $u_{amb} = 5$ cm/s, $\alpha = 45°$, $\Delta y = 100$ km, and $\Delta z = 4000$ m is:

$$\Delta T = 5 \times 10^{-2} \frac{cm}{s} \times \frac{\sqrt{2}}{2} \times 10^5 m \times 4 \times 10^3 m = 14 \times 10^6 m^3/s,$$

which is comparable to the transport differences between the various Gulf Stream events.

Finally, consider the importance of stretching to the mass balance. In ordinary quasi-geostrophic dynamics, to lowest order $u_x + v_y = 0$. At the GUSTO site, however, it is possible that w_z affects the mass balance at lowest order. To test this idea quantitatively, continuity is integrated over a cross-section normal to the Stream, from 575 to 4000 dbar:

$$\int_{y_S}^{y_N} \int_{4000}^{575} \frac{\partial \hat{u}}{\partial x} \, dy \, dz \; + \; \int_{4000}^{575} (\hat{v}_N - \hat{v}_S) \, dz \; + \; \int_{y_S}^{y_N} (w_{575} - w_{4000}) \, dy \; = 0$$

$$(5\text{-}5)$$

If it is assumed that the Stream maintains a steady width (an implicit assumption throughout the analysis thus far), then $\hat{v}_N = \hat{v}_S$ and:

$$\frac{\partial M}{\partial x} = -\int_{y_S}^{y_N} (w_{575} - w_{4000}) \, dy, \qquad M = \int_{y_S}^{y_N} \int_{4000}^{575} \hat{u} \, dy \, dz \qquad (5\text{-}6)$$

Thus, the transport calculated for the "lower layer" can change in the downstream direction if there is squashing or stretching in that part of the water column. The RHS of (5-6) has been estimated for the March and June events. For March, when w_z was basically positive, the RHS has a value of -59.7 m^2/s. For June, $w_z < 0$ and RHS = 49.8 m^2/s. (Notice that the widths of the two events from Table 2-3 are nearly the same.) Estimated transport for the two events differs by 32 x 10^6 m^3/s, about half of which occurs below 575 db. With $\Delta M = 16$ x 10^6 m^3/s, a downstream distance Δx can be estimated, over which squashing or stretching must act to produce the observed transport difference:

$$\Delta x = \frac{16 \times 10^6 \text{ m}^3/s}{(49.8 \text{ to } 59.7) \text{ m}^2/s} = 268 \text{ to } 321 \text{ km.}$$

Over a length scale of about 300 km, a change in transport <u>below 575 db</u> can occur that is comparable to the observed differences between the March and June events. This length scale is intriguingly similar to the downstream spatial growth scale estimated in 5.2. Since velocities have merely been extrapolated to the surface to obtain the total transports, they reflect the changes observed below 575 dbar. However, in the

situation described above, in the "upper layer" w_z generally should have the opposite sign as in the lower layer, and a compensating change in transport ought to be observed in that layer if instruments were there to measure it.

Alternatively, the assumption of a fixed-width Stream may sometimes be violated. Then, balancing the last two terms on the LHS of (5-5) would give (assuming v_N, v_S are approximately barotropic):

$$(\hat{v}_N - \hat{v}_S) \sim 0(50 \text{ m}^2/s) ==> \hat{v}_N - \hat{v}_S \sim 0(1.5 \text{ cm/s}),$$

so that in the presence of stretching (squashing), the Stream would be narrowing (widening) at at rate of 1.5 cm/s or about 1.5 km/day. Clearly, with a single mooring that depends on an assumption of fixed width for horizontal information, such a possibility cannot be tested.

Although the scheme presented here can acccount for some of the peculiarities observed in the data, it is incomplete in the sense that it is not predictive. Even if the behavior of the bottom vertical velocity is known, for example, it is unknown whether a Case I or II type of event is occurring. More serious, perhaps, is not knowing what gives rise to w_B in the first place: is it indeed independent of the response in the rest of the water column, or is it somehow an integral part of that response Closer examination of the velocity time-series at 4000 db suggests that the flow there is actually more complicated than the cross- and long-stream EOF decomposition for the water column would indicate: at times the cross-stream velocities there are bigger than the long-stream component, and up to twice as large as cross-stream velocities in the remainder of the water column. Since GUSTO is the

first example of concurrent deep and thermocline Gulf Stream velocity time-series, it has raised many interesting questions

5.4. Indication for future directions

Now that it is technically feasible to collect long time-series of current and temperature measurements throughout the water column in the Gulf Stream, our understanding of that current should advance dramatically. The GUSTO mooring was the first successful deployment of such a mooring, and the results from the data collected point to the directions that future investigations might take. Analysis of the GUSTO data appears to justify the identification of the Gulf Stream primarily as a discrete feature with a well-defined velocity structure. Thus, a few well-placed moorings can provide considerable coverage of the Stream, if use is made of temperature as a horizontal coordinate, and if a reasonable definition of flow direction is applied. Using the decomposition of velocities into their along- and cross-stream components shows that the vertical structure at the GUSTO mooring site is accounted for by a baroclinic along-stream model and a decoupled, barotropic cross-stream mode. The inferred horizontal information may be used to estimate mass, momentum, and kinetic energy transports of the Gulf Stream. It is also possible to construct a horizontal and vertical profile of the average Stream velocity structure, from which an average potential vorticity section may be constructed. The current meter data have also been used to deduce the existence of strong vertical velocities in the Stream, with maximum rms values at thermocline levels, and a vertical structure resembling the first baroclinic mode.

Certain types of information are required to clear up points that are left ambiguous by the GUSTO data set. Data from the thermocline to the surface are needed to determine whether the velocity structure is sharper on the cyclonic or anti-cyclonic side. Also, the Rossby number has been estimated to be 0.2 or 0.3 at thermocline levels, but could possibly be larger at shallower levels where the relative vorticity $-u_y$ may be quite strong. Finally, results from the GUSTO data have suggested that a two-layer system might adequately model Stream dynamics; information on the velocity structure above the thermocline is necessary to determine whether or not two layers would be sufficient.

Vorticity balances were difficult to determine at the mooring site, but the vertical velocity calculations suggested that stretching was very important. Rudimentary comparison with changes in the Stream path curvature showed that they were probably sufficient to balance the stretching, but careful and detailed inspection of satellite data in conjunction with current meter data will be required to answer this question more fully. The multiple horizontal derivatives involved in the vorticity equation require greater spatial resolution than a single mooring can provide. More than one mooring deployed in the cross-stream direction would be useful in addressing a number of other issues as well. It was found in Section 5.3 that the energy budgets at the mooring site could not be very accurately determined; the analysis of barotropic energy exchanges between eddy and mean flow especially would have benefited from greater cross-stream resolution. Transports could be monitored more accurately with more moorings across the Stream, since it

would take less time for the entire Stream to be profiled in a single passage over the sites; then it might be possible to determine whether transport really changes as dramatically in time as the GUSTO data suggest, or whether apparent changes are due to an ambient velocity field advecting features past the mooring site. It would also be possible to test the extent to which the Stream maintains a constant width.

The most intractable aspect of observational and theoretical Gulf Stream analyses is that of downstream changes in the flow structure, because they are so slight that their signal is swamped by variations in time and in the cross-stream direction. The diagnostic energetic analysis of Chapter 3 yielded several results that might be tested observationally, however. For example, in the jet itself, the terms involved in maintaining the mean kinetic energy budget, particularly in the decelerating portion of the jet, were greater by an order of magnitude than those in the eddy kinetic energy budgets. Analysis of data from moorings separated by as much as 1500 km in the downstream direction might be able to identify whether that is indeed true. (Fofonoff and Hall (1983) tried to address the point but had to take relatively synoptic data as representative of the mean, so that eddy energies had to be ignored.)

One of the major thrusts of this work has been to justify the treatment of the Gulf Stream as a well-defined flow structure in the ocean. This approach gives rise to the most basic philosophical question that investigators must address in the future: when(if ever) is it appropriate to use Eulerian averages in examining regions of Gulf Stream

flow, as was done in the numerical analysis   Our definitions of the general or time-averaged ocean circulation may have to be refined, that we may distinguish between an observable, Eulerian average criculation in the ocean, and the existence of a boundary current with an average structure but variable position and orientation, such that it affects the interior general circulation in order one fashion. It seems that observational tools are sufficiently advanced to resolve these philosophically different approaches in the near future.

Appendix A.1

It is to be shown that

$$\frac{\partial}{\partial x}(u_k \psi_k \nabla^2 \psi_k) + \frac{\partial}{\partial y}(v_k \psi_k \nabla^2 \psi_k) =$$

$$\frac{\partial}{\partial x}(\psi_k \vec{u}_k \cdot \nabla v_k) - \frac{\partial}{\partial y}(\psi_k \vec{u}_k \cdot \nabla u_k) - \nabla \cdot (\frac{\vec{u}_k \, KE_k}{H_k})$$

where k is the layer index and $KE_k = \frac{1}{2}(\psi_{kx}^2 + \psi_{ky}^2)$. For neatness, in the following the subscript k is omitted. Thus:

$$\frac{\partial}{\partial x}(u \, \psi \nabla^2 \psi) + \frac{\partial}{\partial y}(v \, \psi \nabla^2 \psi) =$$

$$\frac{\partial}{\partial x}[u \, \psi(\psi_{xx} + \psi_{yy})] + \frac{\partial}{\partial y}[v \, \psi(\psi_{xx} + \psi_{yy})] =$$

$$\frac{\partial}{\partial x}(u \, \psi \, \psi_{xx}) + \frac{\partial}{\partial y}(v \, \psi \, \psi_{yy}) + u \, \psi \psi_{xyy} + (u \psi)_x \, \psi_{yy} +$$

$$v \, \psi \, \psi_{xxy} + (v \psi)_y \, \psi_{xx} =$$

$$\frac{\partial}{\partial x}(u \, \psi \, \psi_{xx}) + \frac{\partial}{\partial y}(v \, \psi \, \psi_{yy}) + \frac{\partial}{\partial y}(u \, \psi \psi_{xy}) - (u \psi)_y \, \psi_{xy} +$$

$$\frac{\partial}{\partial x}(v \, \psi \, \psi_{xy}) - (v \psi)_x \, \psi_{xy} + (u \psi)_x \, \psi_{yy} + (v \psi)_y \, \psi_{xx} =$$

$$\frac{\partial}{\partial x}(\psi \vec{u} \cdot \nabla \psi_x) + \frac{\partial}{\partial y}(\psi \vec{u} \cdot \nabla \psi_y) - u_y \, \psi \psi_{xy} - u \psi_y \, \psi_{xy} - v_x \, \psi \psi_{xy} -$$

$$\qquad\qquad\qquad\qquad\qquad\qquad [\,A\,] \qquad\qquad\qquad\qquad [\,B\,]$$

$$v \, \psi_x \, \psi_{xy} + u_x \, \psi \, \psi_{yy} + u \, \psi_x \, \psi_{yy} + v_y \, \psi \psi_{xx} + v \, \psi_y \, \psi_{xx} =$$

$$\qquad\quad [\,-A\,] \quad (-v \psi_y \, \psi_{yy}) \quad [\,-B\,] \quad (-u \, \psi_x \, \psi_{xx})$$

$$\frac{\partial}{\partial x}(\psi \vec{u} \cdot \nabla v) + \frac{\partial}{\partial y}(-\psi \vec{u} \cdot \nabla u) - u \frac{\partial}{\partial x}(\frac{1}{2}\psi_y^2) - v \frac{\partial}{\partial y}(\frac{1}{2}\psi_x^2) -$$

$$v \frac{\partial}{\partial y}(\frac{1}{2}\psi_y^2) - u \frac{\partial}{\partial x}(\frac{1}{2}\psi_x^2) =$$

$$\frac{\partial}{\partial x}(\psi \vec{u} \cdot \nabla v) + \frac{\partial}{\partial y}(-\psi \vec{u} \cdot \nabla u) - \vec{u} \cdot \nabla [\frac{1}{2}(\psi_x^2 + \psi_y^2)] =$$

$$\frac{\partial}{\partial x}(\psi \vec{u} \cdot \nabla v) + \frac{\partial}{\partial y}(-\psi \vec{u} \cdot \nabla u) - \nabla \cdot (\vec{u} \frac{KE}{H}).$$

Appendix A.2

It is to be shown that:

$$J(\psi_{k+1/2}, h_{k+1/2}) = J(\psi_k, h_{k+1/2}) = J(\psi_{k+1}, h_{k+1/2})$$

where $\psi_{k+1/2} = \dfrac{H_{k+1}\psi_k + H_k\psi_{k+1}}{H_k + H_{k+1}}$, $h_{k+1/2} = \dfrac{f_0}{g'_{k+1/2}}(\psi_{k+1} - \psi_k)$.

Thus, using the well-known properties of the Jacobian:

I) $J(\psi_{k+1/2}, h_{k+1/2}) = J(\dfrac{H_{k+1}\psi_k + H_k\psi_{k+1}}{H_k + H_{k+1}}, \dfrac{f_0}{g'_{k+1/2}}(\psi_{k+1} - \psi_k)) =$

$$\dfrac{f_0}{g'_{k+1/2}(H_k + H_{k+1})}[J(H_{k+1}\psi_k, \psi_{k+1}) + J(H_k\psi_{k+1}, -\psi_k)] =$$

$$\dfrac{f_0}{g'_{k+1/2}(H_k + H_{k+1})}[H_{k+1}J(\psi_k, \psi_{k+1}) + H_k J(\psi_k, \psi_{k+1})] =$$

$$\dfrac{f_0}{g'_{k+1/2}} J(\psi_k, \psi_{k+1})$$

II) $J(\psi_k, h_{k+1/2}) = J(\psi_k, \dfrac{f_0}{g'_{k+1/2}}(\psi_{k+1} - \psi_k)) = \dfrac{f_0}{g'_{k+1/2}} J(\psi_k, \psi_{k+1})$

III) $J(\psi_{k+1}, h_{k+1/2}) = J(\psi_{k+1}, \dfrac{f_0}{g'_{k+1/2}}(\psi_{k+1} - \psi_k)) =$

$$\dfrac{-f_0}{g'_{k+1/2}} J(\psi_{k+1}, \psi_k) = \dfrac{f_0}{g'_{k+1/2}} J(\psi_k, \psi_{k+1}).$$

References

Bryden, H.L. (1976) Horizontal advection of temperature for low-frequency motions. Deep-Sea Res., 23, 1165-1174.

Bryden, H.L. (1979) Poleward heat flux and conversion of available potential energy in Drake Passage. J. Mar. Res., 37(1), 1-22.

Bryden, H.L. (1980) Geostrophic vorticity balance in midocean. J. Geophys. Res., 85 (C5), 2825-2828.

Bryden, H.L. (1982) Sources of eddy energy in the Gulf Stream recirculation region. J. Mar. Res., 40 (4), 1047-1068.

Chow, J.C. and W.R. Holland (1985) A multi-layer quasi-geostrophic numerical model of ocean circulation. In preparation.

Dewar, W.K., and J.M. Bane (1984) The subsurface energetics of the Gulf Stream near the Charleston Bump. J. Phys. Oceanog., accepted.

Fofonoff, N.P. (1954) Steady flow in a frictionless homogeneous ocean. J. Mar. Res., 13, 254-262.

Fofonoff, N.P. (1962) Dynamics of ocean currents. The Sea: Ideas and Observations on Progress in the Study of the Seas, Vol. 1. Physical Oceanography. M.N. Hill, Ed., Wiley-Interscience, 323-395.

Fofonoff, N.P. (1981) The Gulf Stream System. In: Evolution of Physical Oceanography, B.A. Warren and C. Wunsch, eds., The MIT Press, Cambridge, Massachusetts, 112-139.

Fofonoff, N.P. and M.M. Hall (1983) Estimates of mass, momentum, and kinetic energy fluxes of the Gulf Stream. J. Phys. Oceanog., 13 (10), 1868-1877.

Fuglister, F.C. (1963) Gulf Stream '60. Progress in Oceanography, Vol. 1, Pergamon Press, 265-383.

Haidvogel, D.B., and W.R. Holland (1978) The stability of ocean currents in eddy-resolving general circulation models. J. Phys. Oceanog., 8, 393-413.

Halkin, D. and T. Rossby (1985) The structure and transport of the Gulf Stream at 73° W. J. Phys. Oceanog., submitted.

Hall, M.M. and H.L. Bryden (1985) Profiling the Gulf Stream with a current meter mooring. Geophys. Res. Letters, accepted.

Halliwell, G.R., Jr., and C.N.K. Mooers (1983) Meanders of the Gulf Stream downstream from Cape Hatteras 1975-1978. J. Phys. Oceanog., 13, 1275-1292.

Harrison, D.E. (1979) Eddies and the general circulation of numerical model gyres: an energetic perspective. Rev. Geophys. and Space Phys., 17 (5), 969-979.

Harrison, D.E. and A.R. Robinson (1978) Energy analysis of open regions of turbulent flows -- mean eddy energetics of a numerical ocean circulation experiment. Dyn. Atmos. Oceans, 2, 185-211.

Holland, W.R. (1978) The role of mesoscale eddies in the general circulation of the ocean -- numerical experiments using a wind-driven quasi-geostrophic model. J. Phys. Oceanog., 8, 363-392.

Holland, W.R. (1985) Simulation of mesoscale ocean variability in midlatitude gyres. In: Advances in Geophysics, Vol. xx.

Holland, W.R. and D.B. Haidvogel (1980) A parameter study of the mixed instability of idealized ocean currents. Dyn. Atmos. Oceans, 4, 185-215.

Holland, W.R. and L.B. Lin (1975) On the generation of mesoscale eddies and their contribution to the oceanic general circulation. I. A preliminary numerical experiment. J. Phys. Oceanog., 5, 642-657.

Holland, W.R., and P.B. Rhines (1980) An example of eddy-induced ocean circulation. J. Phys. Oceanog., 10 (7), 1010-1031.

Holland, W.R., and W.J. Schmitz (1985) The penetration scale of the Gulf Stream. J. Phys. Oceanog., submitted.

Johns, W.E. (1985) Dynamics and structure of Gulf Stream meanders northeast of Cape Hatteras, N.C. Ph. D. Thesis, University of Rhode Island, 232 pp.

Johns, W.E. and D.R. Watts (1985) Gulf Stream meanders: Observations on the deep currents. J. Geophys. Res., accepted.

Knauss, J.A. (1969) A note on the transport of the Gulf Stream. Frederick C. Fuglister Sixtieth Anniversary Volume, Deep-Sea Res., 16 (Suppl.),117-123.

Luyten, J.R. (1977) Scales of motion in the deep Gulf Stream and across the Continental Rise. J. Mar. Res., 35 (1), 49-74.

Luyten, J.R., J. Pedlosky and H. Stommel (1983) The ventilated thermocline. J. Phys. Oceanog., 13 (2), 292-309.

Luyten, J.R., and A.R. Robinson (1974) Transient Gulf Stream meandering. Part II: Analysis via a quasi-geostrophic time-dependent model. J. Phys. Oceanog., 4 (20), 256-269.

McCartney, M.S. (1982) The subtropical recirculation of Mode Waters. J. Mar. Res., 40, Suppl., 427-464.

McDowell, S., P. Rhines, and T. Keffer (1982) North Atlantic potential vorticity and its relation to the general circulation. J. Phys. Oceanog., 12 (12), 1417-1436.

Munk, W.H. (1950) On the wind-driven ocean circulation. Journal of Meteorology, 7, 79-93.

Orlanski, I. (1969) The influence of bottom topography on the stability of jets in a baroclinic fluid. J. Atmos. Sci., 26, 1216-1232.

Owens, W.B. (1984) A synoptic and statistical description of the Gulf Stream and subtropical gyre using SOFAR floats. J. Phys. Oceanog., 14, (1), 104-113.

Pedlosky, J. (1970) Finite-amplitude baroclinic waves. J. Atmos. Sci., 27 (1), 15-30.

Pedlosky, J. (1979) Geophysical Fluid Dynamics. Springer-Verlag, 624 pp.

Pedlosky, J. (1982) Finite-amplitude baroclinic waves at minimum critical shear. J. Atmos. Sci., 39 (3), 555-562.

Pratt, L.J. and M.E. Stern (1985) Dynamics of vorticity fronts. J. Fluid Mech., submitted.

Raymer, M.E., A. Spencer, and H.L. Bryden (1985) Temperature correction for mooring motion on GUSTO current meter time series. W.H.O.I. Technical Report, 85-   .

Rhines, P.B. and W.R. Young (1982) Homogenization of potential vorticity in planetary gyres. J. Fluid Mech., 122, 347-368.

Richardson, P.L. (1983a) A vertical section of eddy kinetic energy through the Gulf Stream System. J. Geophys. Res., 88 (C4), 2705-2709.

Richardson, P.L. (1983b) Eddy kinetic energy in the North Atlantic from surface drifters. J. Geophys. Res., 88 (C7), 4355-4367.

Robinson, A.R., J.R. Luyten, and G. Flierl (1975) On the theory of thin

   rotating jets: A quasi-geostrophic time dependent model.

   Geophysical Fluid Dynamics, Vol. 6.

Robinson, A.R. and P.P. Niiler (1967) The theory of free inertial

   currents. I. Path and structure. Tellus, 19, 269-291.

Schmitz, W.J., Jr. (1977) On the deep general circulation in the Western

   North Atlantic. J. Mar. Res., 35 (1), 21-28.

Schmitz, W.J., Jr. (1980) Weakly depth-dependent segments of the North

   Atlantic circulation. J. Mar. Res., 38 (1), 111-133.

Schmitz, W.J., Jr. (1984) Abyssal eddy kinetic energy in the North

   Atlantic. J. Mar. Res., 42, 509-536.

Stommel, H. (1948) The westward intensification of wind-driven ocean

   currents. Trans. Amer. Geophys. Union, 29, 202-206.

Stommel, H. (1950) The Gulf Stream: A brief history of the ideas

   concerning its cause. The Scientific Monthly, 70 (4), 242-253.

Stommel, H. (1965) The Gulf Stream. University of California Press,

   Berkeley, 248 pp.

Talley, L.D. (1982) Instabilities and radiation of thin, baroclinic

   jets. Ph. D. Thesis, Mass. Inst. of Tech./Woods Hole Oceanog.

   Inst., 233 pp.

Warren, B.A. (1963) Topographic influences on the path of the Gulf

   Stream. Tellus, 15, 167-183.

Warren, B.A. and G.H. Volkmann (1968) Measurement of volume transport of

   the Gulf Stream south of New England. J. Mar. Res., 26 (2), 110-126.

Watts, D.R. (1983) Gulf Stream Variability. In: Eddies in Marine Science, A.R. Robinson, ed., Springer-Verlag, 114-144.

Watts, D.R. and W.E. Johns (1982) Gulf Stream meanders: observations on propagation and growth. J. Geophys. Res., 87 (C12), 9467-9476.

Worthington, L.V. (1976) On the North Atlantic Circulation. The Johns Hopkins Oceanographic Studies 6 110 pp.

Wright, D.G. (1981) Baroclinic instability in Drake Passage. J. Phys. Oceanog., 11 (2), 231-246.